NATURAL AND HUMAN INFLUENCES ON BASEFLOW REGIMES: A PHYSICALLY-BASED AND GEOCHEMICAL ANALYSIS

A Dissertation

Presented in Partial Fulfillment of the Requirements for the

Degree of Doctorate of Philosophy

with a

Major in Water Resources

in the

College of Graduate Studies

University of Idaho

by

Ricardo Sánchez-Murillo

May 2014

Major Professor Jan Boll, Ph.D.

Authorization to Submit Dissertation

This dissertation of Ricardo Sánchez-Murillo, submitted for the degree of Doctorate in Philosophy with a major in Water Resources and entitled "Natural and human influences on baseflow regimes: a physically-based and geochemical analysis" has been reviewed in final form. Permission, as indicated by the signatures and dates given below, is now granted to submit final copies to the College of Graduate Studies for approval.

Major Professor	_____	Date _____
	Jan Boll, Ph.D.	
Committee Members	_____	Date _____
	Erin S. Brooks, Ph.D.	
	_____	Date _____
	William Elliot, Ph.D.	
	_____	Date _____
	Esteban Gazel, Ph.D.	
Department Administrator	_____	Date _____
	Jan Boll, Ph.D.	
Agriculture and Life Sciences College Dean	_____	Date _____
	Larry D. Makus, Ph.D.	

Final Approval and Acceptance by the College of Graduate Studies

_____ Date _____

Jie Chen, Ph.D.

Abstract

Baseflow is one of the most important components in the streamflow regime of any ecosystem. Understanding which key factors control baseflow dynamics is an essential mission to pursue future decisions involving the accelerated population growth and climate variability that are currently altering water distribution and availability worldwide. This study combines a series of analyses in natural and human-altered watersheds:

(i) Baseflow recession analysis in the inland Pacific Northwest, USA:

Storage-discharge relationships were analyzed in 26 watersheds in the inland Pacific Northwest of United States (PNW) across a variety of drainage areas (10^0 – 10^3 km^2), land uses, geology units, and climate gradients. Overall, baseflow recession characteristics are not strongly correlated with watershed area. The mean basin slope and the aridity index are the best estimators of baseflow coefficients. Main underlying geology plays a significant role on controlling the characteristic baseflow recession time scales.

(ii) Stable isotope hydrology and geochemical analysis in the inland PNW:

Isotope ratios in precipitation resulted in a regional meteoric water line of $\delta^2H = 7.42 \cdot \delta^{18}O + 0.88$ (n = 316; r^2 = 0.97). Isotope values showed a clear temperature-dependent seasonality. Despite the observed seasonal variation in precipitation, the annual stream $\delta^{18}O$ variation was very small except for one large snowmelt event. Baseflow mean transit times ranged from 0.42 − 0.62 years (human-altered and basalt-dominated landscape), 0.73 – 1.7 years (mining-altered and predominantly sedimentary rocks), and 0.67 − 3.2 years (forested and granitic-dominated watersheds). The best fits between observed and $\delta^{18}O$ ratios were obtained with the exponential and dispersion weighting functions. Baseflow geochemical data supported the relative water age estimates. Greater residence times were represented by more homogenous water chemistry meanwhile smaller residence times resulted in more dynamic composition

(iii) Baseflow geochemical evidence of active serpentinization in a tropical environment:

A baseflow geochemical analysis conducted in the Santa Elena Ophiolite (Costa Rica) provided novel evidence of active serpentinization. Natural springs fluids are characterized by basic conditions (pH>11), high hydroxide, carbonates, and relative low magnesium concentrations. Active methane vents coupled with carbonate deposits ($\delta^{13}C_{CO2}$= −27‰ to −14 ‰; $\delta^{18}O_{CO2}$= −17‰ to − 6‰) also provide evidence for active serpentinization and carbonation. Isotope ratios of the alkaline fluids ($\delta^{18}O$= −7.9‰, $\delta^{2}H$= −51.4‰) and groundwater ($\delta^{18}O$= −7.6‰; $\delta^{2}H$= −48.0‰) suggests that, during baseflow recession, springs are fed by deep groundwater circulation. Methanogenic archaea, which comprises a relatively high percentage of the RNA tag sequences, suggests that biological methanogenesis may play a significant role in the system. Santa Elena's extreme varying weather results in a scenario that could be of significant importance for a) improving the knowledge of conditions on a humid early Earth or Mars that had periodic changes in water supply, b) revealing new insights on serpentinizing solute transport, and c) modeling hydrogeochemical responses as a function of meteoric recharge.

Acknowledgements

First and foremost, I would like to thank my major advisor Dr. Jan Boll for giving me an opportunity to work with his research group at the University of Idaho. His guidance has made this a thoughtful and rewarding journey. It is difficult to overstate my gratitude to him, without his constant enthusiasm, insights, friendship, and great efforts to support me, this journey would not have been possible.

I express my profound gratitude to Dr. Erin Brooks who immersed me in the fascinating (and complex) topic of baseflow regimes. His continuous guide on field monitoring techniques and data analysis facilitated the conclusion of this project. It also was a privilege to work with Dr. William Elliot who allowed me to be part of his funded baseflow project and granted me the access of the Priest River Experimental Forest facilities. Dr. Elliot's insights regarding mountain hydrology processes in the inland Pacific Northwest were highly beneficial for the completion of the baseflow recession analysis. I would like to thank Dr. Esteban Gazel for introduced me into the intriguing study of natural hyperalkaline fluids and its relationships to early Earth life conditions. His geochemical expertise was fundamental for the completion of the interdisciplinary chapter.

I would like to extent my appreciation to all the lab members who helped me in several sampling events, always under rough weather conditions: Bill, Jon, Todd, Ryan, and Levi. Inexorably, I have to extent my deepest thanks to my family and my closest friends who have been supporting me along this journey.

Finally, it is a pleasure to thank those institutions who made this journey possible: National University of Costa Rica, University of Idaho, and USDA-Forest Service Rocky Mountain Station.

Table of Contents

List of Tables

List of Figures

Introduction

1. Baseflow regimes: an overview

Baseflow is one of the most important components of the streamflow regime of any ecosystem. In the past, baseflow significance was commonly analyzed from a single perspective: water supply and hydropower demand. However, baseflow importance can be translated to a wide range of connotations. For instance, low flows provide several ecological services: (i) sustain primary and secondary productivity; (ii) regulate water temperature during summer; (iii) provides continuous habitat to stream biota. Furthermore, knowledge of baseflow characteristics is critical for water management strategies including drought forecasting and water quality assessments.

Future hydro-climate scenarios in temperate semi-arid and tropical regions may translate in severe consequences to (i) the demand of groundwater supplies for food production, electricity generation, clean drinking water, and recreation which may converge in transboundary water rights debates, and (ii) disruption of ecological assemblages (e.g. high water temperatures, low dissolved oxygen levels, and high solute concentrations) along summer flows that are critical to many ecosystems.

Baseflow is described as the cumulative outflow from all upstream riparian aquifers during rainless periods, in the absence of snowmelt or any other hydrologic inputs (Brutsaert, 2005). Baseflow recession has been described as a function of geomorphology (e.g. perennial stream length, drainage area, and porous media) (Knisel, 1963; Brutsaert et al., 1977; Zecharias et al., 1988; Mendoza et al., 1993; Vitvar et al., 2002; Brandes et al., 2005; Biswal et al., 2010) and the structure of riparian aquifers (Troch et al., 1993). While geologic features are clearly invariant at the scale of hydrological studies, recent studies (Peña-Arancibia et al., 2010; van Dijk, 2010) have proposed that climatic attributes should no longer be considered as invariant factors when estimating baseflow recessions, especially, in semiarid, arid or tropical catchments.

Since the 1990s inter-mountainous watersheds have gained increasing attention in science, politics, and economics. Worldwide countries and research institutions have recognized the importance of the water cycle of mountainous water sources, with a special relevance for semiarid and arid regions. Viviroli et al. (2007) described mountainous catchments as the "water towers for humanity" since these systems provide globally 67% and 61% of the discharge in arid and temperate regions, respectively. Yet groundwater contributions are the most poorly understood aspect of mountainous watershed hydrology. In the PNW, efforts to understand hydrological processes have relied on the use of conservative tracers such as $\delta^{18}O$ and $\delta^{2}H$ (Larson et al., 2000; Koeniger et al., 2008; Takeuchi et al., 2009; Moravec et al., 2010). These naturally-occurring tracers have been useful to identify contributions of pre-event water, event water, and mean transit times; however the conjunction of stable isotopes signatures, geochemical characterization, and climate variability may give new insights to understand key hydrological processes in complex mountainous watersheds, especially, processes that dictate how water is delivered to streams under baseflow conditions.

2. Chapter descriptions

The first chapter describes the storage-discharge relationships in 26 watersheds within the inland Pacific Northwest of the United States across a variety of basin areas, geologic formations, land uses, and temperature and precipitation gradients of eastern Washington and central and northern Idaho. Baseflow recession coefficients were obtained using several statistical and graphical methods. The main objectives of Chapter I were to: *a)* evaluate the main terrain characteristics controlling the natural release of water as baseflow; *b)* to estimate the role that climate plays in the baseflow recession process; and *c)* to determine the regional variability of the characteristic recession time scale *K* and minimum annual storage across the inland PNW. This study presents the first comprehensive baseflow recession analysis for the inland PNW. By understanding the main factors controlling baseflow recession characteristics, environmental agencies could prioritize efforts in areas where future

droughts and land use changes may affect ecological assemblages and socio-economic activities.

Chapter II presents a stable isotope hydrology assessment of precipitation and surface waters in the inland PNW of Washington and Idaho. The objectives of this study were to: *a)* establish foundational regional and local meteoric water lines in the inland PNW; *b)* describe spatial and temporal isotopic variations in precipitation and surface waters; and *c)* evaluate differences in mean transit times and transit distribution functions at variable catchment scales (10^0 – 10^2 km^2), land uses (i.e. agricultural-urban, mining, and forested), climatic gradients, and main underlying geology (i.e. basalt, granitic, metamorphic, and sedimentary). Mean transit time input-output relationships were constructed from $\delta^{18}O$ ratios in precipitation and surface waters over a sampling period of 2 years in most of the selected watersheds. To complement the stable isotope data, a baseflow geochemical analysis was conducted in five natural and human-altered watersheds to evaluate water quality conditions in these systems during the critical summer months. Stable isotope and geochemical data are needed to create a baseline for future water resources assessments and modeling efforts in the inland PNW.

Chapter III presents geochemical evidence of a new tropical active serpentinization end-member discovered early in 2013 within the Santa Elena Ophiolite, Costa Rica. Extreme varying climate conditions between dry and wet seasons result in a unique hydrogeological scenario that could be of significant importance for a) improving current knowledge of conditions on a humid early Earth or Mars that had periodic changes in water supply, b) revealing new insights on serpentinization processes and the natural release of hyperalkaline fluids as baseflow, and c) modeling hydrogeochemical responses as a function of meteoric water recharge and baseflow recession in present-day continental serpentinization environments.

2. References

Biswal, B., and Marani, M. 2010. Geomorphological origin of recession curves. *Geophysical Res. Letters,* 37:L24403, doi:10.1029/2010GL045415.

Brandes, D., Hoffman, J., Mangarillo, J.T. 2005. Baseflow recession rates, low flows, and hydrologic features of small watersheds in Pennsylvania, USA. *JAWRA.,* 41(5):1177-1186.

Brutsaert, W. 2005. Hydrology: an introduction. Cambridge University Press. Cambrigde, United Kingdom.

Brutsaert, W., and Lopez, J.P. 1998. Basin-scale geohydrologic drought flow features of riparian aquifers in the southern Great Plains. *Water Resour. Res.,* 34 (2), 233-240.

Knisel, W. 1963. Baseflow recession analysis for comparison of drainage basins and geology. *Geophysical Research*, 68(12):3649-3653.

Koeniger, P., Hubbart, J. A. Link, T., and Marshall, J.D. 2008. Isotopic variation of snow cover and streamflow in response to changes in canopy structure in a snow-dominated mountain catchment. *Hydrol. Process*. 22:557–566.

Larson, K.R., Keller, C.K., Larson, P.B., and Allen-King, R.M., 2000. Water resource implications of 18O and 2H distributions in a basalt aquifer system. *Groundwater,* 38:947– 953.

Mendoza, G.F., Steenhuis, T. S., Walter M. T., and Parlange, J.Y. 2003. Estimating basin-wide hydraulic parameters of a semi-arid mountainous watershed by recession-flow analysis. *Hydrology,* 279:57–69.

Moravec, B C., Keller, K.C., Smith, J.L., Allen-King, R-M., Goodwin, A.J., Fairley, J.P., and Larson, P.B. 2010. Oxygen-18 dynamics in precipitation and streamflow in a semi-arid agricultural watershed, Eastern Washington, USA . *Hydrol. Process.,* 24:446–460.

Peña-Arancibia, J.L., van Dijk, A.I.J.M., Mulligen, M., and Bruijzeel, L.A. 2010. The role of climatic and terrain attributes in estimating baseflow recession in tropical catchments. *Hydrol. Earth Syst. Sci. Discuss.,* 7:4059-4087.

Takeuchi, A., Goodwin, A.J., Moravec, B., Larson, P.B., and Keller, C.K. 2009. Isotopic evidence for temporal variation in proportion of seasonal precipitation since

the last glacial time in the inland Pacific Northwest of the USA. *Quaternary Research,* 72:198–206.

van Dijk., A.I.J.M. 2010. Climate and terrain factors explaining streamflow response and recession in Australian catchments. *Hydrol. Earth Syst. Sci. Discuss.,* 14:159-169.

Vitvar, T., Burns, D.A., Lawrence, G.B., McDonnell, J.J., and Wolock, D.M. 2002. Estimation of baseflow residence times in watersheds from the runoff hydrograph recession: method and application in the Neversink watershed, Catskill Mountains, New York. *Hydrol. Process.* 16:1871–1877.

Zecharias, Y., and Brutsaert, W. 1988. Recession characteristics of groundwater outflow and base flow from mountainous watersheds. *Water Resour. Res.,* 24 (10):1651-1658.

CHAPTER I

Baseflow Recession Analysis in the Inland Pacific Northwest, USA

R. Sánchez-Murillo, E. S. Brooks, W. J. Elliot W.J, E. Gazel, and J. Boll.

In review. Submitted to Hydrogeology Journal on April 4th, 2014.

Abstract

This study analyzed storage-discharge relationships of 26 watersheds in the inland Pacific Northwest of the United States, specifically in the inter-mountainous region of eastern Washington and central and northern Idaho. Four fitting methods were used to obtain the baseflow coefficients: lower envelope, organic correlation, and ordinary and inverse least squares. Several climatic and terrain attributes were evaluated as potential predictors of baseflow coefficients and minimum annual storage. Watersheds dominated by basalt and flatter landscapes exhibited the smallest characteristic recession time scales (*K*) (12.5-20 days). Greater *K* values (33-67 days) were obtained over catchments dominated by metamorphic and sedimentary underlying geology and steeper mean basin slopes. Overall, mean *K* corresponded to 33±15 days with extremes of 12.5 and 67 days. The mean basin slope and the aridity index were found to be the best estimators of baseflow coefficients. Baseflow contributions in relatively flat basalt landscapes located in dry, warm climates, such as those found in lower elevations of eastern Washington and northern Idaho, decrease rapidly during summer months and are most sensitive to potential future droughts and warming climates. Groundwater systems feeding streams during the driest months can drop to less than 1 mm of effective storage in these sensitive systems. In contrast the minimum annual storage amount in steep, high elevation systems, in cooler climates can have greater than 10 mm effective

storage, and are likely more resilient to climate change. The baseflow recession characteristics provided in this study will enhance physically-based modeling by reducing the use of trial and error approach to calibrate baseflow or deep percolation coefficients. By understanding the main factors controlling baseflow periods and their recession characteristics, land managers and environmental agencies could prioritize efforts and resources in areas where potential future droughts and land use changes may drastically affect ecological assemblages and socio-economic activities.

Keywords: Baseflow recession analysis; storage; geology; climate; watershed management.

1. Introduction

Climate change is anticipated to increase evaporation and precipitation across the globe resulting in an intensification or acceleration of the water cycle in the coming decades (DelGenio et al., 1991; Nijssen et al., 2001; Huntington, 2006, Durack et al., 2012), which may significantly alter the magnitude and timing of streamflow regimes (Tang and Lettenmaier, 2012; Döll and Zhang, 2010; Döll and Schmied, 2012; Arnell and Gosling, 2013). Consequently, international efforts (e.g. International Flood Initiative, http://www.ifi-home.info/) and government attention has been geared to prevent and mitigate the effects of extreme flood events (Plate, 2002), especially in developing countries. A broad spectrum of human activities (e.g. food production, drinking water, and transportation) and ecological assemblages (e.g. habitat volume for aquatic biota, biochemistry and thermal regimes) rely on sustained baseflow conditions. Despite its importance, however, current understanding of future impacts on long-term groundwater storage and baseflow regimes is limited (Dams et al., 2012; Brutsaert, 2012).

Baseflow is described as the cumulative outflow from all upstream riparian aquifers during rainless periods, in the absence of snowmelt or any other hydrologic inputs (Brutsaert, 2005). Changes in groundwater storage and baseflow discharge constitute a critical component of any ecosystem. For example, baseflow plays an important role in regulating stream chemistry, water temperature, dissolved oxygen during critical summer months, and provides continuous habitat volume to endangered aquatic species in temperate regions (Sánchez-Murillo et al., 2013). Furthermore, information of baseflow characteristics and groundwater storage is important for decision making related to effective allocation of resources, water quality standard assessments and regulations, and prioritization of water conservation efforts in areas of accelerated potential future droughts or population growth.

The Pacific Northwest of the United States (PNW) has been recognized as a particularly sensitive region to climate variability (Miles et al., 2000; Elsner et al., 2010). Since the 1940s, a decreasing trend in snow water equivalent has been

observed while water consumption has increased (Mote, 2003; Stewart et al., 2005; McCabe et al., 2005; Van Kirk and Naman, 2008). Overall, a consensus exists that snow-dominated watersheds within the PNW will potentially experience spring runoff episodes up to four weeks earlier. Future climate scenarios for the PNW (Mote and Salathé, 2010) project a warming of 0.1°C to 0.6°C per decade. Mayer (2012) found that baseflow is one of the major factors controlling summer thermal regimes across the region with a mean sensitivity of 0.47°C (stream)/°C (air). Hence, one immediate consequence of increasing temperatures may be the disruption of stream thermal regimes throughout the summer, indicating a need to improve our understanding of how seasonal variability in baseflow impacts stream environments.

Over the last half century the PNW has been experiencing declines in summer baseflow. Clark (2010) found a decrease of 25% in daily minimum streamflow across Idaho, western Wyoming, and northern Nevada. Luce and Holden (2009) examined 43 stream stations throughout the PNW and found a significant decline in the 25th percentile of annual flow in 72% of the stations. Half the stream stations showed a 29% decline in the 25th percentile of flow between 1948 and 2006 with records from one station indicating a 47% drop. Leppi et al. (2012) examined 50 year records from 153 stream stations in the Central Rocky Mountain Region and found declining trends in the mean monthly flow in August in 89% of the stations. Fu et al. (2010) noted similar differences in mean annual flow at 35 stations in Washington State. Understanding long-term patterns of baseflow recession emerges as a fundamental mission. It is essential that new methods are developed to support future decisions responding to how accelerated population growth and climate variability and impact alter water distribution systems in the PNW and elsewhere (Milly et al., 2005; Hungtington, 2006; Bates et al., 2008; Zhou et al., 2011).

In this study we analyzed the storage-discharge relationships across 26 watersheds in the inland PNW with a variety of basin areas, geologic formations, land uses, and temperature and precipitation gradients. We present a modified methodology for baseflow analysis applicable for steep and flat landscapes. To our knowledge a comprehensive baseflow recession analysis has not yet been conducted for the inland PNW. The specific objectives were: *a)* to evaluate the main

terrain characteristics controlling the natural release of water as baseflow; *b)* to estimate the role that climate plays in the baseflow recession process; and *c)* to determine the regional variability of the *K* and minimum annual storage across the inland PNW.

1.1 Baseflow recession analyses methods

Generally, baseflow is examined using low frequency analysis such as $Q_{7,10}$ (i.e. 7-day, 10-year return period discharge) (Vogel and Kroll, 1992; Brandes et al., 2005), baseflow indices (Wolock, 2003; Bloomfield et al., 2009), and recession analysis methods (Tallaksen, 1995). Detailed reviews of recession analysis have been reported elsewhere (Hall, 1968; Wittenberg, 1999; Smakhtin, 2001; Kirchner, 2009; Price, 2011). To overcome the uncertainties involved in defining the time at which the recession begins, Brutsaert and Nieber (1977) proposed a method to parameterize a storage-discharge relationship based on the Boussinesq equation (i.e. flow from an unconfined horizontal aquifer,) (Supplemental Fig. 1). This method consists of plotting the decline in discharge ($-dQ/dt$) [L T^{-2}] versus average discharge (Q) [L T^{-1}] (Eq. 1, Fig. 1). The main advantage of representing the recession curve in the form shown in Eq.1 is the elimination of time as a dependent variable, thus, it is unnecessary to select the precise beginning of the recession.

$$-\frac{dQ}{dt} = f(Q) \quad (1)$$

where *f* is a characteristic function for a given watershed and *Q* [L/T] is streamflow. When using actual discharge data, Eq. 1 can be expressed as follows:

$$\left(\frac{Q_i - Q_{i-1}}{\Delta t}\right) = f\left(\frac{Q_i + Q_{i+1}}{2}\right) \quad (2)$$

where the subscript *i* represents a counter in the discharge time series. Change in underground water storage in a particular watershed over a period of time is described by the conservation of mass equation:

$$\frac{dS}{dt} = P - ET - Q - L \ (3)$$

where *S* [L] is the volume of water stored in the watershed, *P* [LT^{-1}] is precipitation, *ET* [LT^{-1}] is evapotranspiration, *Q* [LT^{-1}] is discharge, and *L* [LT^{-1}] is deep percolation loss. In the absence of aquifer recharge during the late summer, when *P*, *ET*, and *L* are negligible, baseflow dominates stream discharge and Eq. (3) can be written as:

$$\frac{dS}{dt} = -Q \ (4)$$

Linear reservoir theory assumes that outflow *Q* from the bedrock or riparian aquifer is linearly dependent on the storage *S* (Tallaksen, 1995):

$$Q = aS \ (5)$$

where *a* is a constant [T^{-1}]. Substituting Eq. (5) into Eq. (4), the mass balance equation yields a power law relationship between *–dQ/dt* and discharge *Q*:

$$-\frac{dQ}{dt} = aQ^b \ (6)$$

where *b* is an exponent; *b=1* yields the linear reservoir special case. One of the advantages of representing the recession process in a power form such as Eq.6 is that three well known analytical solutions (Table 1) to the Boussinesq equation for an unconfined horizontal aquifer can be also expressed in a power form where coefficient *a* is a function of the hydraulic properties of the system.

Equation 6 can be also log-transformed to:

$$\log(-dQ/dt) = \log(a) + b\ log(Q) \ (7)$$

In the method of Brutsaert and Nieber (1977), when plotting the decline in discharge (*–dQ/dt*) [LT^{-2}] versus average discharge (*Q*) [$L\ T^{-1}$] on a log-log scale a natural cloud of data points is obtained, where the lower envelope represents the lowest *dQ/dt* for a given *Q* (Fig. 1). The lower envelope can be analyzed using three fixed slopes *b* equal to 1, 1.5, and 3 (Brutsaert and Lopez, 1998). A slope of 1 represents a linearized outflow from a rectangular aquifer into a fully penetrated channel. A slope of 1.5 describes a situation in which the shape of the water table remains curvilinear for a long time. Finally, a slope of 3 describes a high flow

scenario based on the assumption that the aquifer boundary at the divide stays infinitely distant from the channel (Shaw and Riha, 2012). Others (Wittenberg, 1994, 1999; Wittenberg and Sivapalan, 1999; Aksoy and Wittenberg, 2011) have found from an analysis of more than 80 river gauging stations in Germany a widespread non-linear relationship with an exponent $b < 1$.

The selection of the exact lower envelope position has also been a matter of discussion (Ajami et al., 2011; Stoelzle et al., 2012), because there is some degree of subjectivity or uncertainty related with this procedure. Kirchner (2009) suggested estimating the central tendency of $-dQ/dt$ instead of the lower envelope as a better average descriptor of a watershed's natural behavior. Several fitting techniques have been used to estimate the baseflow coefficients (i.e. a and b) from linear regression models (Brutsaert and Lopez, 1998) to binning means (Parlange et al., 2001; Kirchner 2009; Palmroth et al., 2010), and mean relative errors (Peña-Arancibia et al., 2010; van Dijk, 2010). Rupp and Selker (2006) reported that the lower envelope may be affected by precision and noise in the streamflow data causing scattering and discretization at low flows. These two factors, illustrated by the horizontal artifacts when plotting $-dQ/dt$ versus average discharge Q (Fig. 2), may lead to misinterpretation of the recession phenomena.

Despite the variety of approaches used to determine the baseflow coefficients, the Brutsaert and Nieber (1977) method has been successfully used to determine basin-scale effective groundwater parameters (i.e. aquifer thickness, hydraulic conductivity, drainage porosity) (Zecharias and Brutsaert, 1988; Troch et al., 1993; Brutsaert and Lopez, 1998; Szilagyi et al., 1998; Mendoza et al., 2003); mountain block recharge (Ajami et al., 2011), human influences on baseflow (Wittenberg, 2003; Wang and Cai, 2009, 2010 a,b), and long-term minimum annual storage trends (Brutsaert, 2008, 2012; Brutsaert and Sugita, 2008). The latter application provides meaningful information to evaluate water management under changing climate conditions and may be a potential tool to estimate water availability in ungauged basins.

The minimum annual storage in a particular basin can be evaluated as:

$$S = Ky \quad (8)$$

where $y=Q/A$ is the rate of flow per unit of drainage area [LT^{-1}] and K (i.e. a^{-1}, see Eq. 5) is the characteristic recession time scale [T]. Brutsaert (2012) reported the annual lowest seven-day daily mean flow (i.e., y_{L7}) as a plausible measure to evaluate the minimum annual basin storage. Additionally, several studies (Brutsaert 2008, 2010, 2012; Brutsaert and Sugita, 2008) have found on average a K of 45±15 days for large basins (i.e. >100 km^2). Brutsaert and Lopez (1998) found a mean K of 31.6 days for 22 subbasins in the southern Great Plains of the United States with extremes of 12.5 and 66.5 days.

2. Methodology

2.1. Data selection and watersheds characteristics

Long-term daily discharge and precipitation records were obtained for 26 watersheds throughout eastern Washington and central and northern Idaho (Fig. 3, Table 2) from the United States Geological Survey National Water Information System (USGS, http://waterdata.usgs.gov/usa/nwis/rt) and the National Oceanic and Atmospheric Administration (NOAA, National Climate Data Center, http://www.ncdc.noaa.gov/cdo-web/), respectively. In selecting the watersheds, we avoided hydrological alterations such as dams, reservoirs, irrigation, and return flows. Therefore, most of watersheds represent near-natural conditions corresponding to inter-mountainous forested or semi-arid areas. Daily streamflow records were normalized to unit area discharge [$L\ T^{-1}$].

Several geomorphic and climatic attributes were determined for each watershed (Table 2) based on Digital Elevation Models (30 x 30 m, Seamless, USGS) and the Parameter-Elevation Regressions on Independent Slopes Model (PRISM, Climate Group, USA) using ArcGIS version 9.3.1. (ESRI, USA). The study watersheds cover a wide range of climate gradients and terrain characteristics. A detailed summary of main underlying geology in each watershed is presented in Table 3 and Fig. 4.

2.2. Recession extraction and analysis

To ensure comparability of the recession analysis, several procedures were applied according to the Brutsaert and Nieber (1997) method. Data points within a recession period were extracted in accordance with the following steps: *i)* positive or zero *dQ/dt* values were eliminated; *ii)* $-dQ/dt$ values were only considered after 3 days of any precipitation event, to avoid the influence of surface flows; *iii)* days with recorded precipitation were excluded; *iv)* due to precision errors at low flows, a trial and error threshold was applied ($1-Q_{i+n}/Q_i>0.1$) to avoid horizontal artifacts, where Q_i is the initial discharge and Q_{i+n} is the discharge corresponding to the selected time step (*dt*).

Four fitting methods were used to obtain the recession intercepts and slopes: *i)* lower envelope (LE) with a fixed slope $b=1$; *ii)* organic correlation (OC); *iii)* ordinary least squares (OLS); and *iv)* inverse least squares (ILS) (See Appendix A for fitting method details). The intercept *a* can be seen as an indicator of storage volume whereas slope *b* is usually linked to the rate and dynamic of the recession process (Stoelzle et al., 2012). Variation in minimum annual storage *S* [L] was conducted using Eq. 8 (Brutsaert, 2008) where the y_{L7} is used as a reasonable measure of minimum baseflow conditions. Minimum annual storage was computed using an average characteristic drainage timescale of 45 days (*K*) (Brutsaert, 2012) and *K* values calculated for each watershed using the lower envelope method (See supplementary Table S1).

Statistically significant differences for intercepts, slopes, characteristic recession timescales, and minimum annual storage were evaluated using Tukey's multiple comparison procedure. Tukey's procedure is more conservative than the commonly used Least Significance Difference (LSD) or Student-Newman-Keuls (SNK) methods, thus, declares fewer significant differences among *t* population means (Ott and Longnecker, 2008).

2.3. Regression analyses

Pearson's product moment correlation coefficient, including statistical significance, was calculated between baseflow coefficients, geomorphic parameters, and climatic attributes. Regression modeling between the remaining catchment attributes and baseflow coefficients was conducted to select the best individual predictor for intercept *a*, slope *b*, and minimum annual storage *S*. Multiple regression models were excluded based on the premise that commonly these types of models tend to duplicate or replicate data points rather than finding a predictor that can be potentially linked to a physically-based process. A correlation matrix per individual fitting method is presented in Supplementary Table S2.

3. Results

3.1. Estimation of baseflow recession characteristics

The overall mean intercept *a* (i.e. lower envelope, b=1) for the 26 watersheds analyzed was 0.037 ± 0.016 (1σ) d^{-1} with extremes ranging from 0.015 up to 0.08 d^{-1} (Fig. 5a). Intercepts *a* calculated from other fitting methods (where slopes are greater than 1) are presented in Fig.5a, intercept a units are represented as mm1-bd All distributions were positively skewed for intercepts *a*. Greater intercepts were found in steeper and forested catchments and lower values in flatter semi-arid catchments. Slopes *b* varied from 0.823 up to 1.541 with a mean of 1.178 ± 0.129 (1σ) (Fig. 5b). Distribution of slope *b* from OLS was negatively skewed. Values of *b* from OLS and ILS were found to be significantly different ($p < 0.001$).

The characteristic recession time scales *K* (i.e. lower envelope) were fairly variable with extremes ranging from 12.5 days up to 67 days. Mean *K* value was 33 ± 15 days (1σ). The minimum annual storage ranged from less than 0.1 mm up to 15.9 mm. An additional minimum annual storage condition was analyzed using a *K* value

of 45 days as proposed by Brutsaert (2008), resulting in a greater median storage of 7.4 mm.

Faster recessions and lower minimum annual storage values were found in flatter and semi-arid catchments dominated by basalt features and eolian-originated soils (e.g. Asotin Creek, Union Flat Creek, and South Fork Palouse River). Longer recessions and greater storage were found consistently where granitic, metamorphic or sedimentary rock composition is the dominant underlying geology (e.g. Crumarine Creek, Pine Creek, Mica Creek, and Saint Maries River). These catchments are also characterized by greater mean basin slopes. Individual log-log scatter plots $-dQ/dt$ versus average Q including all four fitting methods are shown in Fig. 6. The natural spectrum of data points observed is largely the result of non-uniform distribution of characteristics across the watersheds and the evolution of the recession process from faster depletion in surface runoff (i.e. upper envelope) to lower rates of depletion from the gentler parts of the aquifer (i.e. lower envelope). Interestingly, the intercept a_3 calculated with a fixed slope $b=3$ exhibited a strong power regression with drainage area (r^2=0.74) (Fig. 7) and total stream length (r^2=0.67, not shown in Fig. 7). High variability in a_3 was observed for drainage areas less than 1,116 km^2 whereas more predictable values were found as area increases. The power exponent (a_3=10*A$^{-2.16}$) is close to the theoretical value of −2 described by Brutsaert and Lopez (1998). This shows that a_3 may be used as an alternative predictor of scale dependent hydraulic parameters such as hydraulic conductivity and drainable porosity (Table 1).

3.2. Climatic and terrain relationships

In general, baseflow coefficients were poorly correlated with catchment scale parameters such as drainage area, perennial stream length, drainage density, and total relief (See Supplementary Table S2). Intercept a was weakly correlated with drainage area for all fitting models (− 0.26 to 0.09). For the lower envelope method, the best individual regression (r^2=0.33) was assessed with mean basin slope as a

single predictor of intercept *a* (Fig. 8a). The minimum annual storage was strongly correlated with mean basin slope. The power regression (r^2=0.73) between minimum annual storage versus mean basin slope is shown in Figure 8b. The characteristic recession timescale *K* shows a similar pattern of correlation found with intercept *a* where the best correlation is linked to the mean basin slope, however, due to their high collinearity; *K* was not used in the regression analysis. Brutsaert's approach using a constant *K* of 45 days to calculate storage for watersheds with area greater than 100 km^2 tends to overestimate the minimum annual storage in comparison with the fitting methods.

The aridity index (i.e. AI = Mean Annual Precipitation/Potential Evapotranspiration) ranged from 1.09 up to 2.70. A moderate power regression (a_{LE}=0.051$AI^{-0.89}$; r^2=0.30) was found between intercept *a* and the aridity index (Fig. 9) Semi-arid watersheds with greater ET exhibited lower aridity index values, therefore, lower recession timescales. Forested areas with greater mean annual precipitation and lower ET tend to have longer recession depletions and greater minimum annual storage. This is similar to a relationship reported by Arancibia et al. (2010) in a study of 167 subtropical and tropical watersheds.

4. Discussion

As baseflow will likely continue to decrease in the coming century, understanding the processes that impact baseflow at catchment scales and over a range of climate gradients and land use scenarios can inform management of the ecosystem services that society and nature derive from watersheds. This study analyzed a wide range of storage-discharge relationships to attempt a regionalized baseflow characterization in the inland Pacific Northwest that can be translated to ungauged basins sharing similar climate and underlying geological features.

Consistently, no significant relationship was found between drainage area and baseflow coefficients *a* and *b.* Similar findings have been reported elsewhere (Lacey and Grayson, 1998; Peña-Arancibia et al., 2010; Price, 2011; Stoelzle et al., 2012). Generally, small intercepts were associated with longer characteristic recession times

and larger minimum annual storage. Catchments with underlying basalt tended to be drier, had flatter slopes, and exhibited shorter recession times and lower storages values. These watersheds are also characterized by a lower aridity index (i.e. lower P and greater ET) that may accelerate the rate of recession. The potential for increased ET with warming climates could lead to even higher recession depletions in these areas where food production is an essential activity. Forested areas resulted in longer recession times and greater minimum storage. These near-natural forested areas, mainly underlain by granitic, metamorphic, and sedimentary features, with lower hydraulic conductivity relative to fractured basalt, may play a significant role in the groundwater storage and baseflow contributions (Fig. 10). Additionally, the mean basin slope appeared to be the best estimator of intercept *a* in a power function followed by the climatic aridity index. This could potentially be used to characterize baseflow conditions in ungauged basins across the inland Pacific Northwest.

Several authors have identified that the variability of slope *b* could bring useful information about aquifer behavior. In this study, watersheds located in eastern Washington and western Idaho dominated by flatter landscapes, shallow eolian-originated soils, and basalt geology exhibited a predominant linear behavior. In contrast, watersheds in northern and east-central Idaho dominated by steeper forested terrains resulted in greater slopes that may be a result of more active channel storage and lateral flow pathways. Overall, slope *b* was in the range of literature values (Brutsaert and Lopez, 1998; Palmroth et al. 2010; Biswal and Marani, 2010; Wang, 2011; Shaw and Riha, 2012). Since the values of *b* evolve and denote distinct stages of the recession phenomena, when analyzed as individual recession events (Shaw and Riha, 2012), an analysis of all recession events might mask other relationships with geomorphic characteristics of the riparian aquifers that do not emerge at the watershed scale.

Probably, the most useful application of knowing the characteristic recession timescale of any catchment is the estimation of storage conditions. It is well known that long-term records of groundwater storage are scarce within the inland Pacific Northwest and over many regions of the world; therefore, estimation of minimum annual storage becomes critical for noteworthy diagnoses of water availability under

different land use and climate change scenarios. This analysis suggested that watersheds located in eastern Washington and north-western Idaho due to a combination of several factors such as flatter basalt landscapes, low precipitation and high ET rate could confront even lower recession times and less than 1 mm of minimum annual storage in several water catchments (Fig. 5). Lower storage can result in decreased summer flows that with the same pollutant inputs could lead to declining water quality, recreation opportunities, and availability of ecological habitat for endangered species such salmonids. Additionally, forested areas of northern and eastern Idaho characteristically have longer recession times and greater minimum annual storage volumes with S values greater than 20 mm.

5. Conclusions

Baseflow recession characteristics and their relationship to landscape, geomorphic, and climatic attributes have been a matter of debate among the hydrology community for several decades. Despite this debate, the spatial heterogeneity and intrinsic complexity of baseflow processes have turned the attention of researchers to *a)* physically-based efforts that permit the parameterization of hydraulic parameters over meso (10^2 km^2) and large (10^3 km^2) catchment areas and *b)* regional analyses that provide a systematic perspective of water sustainability (i.e. surface and groundwater resources) for the upcoming decades. For the inland Pacific Northwest, water managers, understanding how the combination of potential greater ET, earlier spring runoff, and prolonged droughts will affect baseflow regimes has become an imperative.

The long term trend of declining summer baseflow in the PNW and the threat of continued and potentially more significant declines in the future due to climate change depicts future hydro-climate scenarios that may translate in severe consequences to *i)* the demand for groundwater for food production, electricity generation, clean drinking water, and recreation. This increase in demand may lead to individual and inter-state water rights debates, and disruption of ecological

attributes (e.g. high water temperatures, low dissolved oxygen concentrations) during summer flows that are critical to many ecosystems such as steelhead/salmon rearing habitats.

Our findings indicate that baseflow coefficients are not strongly related with drainage scale. The most significant parameter controlling the natural release of water as baseflow resulted to be the mean basin slope. The climatic aridity index also could be a useful estimator of baseflow parameters; however, a better understanding of potential changes in precipitation regimes and air temperature is needed. Our findings suggest that watersheds located in eastern Washington and northwestern Idaho due to a combination of several factor such as flatter basalt landscapes, low precipitation, and high ET rates could experience even lower recession times and less than 1 mm of minimum annual storage.

The baseflow recession characteristics provided in this study may enhance physically-based modeling by reducing the use of trial and error approach to calibrate baseflow or deep percolation conditions. By knowing baseflow characteristics such as minimum annual storage and recession timescales, land managers and environmental agencies could prioritize efforts and resources in areas where potential future droughts may drastically affect overall ecosystems services.

6. Acknowledgments

This project was funded by the joint venture agreement (No. 10-JV-11221634-252) between USDA-Forest Service Rocky Mountain Research Station) and the University of Idaho. The authors thank the insights and useful comments from two anonymous reviewers.

7. Fitting methods additional information

To estimate the baseflow coefficients (i.e. *a* and *b*) four different fitting methods were used: lower envelope, the organic correlation technique (Eq. A1 and A2), ordinary (Eq. A3, A4) and inverse (A5, A6) least square estimation. The organic

correlation technique (Hirsch and Gilroy, 1984) minimizes the sum of the squared geometric means of the distances in both the vertical and horizontal directions. This technique is not suited for minimizing estimation errors, but is most applicable for establishing equivalence between (*Q*) and (*dQ/dt*).

$$\alpha = \left[average\left(\frac{dQ}{dt}\right) - average(Q)\right] * sign[correl\left(Q, \frac{dQ}{dt}\right)] * \frac{StdevP\left(\frac{dQ}{dt}\right)}{StdevP(Q)} \quad (A1)$$

$$b = sign\left[correl\left(Q, \frac{dQ}{dt}\right)\right] * \frac{StdevP(\frac{dQ}{dt})}{StdevP(Q)} \quad (A2)$$

$$\alpha = \left[average\left(\frac{dQ}{dt}\right) - average(Q)\right] * correl\left(Q, \frac{dQ}{dt}\right) * \frac{StdevP\left(\frac{dQ}{dt}\right)}{StdevP(Q)} \quad (A3)$$

$$b = correl\left(Q, \frac{dQ}{dt}\right) * \frac{StdevP(\frac{dQ}{dt})}{StdevP(Q)} \quad (A4)$$

$$\alpha = \left[average\left(\frac{dQ}{dt}\right) - average(Q)\right] / correl\left(Q, \frac{dQ}{dt}\right) * \frac{StdevP\left(\frac{dQ}{dt}\right)}{StdevP(Q)} \quad (A5)$$

$$b = StdevP(\frac{dQ}{dt}) / correl\left(Q, \frac{dQ}{dt}\right) / StdevP(Q) \quad (A6)$$

8. References

Ajami H., Troch P., Maddock T., Meixner T., Eastoe C. 2011. Quatifying mountain block recharge by means of catchment-scale storage-disccharge relationships. *Water Resources Research*, 47, W04504, doi:10.1029/2010WR009598.

Aksoy H., Wittenberg H. 2011. Nonlinear baseflow recession analysis in watersheds with intermittent streamflow. *Hydrological Sciences*, 56:2, 226–237. http://dx.doi.org/10.1080/02626667.2011.553614.

Arnell N.W., Gosling S.N. 2013. The impacts of climate change on river flow regimes at the global scale. *Hydrology*, 486: 351–364.

Bates, B.C., Kundzewicz, Z.W., Wu, S., Palutikof, J.P. 2008. Climate change and water. Technical Paper of the Intergovernmental Panel on Climate Change, IPCC Secretariat, Geneva, 210 pp.

Biswa, B. and Marani, M. 2010. Geomorphological origin of recession curves. Geophys. Res. Lett., 37 L24403, doi: 10.1029/2010GL045415.

Brandes D., Hoffman J., Mangarillo J.T. 2005. Baseflow recession rates, low flows, and hydrologic features of small watersheds in Pennsylvania, USA. *Journal of the American Water Resources Association*, 41(5):1177–1186.

Bloomfield J.P., Allen D.J., and Griffiths K.J. 2009. Examining geological controls on baseflow index (BFI) using regression analysis: an illustration from the Thames Basin, Uk. *Hydrology*, 373:164–176.

Brutsaert, W., and Nieber, J. 1977. Regionalized drought flow hydrographs from a mature glaciated plateau. *Water Resour. Res.,* 13 (3):637–643.

Brutsaert, W., and Lopez, J.P. 1998. Basin-scale geohydrologic drought flow features of riparian aquifers in the southern Great Plains. *Water Resour. Res.,* 34 (2), 233–240.

Brutsaert, W. 2005. Hydrology: an introduction. Cambridge University Press. Cambrigde, United Kingdom. 605 pp.

Brutsaert, W. and Sugita, M. 2008. Is Mongolia's groundwater increasing or decreasing? The case of the Kherlen River basin. *Hydrol. Sci.,* 53, 1221–1229, 2008.

Brutsaert W. 2008. Long-term groundwater storage trends estimated from streamflow records: climatic perspective. *Water Resources Research,* 44, W022409, doi:10.1029/2007WR006518.

Brutsaert W. 2010. Annual drought flow and groundwater storage trends in the eastern half of the United States during the past two-third century. *Theoretical and Applied Climatology*, 100: 93–103. doi: 10.1007/s00704-009-0180-3.

Brutsaert W. 2012. Are the North American deserts expanding? Some climate signals from groundwater storage conditions. Ecohydrology, 5, 541–549, doi: 10.1002/eco.263.

Boussinesq, J. 1903. Sur le débit, en temps de sécheresse, d´ une source alimentée par une nappe d´eaux infiltration. C. R. Hebd. Seanc. Acad. Sci., 136:1511–1517.

Boussinesq, J. 1904. Recherches theories sur l´écoulement des nappes d´eau

infiltrées dans le sol et sur débit sources. *J. Math. Pures Appl*., 10:5–78.

Clark, G.M. 2010. Changes in patterns of streamflow from unregulated watersheds in Idaho, Western Wyoming, and Northern Nevada. Journal of the American Water Resources Association, 46 (3):486–497.

Dams J., Salvadore E., Van Daele T., Ntegeka V., Willems P., Batelaan O. 2012. Spatio-temporal impact of climate change on the groundwater system. Hydrol. Earth Syst. Sci., 16: 1517–1531.

DelGenio, A.D., Lacis, A.A., Ruedy, R.A., 1991. Simulations of the effect of a warmer climate on atmospheric humidity. *Nature,* 351:382–385.

Döll, P., Zhang, J., 2010. Impact of climate change on freshwater ecosystems: a global-scale analysis of ecologically relevant river flow alterations. *Hydrol. Earth Syst. Sci.,* 14 (5):783–799.

Döll, P., Müller Schmied, H. 2012. How is the impact of climate change on river flow regimes related to the impact on mean annual runoff? A global-scale analysis. *Environ. Res. Lett.,* 7 (1). http://dx.doi.org/10.1088/1748-9326/7/1/014037.

Durack P., Wijffels S.E., Matear R.J. 2012. Ocean salinities reveal strong global water cycle intensification during 1950 to 2000. *Science,* 336: 455–458. DOI: 10.1126/science.1212222

Elsner M.M., Cuo L., Voisin N., Deems J.S., Hamlet A.F., Vano J.A., Mickelson K., Lee S., Lettenmaier D.P. 2010. Implications of 21st century climate change for the hydrology of Washington State. *Climatic Change,* 102: 225–260 DOI 10.1007/s10584-010-9855-0

Fu G., Barber M.E., Chen S. 2010. Hydro-climatic variability and trends in Washington State for the last 50 years. *Hydrological processes*, 24 (7):866–878.

Hall F.R. 1968. Base-flow recession. A review. *Water Resources Research,* 4(5):973–983.

Hirsch, R.M. and E.J. Gilroy. 1984. Methods of fitting a straight line to data: Examples in water resources, *Water Resour. Bull*., 20:705–711.

Huntington T.G. 2006. Evidence for intensification of the global water cycle: review and synthesis. Hydrology, 319: 83–95.

Kirchner, J.W. 2009. Catchments as simple dynamical systems: Catchment characterization, rainfall-runoff modeling, and doing hydrology backward. *Water Res. Research,* 45:1-34. W02429, doi:10.1029/2008WR006912

Lacey, G.C. and Grayson, R.B. 1998. Relating baseflow to catchment properties in south-eastern Australia. *Hydrology,* 204: 231-250.

Leppi J.C., DeLuca T.H., Harrar S.W., and Running S.W. 2012. Impacts of climate change on August stream discharge in the Central-Rocky Mountains. *Climatic Change*, 112:997–1014 Doi 10.1007/s10584-011-0235-1.

Luce C.H., and Holden Z.A. 2009. Declining annual streamflow distributions in the Pacific Northwest United States, 1948–2006. *Geophysical Research Letters*, 36, L16401, doi:10.1029/2009GL039407.

Mayer T.D. 2012. Controls of summer stream temperature in the Pacific Northwest. Hydrology, 475: 323–335.

McCabe, G.J., and Clark, M.P. 2005. Trends and variability in snowmelt runoff in the Western United States. *Hydrometeorology,* 6 (4):476-482.

Mendoza, G.F., Steenhuis, T. S., Walter M. T., and Parlange, J.Y. 2003. Estimating basin-wide hydraulic parameters of a semi-arid mountainous watershed by recession-flow analysis. *Hydrology,* 279:57–69.

Miles E.L. Snover A.K., Hamlet A.F., Callahan B., Fluharty, D. 2000. Pacific Northwest Regional Assessment: The impacts of climate variability and climate change on the water resources of the Columbia River Basin. *American Water Resources Association*, 36 (2): 399-420.

Milly, P.C.D., Dunne, K.A., and Vecchia, A.V. 2005. Global pattern of trends in streamflow and water availability in a changing climate. Nature letters, 438:347-350.

Mote P. W. 2003. Trends in snow water equivalent in the Pacific Northwest and their climatic causes. *Geophys. Res. Lett.,* 30:1601, doi:10.1029/2003GL017258.

Mote P.W., and Salathé E.P. 2010. Future climate in the Pacific Northwest. Climatic Change. DOI 10.1007/s10584-010-9848-z

Nijssen B., O'Donnell G.M., Hamlet A.F., Lettenmaier D.P. 2001. Hydrologic sensitivity of global rivers to climate change. *Climatic Change* 50: 143–175.

Ott R., and Longnecker M. 2008. An introduction to statistical methods and data analysis. Brooks/Cole, Cengage Learning. Canada. 1280 pp.

Pale E.J. 2002. Flood risk and flood management. *Hydrology,* 267: 2–11.

Palmroth, S., Katul, G. G., Hui, D., McCarthy, H. R., Jackson, R. B., and Oren, R. 2010. Estimation of long-term basin scale evapotranspiration from streamflow time series. *Water Resour. Res.,* 46, W10512, doi:10.1029/2009WR008838.

Peña-Arancibia, J.L., van Dijk, A.I.J.M., Mulligen, M., and Bruijzeel, L.A. 2010. The role of climatic and terrain attributes in estimating baseflow recession in tropical catchments. *Hydrol. Earth Syst. Sci. Discuss.,* 7:4059-4087.

Parlange, J., Stagnitti, F., Heilig, A., Szilagyi, J., Parlange, M., Steenhuis, T., Hogarth, W., Barry, D., and Li, L.: Sudden drawdown and drainage of a horizontal aquifer. Water Resour. Res., 37, 2097–2101, 2001.

Polubarinova-Kochina, P.Y. 1962. Theory of groundwater movement. Princeton University Press, Princeton, N.J.

Price K. 2011. Effects of watershed topography, soils, land use, and climate on baseflow hydrology in humid regions: A review. Progress in Physical Geography, 35(4): 465-492.

Plate E. 2002. Flood risk and flood management. *Hydrology*, 267:2-11, http://dx.doi.org/10.1016/S0022-1694(02)00135-X

Rupp, D. E., and Selker, J.S. 2006. Information, artifacts, and noise in *dQ/dt-Q* recession analysis. *Advances in Water Resources,* 29:154-160.

Rupp, D.E., Schmidt, J., Woods, R. A., Vincent, J.B. 2009. Analytical assessment and parameter estimation of a low-dimensional groundwater model. *Hydrology,* 377:143-154.

Sánchez-Murillo, R., Brooks E.S., Sampson L., Boll J., Wilhelm F. 2013. Ecohydrological analysis of Steelhead (Oncorhynchus mykiss) habitat in an effluent dependent stream in the Pacific Northwest, USA. Ecohydrology, doi: 10.1002/eco.1376

Shaw, S.B., and Riha, S.J. 2012. Examining individual recession events instead of a data cloud: Using a modified interpretation of dQ/dt–Q streamflow recession in glaciated watersheds to better inform models of low flow. Hydrology, 434-435: 46-54, http://dx.doi.org/10.1016/j.jhydrol.2012.02.034

Smakhtin, V. U. 2001. Low flow hydrology: a review. *Hydrology,* 240:147–186.
Stewart, I.T., Cayan, D.R., and Dettinger, M.D. 2005. Changes toward earlier streamflow timing across Western North America. *Climate*, 18:1136-1155.

Stoelzle, M., Stahl, K., and Weiler, M. 2012. Are streamflow recession characteristics really characteristic? Hydrol. Earth Syst. Sci., 9, 10563–10593, doi:10.5194/hessd-9-10563-2012

Szilagyi J., Parlange M.B., and Albertson J.D. 1998. Recession flow analysis for aquifer parameter determination. Water Resources Research, 34(7): 1851-1857.

Tallaksen, L. M. 1995. A review of baseflow recession analysis. Hydrology, 165: 349–370.

Tang, Q.H., Lettenmaier D.P. 2012. 21st century runoff sensitivities of major global river basins. *Geophys. Res. Lett.,* 39: L06403. http://dx.doi.org/10.1029/2011gl050834.

Troch, P., De Troch, F., and Brutsaert, W. 1993. Effective water table depth to describe initial conditions prior to storm rainfall in humid regions. *Water Res. Research*, 29 (02):427-434.

van Dijk., A.I.J.M. 2010. Climate and terrain factors explaining streamflow response and recession in Australian catchments. *Hydrol. Earth Syst. Sci. Discuss.,* 14:159-169.

van Kirk R.W., and Naman S.W. 2008. Relative effects of climate and water use on base-flow trends in the lower Klamath basin. *American Water Resources Association,* 44(4): 1032-1052.

Vogel R.M., and Kroll C.N. 1992. Regional geohydrologic-geomorphic relationships for the estimation of low-flow statistics. Water Resources Research, 28(9): 2451-2458.

Wang, D. and Cai, X. 2009. Detecting human interferences to low flows through base flow recession analysis, *Water Resour. Res.,* 45, W07426, doi:10.1029/2009WR007819, 2009.

Wang, D. and Cai, X. 2010a.Comparative study of climate and human impacts on seasonal baseflow in urban and agricultural watersheds. *Geophys. Res. Lett.,* 37, L06406, doi:10.1029/2009GL041879, 2010.

Wang D., and Cai X. 20100b. Recession slope curve analysis under human interferences. *Advances in Water Resources,* 33 (2010) 1053–1061.

Wang D. (2011), On the base flow recession at the Panola Mountain Research Watershed, Georgia, USA, *Water Resources Research*, 47, W03527, doi:10.1029/2010WR009910.

Wittenberg H. 1994. Nonlinear analysis of flow recession curves. In FRIEND: Flow Regimes from International Experimental and Network Data, Seuna P, Gustard A, Arnell NW, Cole GA (eds). IAHS Publication 221. IAHS Press: Wallingford; 61–67.

Wittenberg H. 1999. Baseflow recession and recharge as nonlinear storage processes. *Hydro. Processes*,13:715–726.

Wittenberg H., and Sivapalan, M. 1999. Watershed groundwater balance estimation using streamflow recession analysis and baseflow separation. Hydrology, 219:20-33, http://dx.doi.org/10.1016/S0022-1694(99)00040-2

Wittenberg H. 2003. Effects of season and man-made changes on baseflow and flow recession: case studies. *Hydrol. Process.* 17, 2113–2123. DOI: 10.1002/hyp.1324.

Wolock, D. 2003. Base-flow index grid for the conterminous United States. U.S. Geological Survey Open-File Report 03-146. Digital dataset available on http://water.usgs.gov/GIS/dsdl/bfi48grd.zip

Zecharias, Y., and Brutsaert, W. 1988. Recession characteristics of groundwater outflow and base flow from mountainous watersheds. *Water Resour. Res.,* 24 (10):1651-1658.

Zhou, Y.P., Xu Kuan-Man., Sud, Y.C., Betts, A.K. 2011. Recent trends of the tropical hydrological cycle inferred from Global Precipitation Climatology Project and International Satellite Cloud Climatology Project data. Geophysical Res., 116, D09101, doi:10.1029/2010JD015197.

Table 1: Solutions to Boussinesq equation for an unconfined rectangular aquifer placed on a horizontal impermeable layer draining into a fully penetrating stream channel.

Linearity	Time domain	Slope *b*	Outflow time *a* [T^{-1}]	Source
Non-linear	Short	3	$\frac{1.1334}{k\varphi D^3 L^2}$	Polubarinova-Kochina [1962]
Non-linear	Long	1.5	$\frac{4.804k^{1/2}L}{\varphi A^{3/2}}$	Boussinesq [1904]
Linearized	Long	1	$\frac{\pi pkDL^2}{\varphi A^2}$	Boussinesq [1903]

k:hydraulic cond., φ:drainable porosity; D: aquifer depth; L: upstream length; A: drainage area; p:(0.3465).

Table 2: Summary of geomorphic and climatic watershed characteristics.

ID	Site	Q [mm/yr]	ET [mm/yr]	P [mm/yr]	AI	Mean T. [˚C]	Mean Slope [%]	Mean E. [m]	Area [km^2]	Total stream length [km]	D. density	Total Relief [m]
1	Lawyer Creek	109	473	582	1.23	6.8	9.2	1192	368	460	1.25	927
2	Asotin Creek	186	419	605	1.44	8.1	37.5	1187	269	760	2.83	1478
3	Fish Creek	109	1202	1311	1.09	5.8	36.1	1360	228	310	1.36	1409
4	Big Creek	406	480	886	1.85	1.8	45.7	2130	1168	1358	1.16	1647
5	Pine Creek	703	522	1225	2.35	5.5	46.5	1221	190	231	1.22	1240
6	Canyon Creek	754	559	1313	2.35	3.8	46.3	1515	60	64	1.06	1220
7	Mica Creek	502	786	1288	1.64	5.7	29.9	1241	12.25	12	1.00	476
8	Salmon River, Stibnite	472	470	942	2.00	1.3	41.7	2320	50	105	2.11	1037
9	Clearwater River, Kamiah	591	473	1064	2.25	4.8	37.2	1511	12357	15733	1.27	2501
10	Little Pend Oreille River	155	687	842	1.23	5.5	19.8	1056	342	623	1.82	1109
11	Union Flat Creek	155	461	616	1.34	8.5	11.2	820	489	801	1.64	556
12	Asotin Creek	103	420	523	1.25	8.6	28.0	1025	836	1382	1.65	1659
13	Johnson Creek	522	593	1115	1.88	1.8	28.9	2175	564	568	1.01	1362
14	Saint Maries River	443	682	1125	1.65	6.1	26.1	1095	699	1445	2.07	1155
15	Crumarine Creek	230	801	1031	1.29	7.3	28.4	1121	6.35	8	1.29	659
16	SF Clearwater River	342	637	979	1.54	4.3	25.1	1553	676	989	1.46	1098
17	Paradise Creek	146	601	747	1.24	8.0	12.7	866	45	60	1.33	552
18	SF Palouse River	97	573	670	1.17	8.2	12.0	832	342	586	1.71	807

Q = Discharge; ET = Evapotranspiration; P = Precipitation; AI = Aridity Index (precipitation/evapotranspiration); T = Temperature; E = Elevation; D = Drainage.

Table 2: (continued)

ID	Site	Q [mm/yr]	ET [mm/yr]	P [mm/yr]	AI	Mean T. [˚C]	Mean Slope [%]	Mean E. [m]	Area [km^2]	Total stream length [km]	D. density	Total Relief [m]
19	Palouse River, Potlatch	283	567	850	1.5	6.7	22.3	965	821	1322	1.61	872
20	Tucannon River	146	518	664	1.3	8.9	27.0	896	1116	1821	1.63	1715
21	NF Couer D'Alene River	720	505	1225	2.4	5.2	42.2	1203	858	1259	1.47	1138
22	Boundary Creek	416	551	967	1.7	4.2	36.4	1361	428	237	0.09	1562
23	Lochsa River	817	481	1298	2.7	4.3	39.5	1583	3060	3279	1.07	2240
24	Selway River	666	449	1115	2.5	3.9	45.3	1680	4950	6470	1.31	2365
25	Salmon River, Salmon	175	411	586	1.4	2.8	34.4	2255	9740	14117	1.45	2660
26	Palouse River, Hooper	85	461	546	1.2	8.5	12.2	727	6472	9195	1.42	1301
	Mean	359	569	927	1.7	5.6	30	1342	1775	2431	1.4	1336
	Standard deviation	239	167	269	0.5	2.3	12	458	3152	4226	0.5	593
	Maximum	817	1202	1313	2.7	8.9	47	2320	12357	15733	2.8	2660
	Minimum	85	411	523	1.1	1.3	9	727	6	8	0.1	476

Q = Discharge; ET = Evapotranspiration; P = Precipitation; AI = Aridity Index (precipitation/evapotranspiration); T = Temperature; E = Elevation; D = Drainage

Table 3: Summary of main geologic features in the study watersheds.

Site	Percent of main geologic features									
	Alluvial	Granitic	Basalt	Eolian	Mafic	Metamorphic	Sedimentary	Glacial drift	Volcanic	Unconsolidated material
Lawyer 1Creek	0.0	12.3	77.1	0.0	0.0	10.6	0.0	0.0	0.0	0.0
Asotin Creek	0.0	0.0	0.0	4.8	95.2	0.0	0.0	0.0	0.0	0.0
Fish Creek	0.0	100.0	0.0	0.0	0.0	0.0	0.0	0.0	0.0	0.0
Big Creek	0.6	38.0	0.0	0.0	0.0	27.1	0.0	0.0	34.3	0.0
Pine Creek	0.0	0.0	0.0	0.0	0.0	63.1	36.9	0.0	0.0	0.0
Canyon Creek	12.9	3.2	0.0	0.0	0.0	66.1	17.8	0.0	0.0	0.0
Mica Creek	0.0	0.0	0.0	0.0	0.0	0.0	100.0	0.0	0.0	0.0
Salmon River, Stibnite	0.0	57.1	0.0	0.0	0.0	13.4	0.0	0.0	29.5	0.0
Clearwater River, Kamiah	0.8	60.0	11.3	0.0	0.0	26.9	0.4	0.1	0.5	0.0
Little Pend Oreille River	0.0	39.6	0.0	0.0	0.0	2.3	1.2	56.6	0.0	0.4
Union Flat Creek	6.7	10.3	0.0	75.5	7.6	0.0	0.0	0.0	0.0	0.0
Asotin Creek	0.1	0.0	0.0	36.7	62.6	0.0	0.6	0.0	0.0	0.0
Johnson Creek	0.6	81.9	0.0	0.0	0.0	9.0	0.0	8.4	0.0	0.0
Saint Maries River	3.8	1.4	7.6	0.0	0.0	39.9	47.3	0.0	0.0	0.0
Crumarine Creek	0.0	100.0	0.0	0.0	0.0	0.0	0.0	0.0	0.0	0.0
SF Clearwater River	0.2	18.7	0.0	0.0	0.0	78.2	2.9	0.0	0.0	0.0
Paradise Creek	0.9	34.1	0.0	65.1	0.0	0.0	0.0	0.0	0.0	0.0
SF Palouse River	5.8	28.7	0.1	58.9	5.8	0.7	0.0	0.0	0.0	0.0
Palouse River, Potlatch	3.8	15.2	0.8	15.8	0.0	54.7	9.7	0.0	0.0	0.0
Tucannon River	1.1	0.1	0.0	43.6	54.8	0.0	0.3	0.1	0.0	0.0
NF Couer D'Alene River	3.3	0.0	0.0	0.0	0.0	63.7	33.0	0.0	0.0	0.0
Boundary Creek	0.6	86.5	0.0	0.0	0.0	4.1	8.8	0.0	0.0	0.0
Lochsa River	0.1	76.9	0.0	0.0	0.0	22.1	0.0	0.0	0.8	0.1
Selway River	0.6	82.2	0.0	0.0	0.0	17.2	0.0	0.0	0.0	0.1
Salmon River, Salmon	15.4	11.0	0.0	0.0	0.0	10.5	16.2	5.1	41.7	0.2
Palouse River, Hooper	4.9	5.0	0.2	54.5	22.8	7.7	2.4	2.3	0.0	0.2

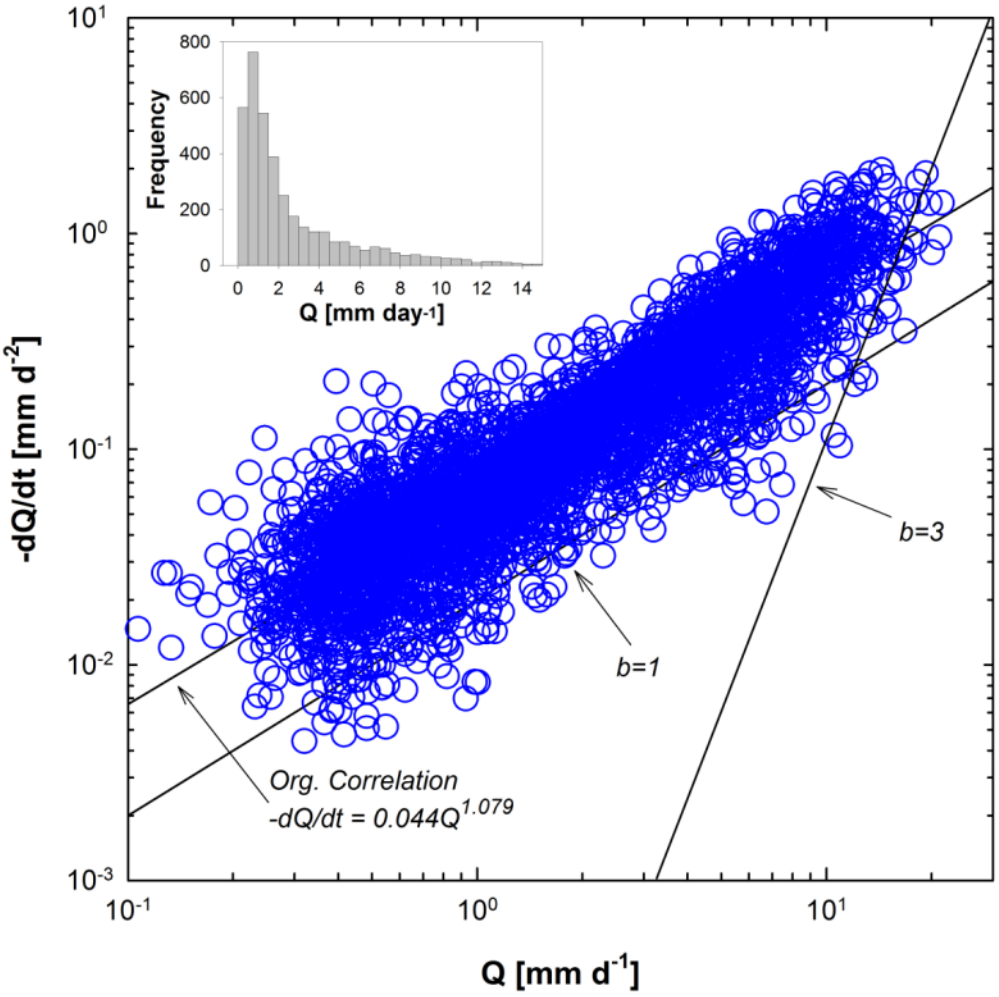

Figure 1: Natural spectrum of data points –dQ/dt [mm d^{-2}] versus the average Q [mm d^{-1}] during the period 1939-2011 on Lochsa River, Lowell, Idaho. The drainage area is 3,060 km^2. The lower envelopes are represented by the lines with slopes of 1 and 3. The organic correlation fitting method exhibits a slope of 1.079. The inset shows the distribution of average discharge Q [mm d^{-1}].

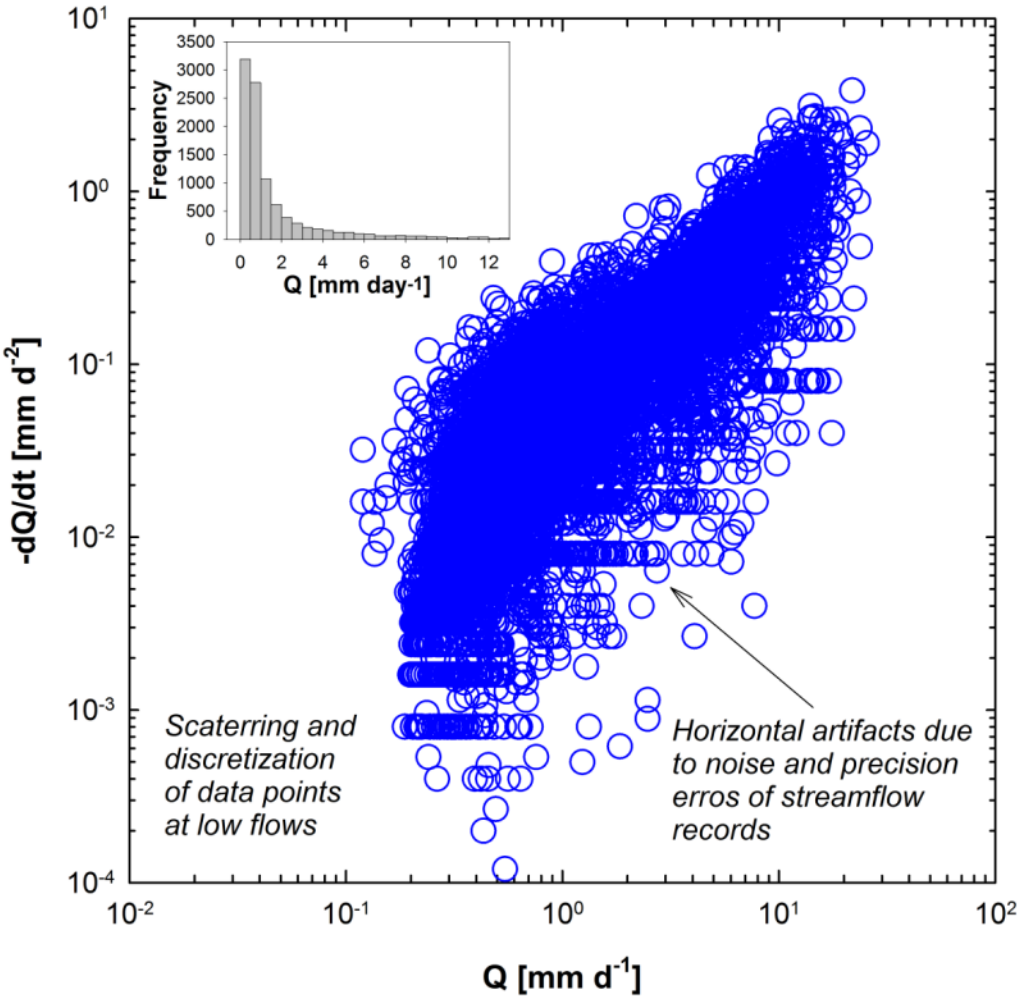

Figure 2: Example of horizontal artifacts due to noise and precision errors of streamflow records at lower flow rates when plotting $-dQ/dt$ [mm d^{-2}] versus the average Q [mm d^{-1}] during the period 1939-2011 on Lochsa River, Lowell, Idaho. The drainage area is 3,060 km^2. The inset shows the distribution of average discharge Q [mm d^{-1}].

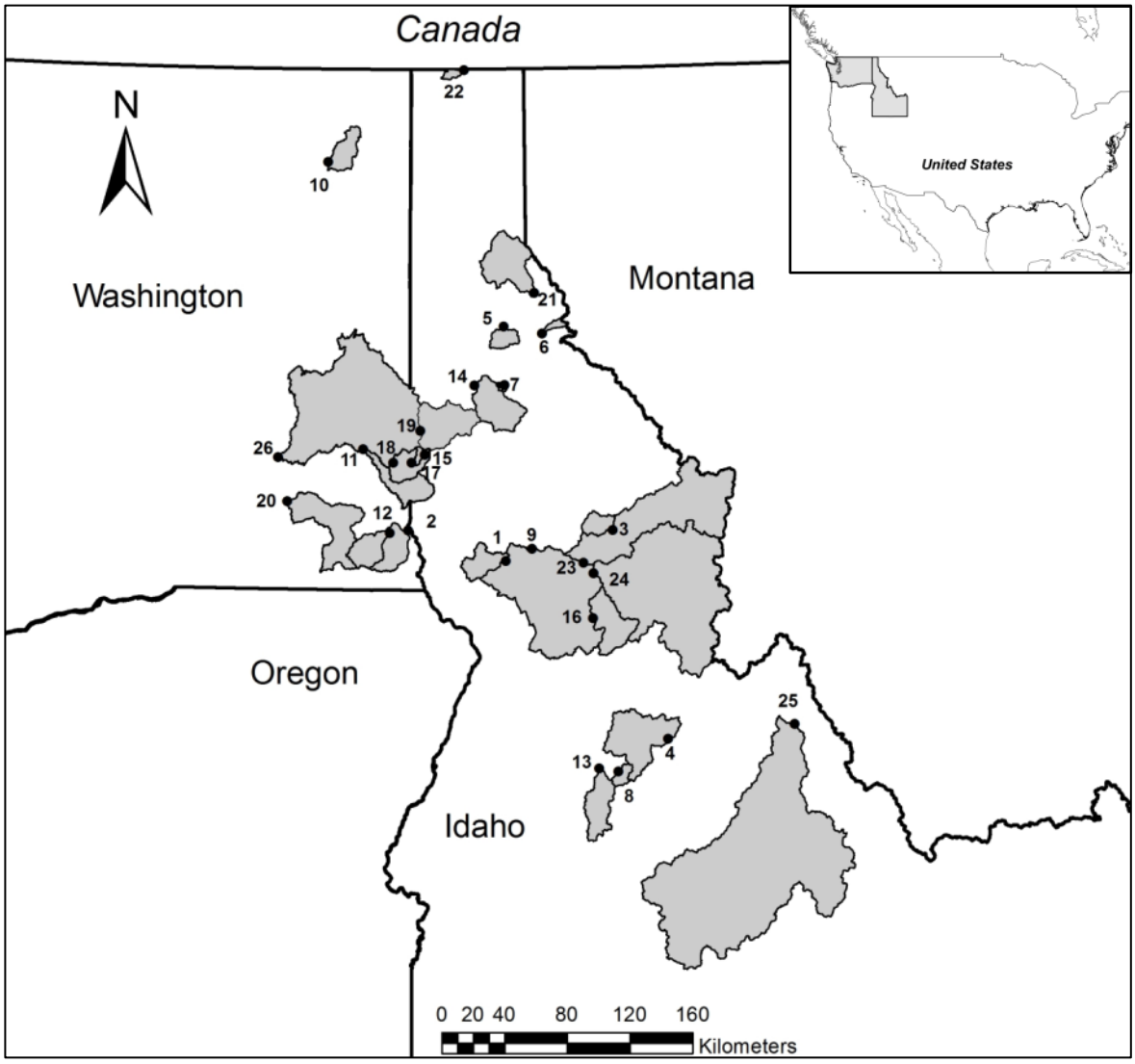

Figure 3: Study area including watershed boundaries across eastern Washington and northern/central Idaho. Inset highlights the location of Washington and Idaho states within the Pacific Northwest of the United States.

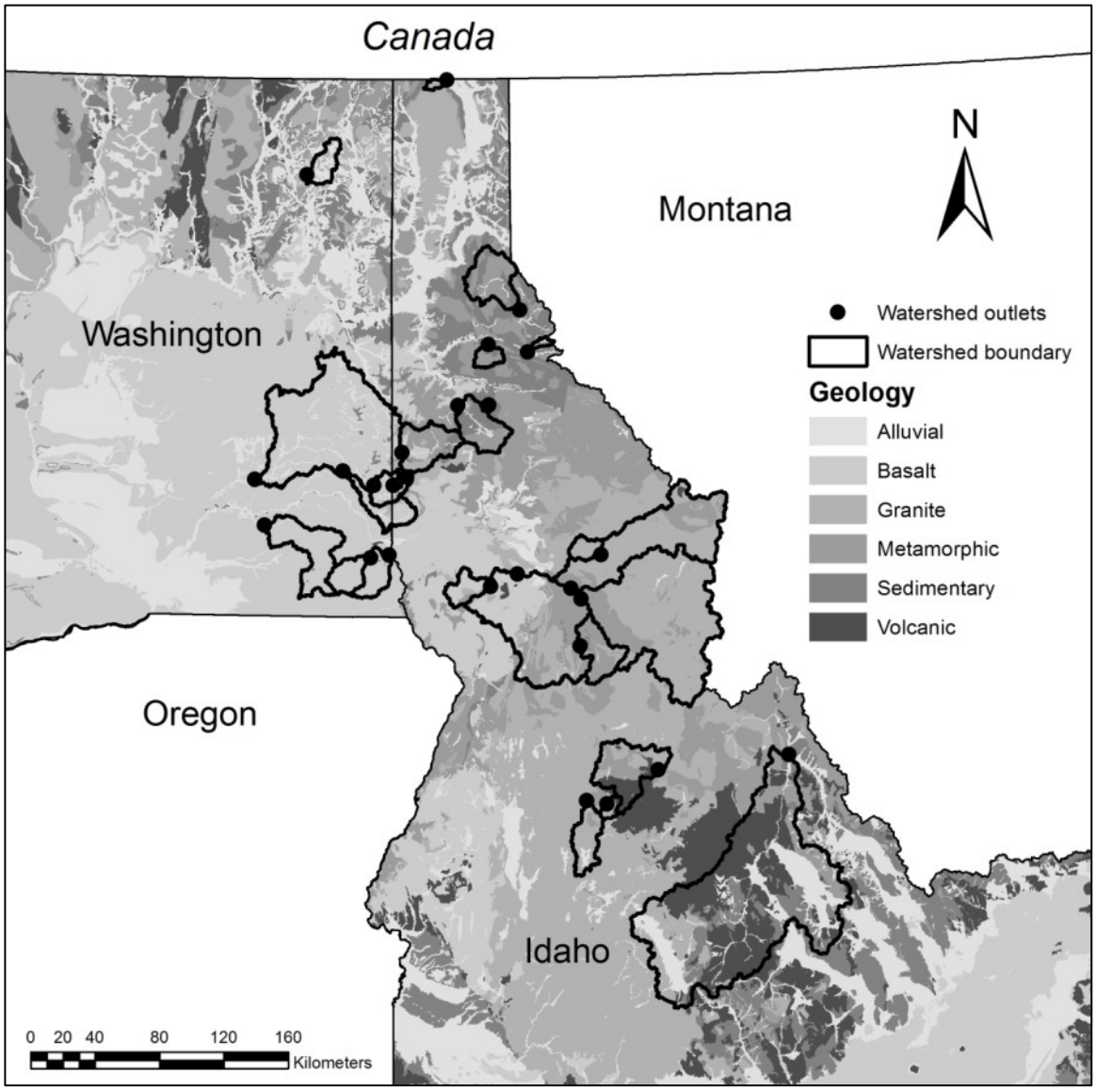

Figure 4: Study area including watershed boundaries and main geology units.

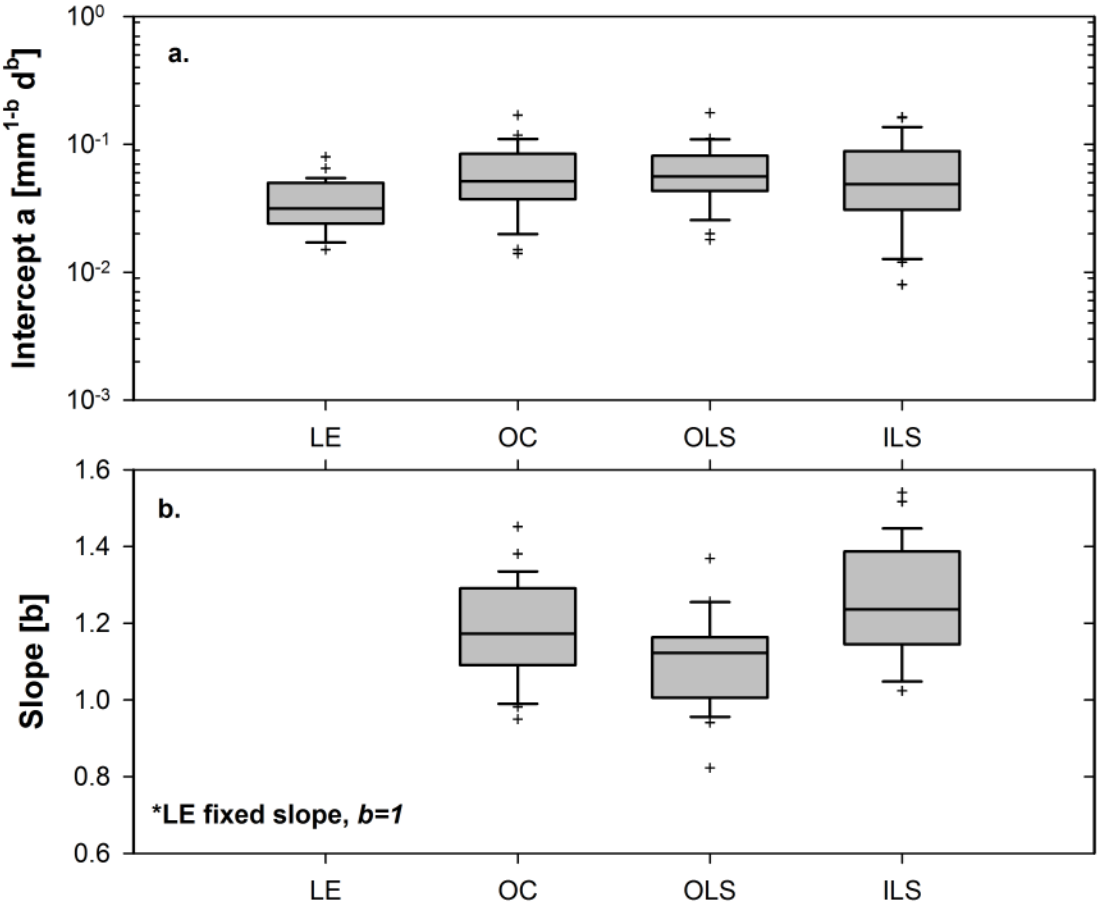

Figure 5: Distribution of intercept a **(a) and** slope b **(b).** Box plots include median, 5th and 95th percentiles and error bars. Crosses denote the number of outliers per fitting method.

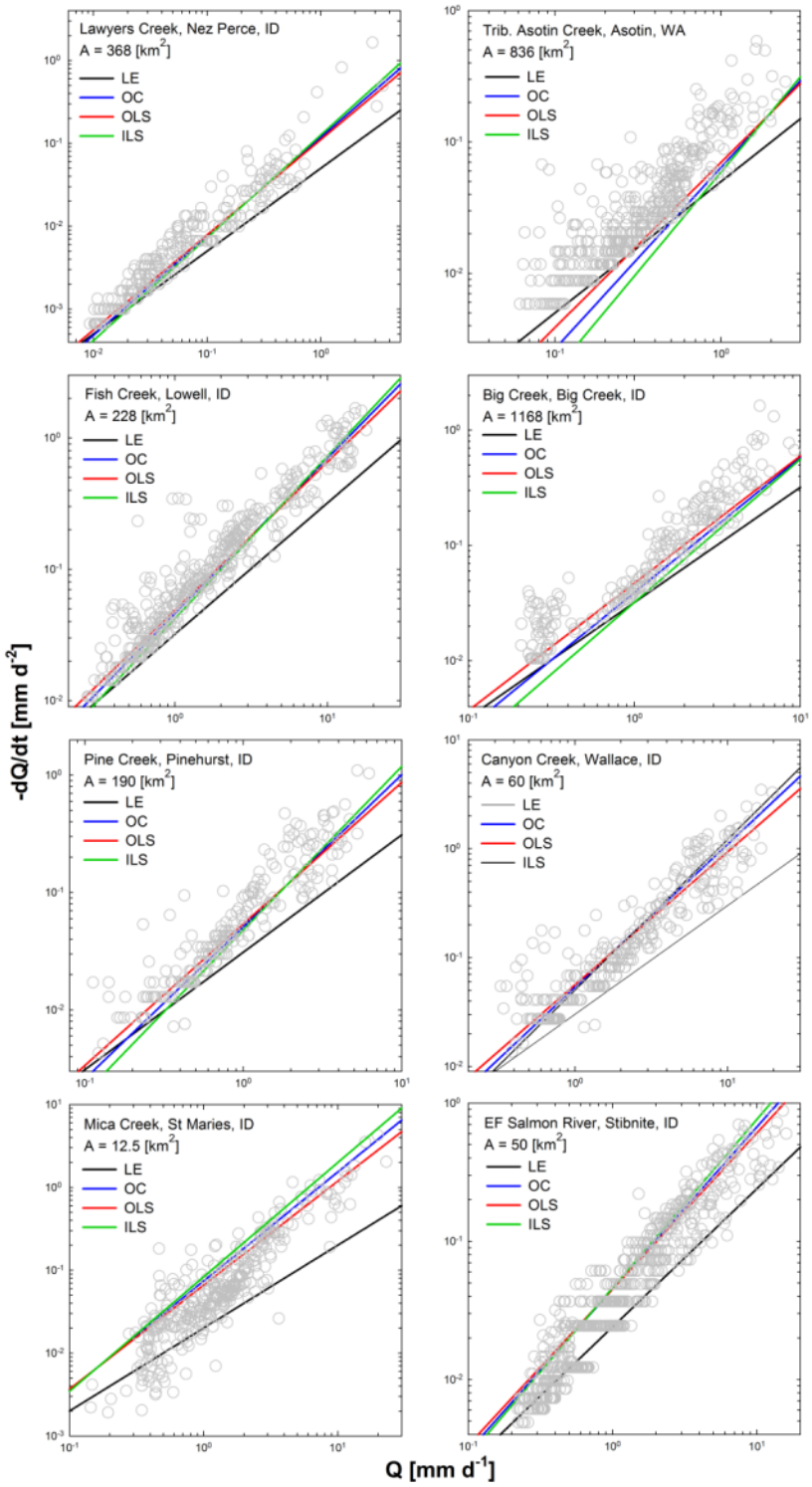

Figure 6: Recession plots showing –dQ/dt [mm d^{-2}] versus the average Q [mm d^{-1}] and four different fitting procedures. Black line represents the lower envelope (LE) (b=1) method. Organic correlation (OC) is represented by blue lines. Ordinary (OLS) and inverse least squares (ILS) are represented by red and green lines, respectively. Plots are organized by the increasing number of record years (Table 1).

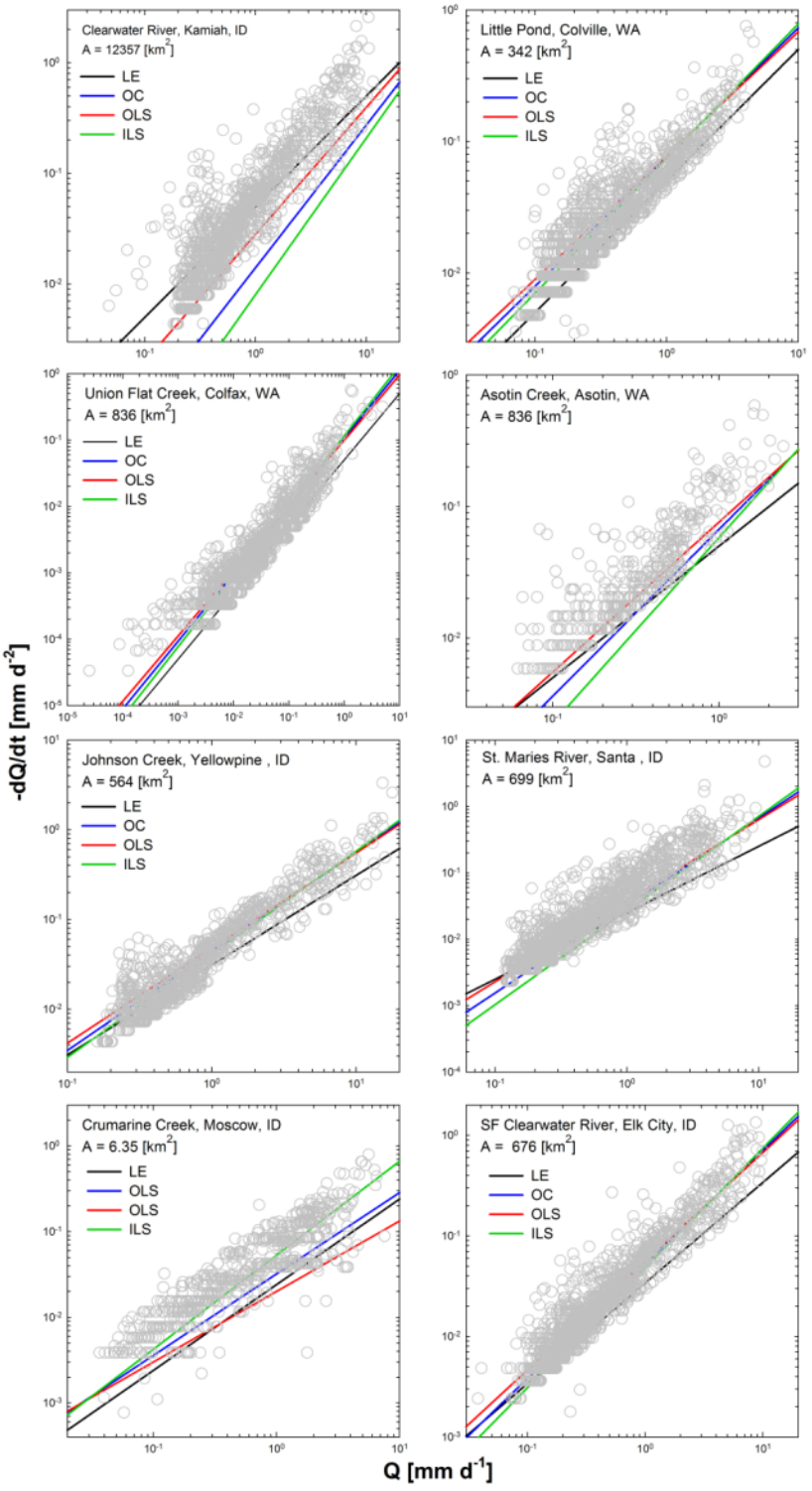

Figure 6: (continued)

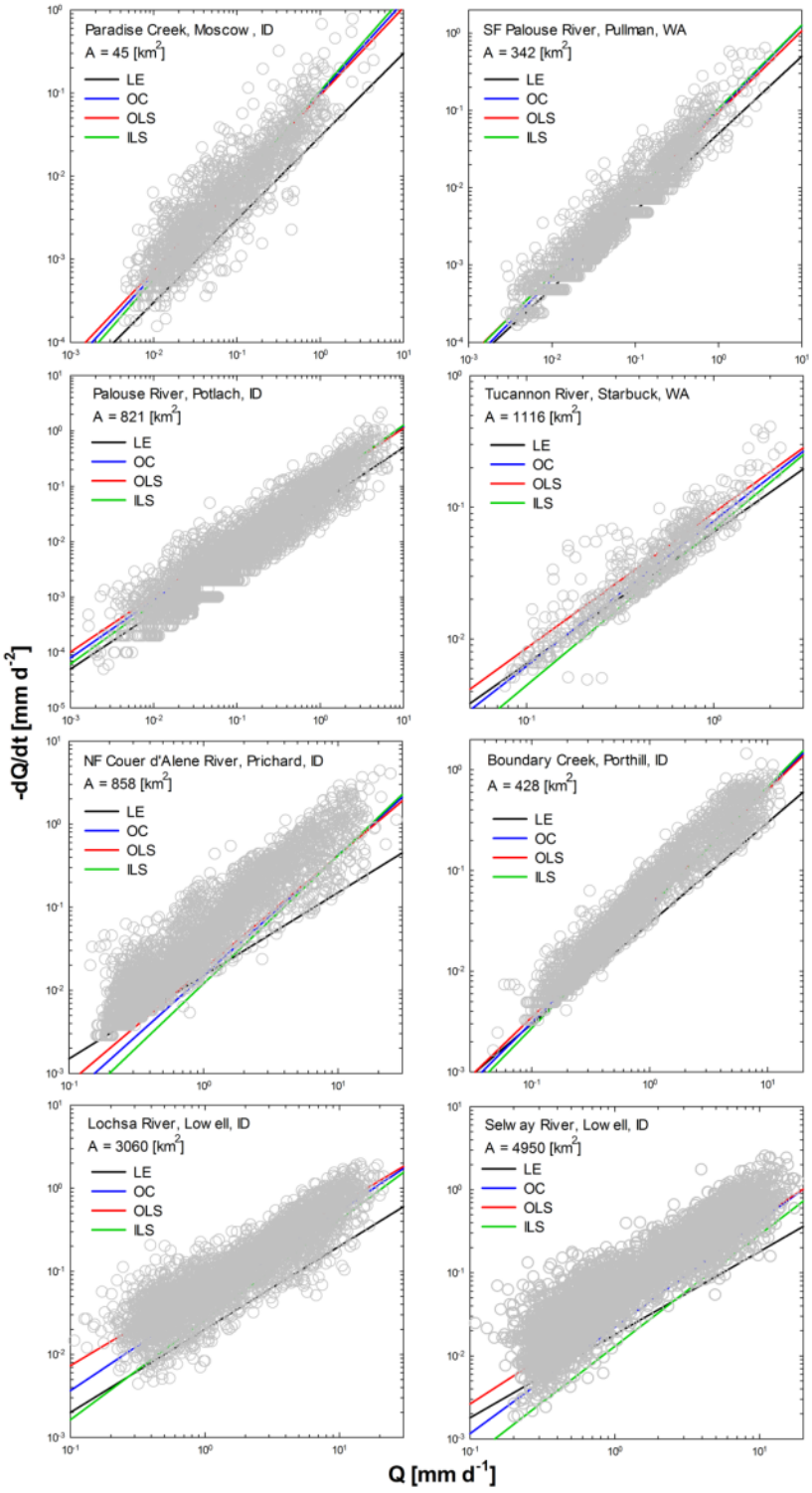

Figure 6: (continued)

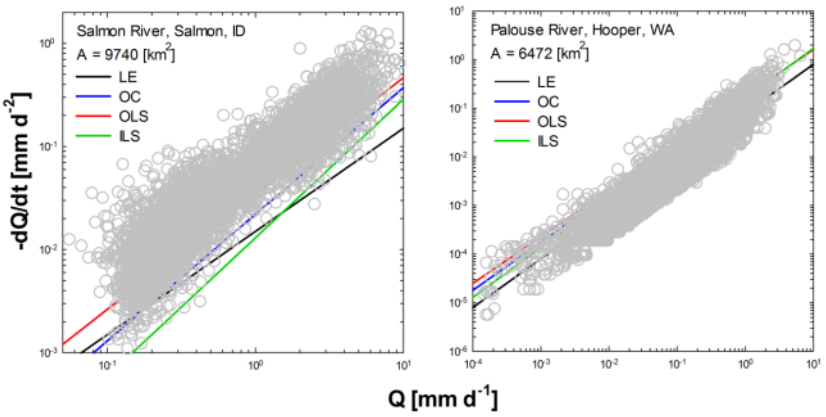

Figure 6: (continued)

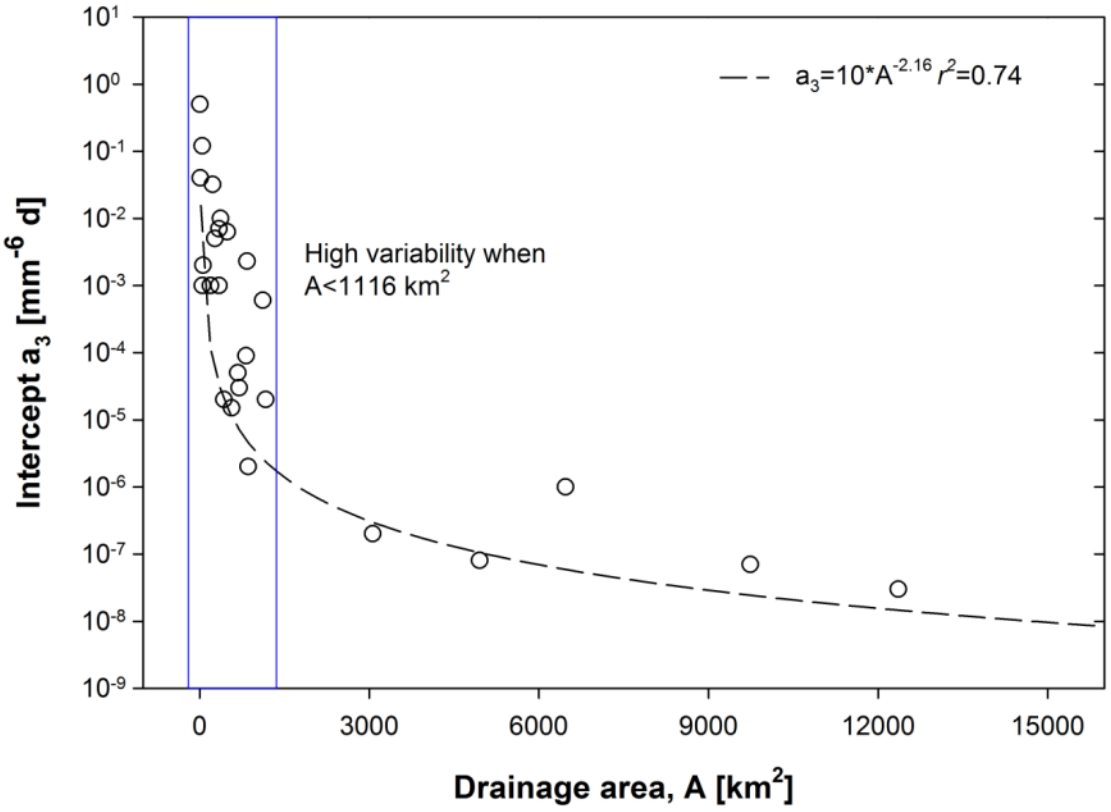

Figure 7: Intercept a3 versus drainage area A. Dotted line is the best fit power curve for the observed data.

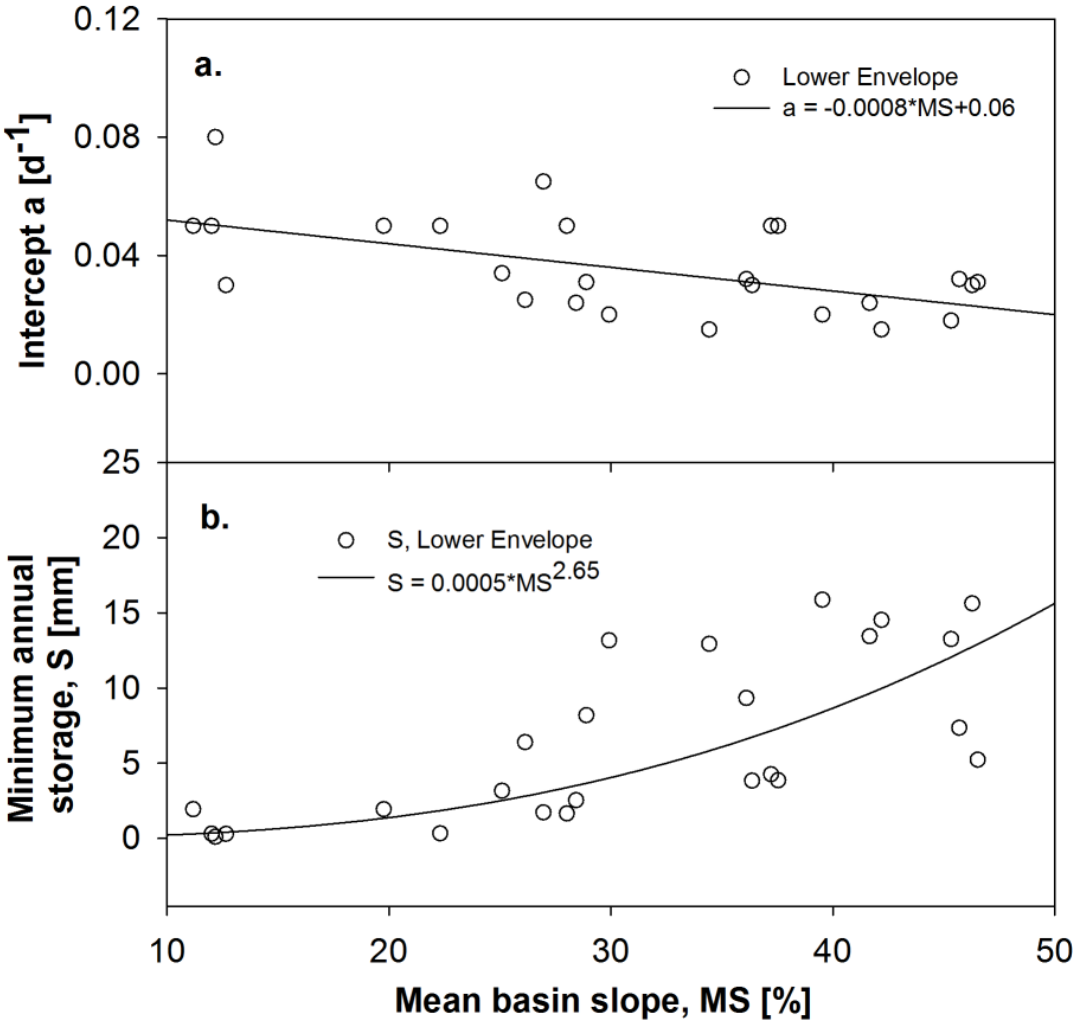

Figure 8: Scatter plots of mean basin slope versus (a) intercept a and (b) minimum annual storage S for the lower envelope method.

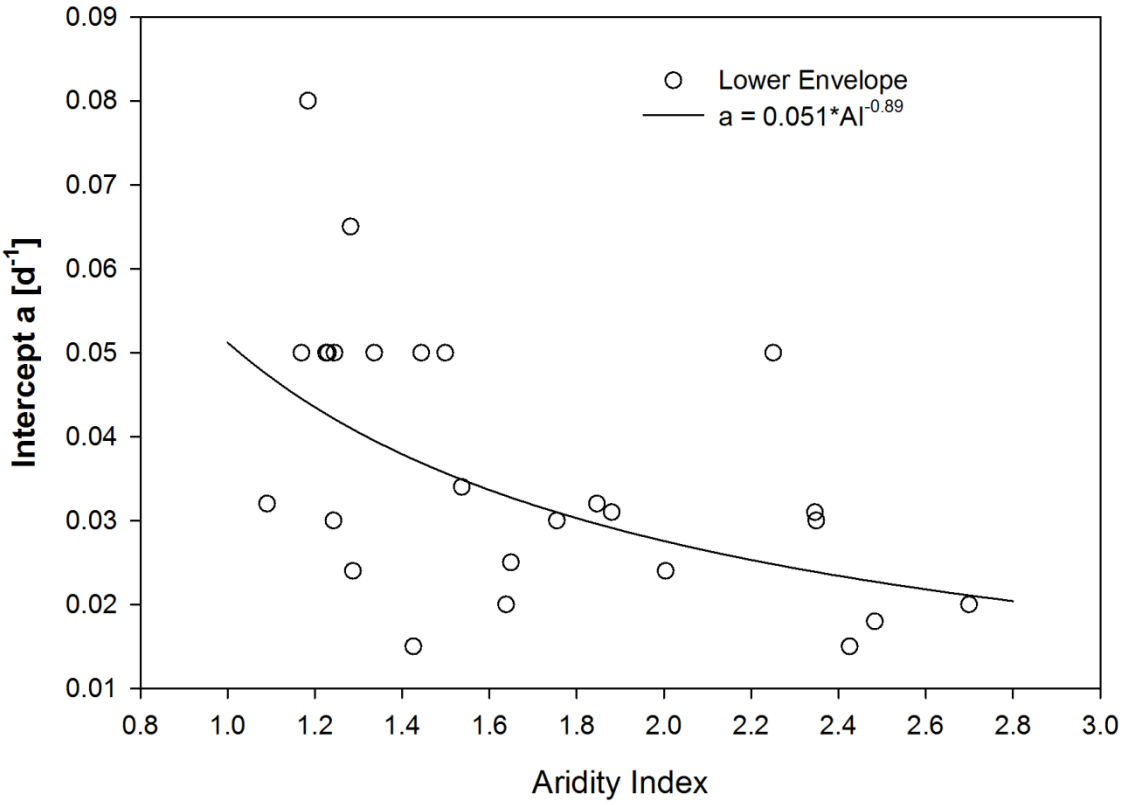

Figure 9: Scatter plot of mean intercept *a* versus aridity index.

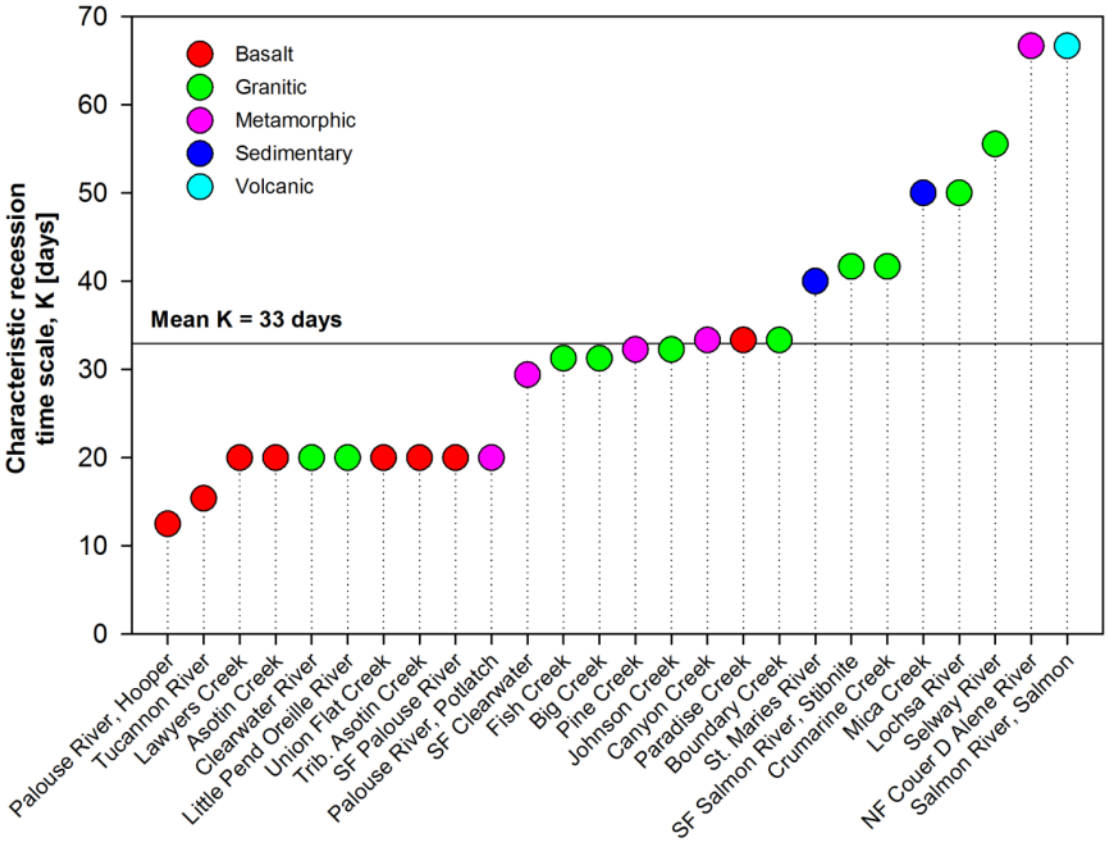

Figure 10: Relationship of characteristic recession time scale *K* [days] and main underlying geology among the study watersheds.

Supplementary Tables

Supplementary tables S1 and S2 are provided in digital format.

Table S1: Summary of baseflow coefficients, characteristic recession time scales, and minimum annual storages for all fitting methods.

Table S2: Pearson product moment correlation matrix of baseflow coefficients and watershed attributes. Significant correlations at α=0.05 level are shown in bold.

Supplementary Figure

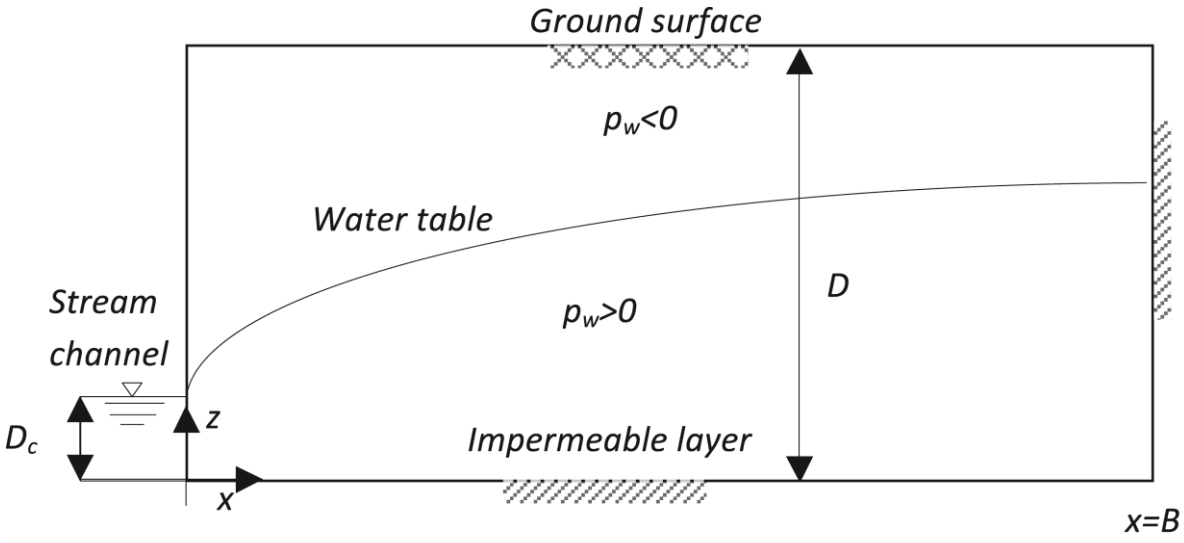

Figure S1: Schematic representation of an unconfined rectangular aquifer placed on a horizontal impermeable layer draining into a fully penetrating stream channel. This system is also known as the "Dupuit-Boussinesq" aquifer (Brutsaert and Nieber, 1977), in which *D* is the aquifer depth, D_c is the water depth in the stream channel, and *B* is the aquifer breadth. Modified from Brutsaert (2005).

CHAPTER II

Isotope Hydrology and Baseflow Geochemistry in Natural and Human-Altered Watersheds in the Inland Pacific Northwest, USA

R. Sánchez-Murillo, Brooks E.S, Elliot W.J, and Boll J.

Abstract

This study presents a stable isotope hydrology and geochemical analysis across three areas of particular interest in the inland Pacific Northwest of the United States (PNW): Palouse Region, Silver Valley, and Priest River area. Isotope ratios (δ^2H, δ^{18}O) were used to estimate mean transit times (MTT) in natural and human-altered watersheds. Input-output relationships were obtained from observed δ^{18}O (‰) ratios in precipitation and surface waters using the computer program FLOWPC and sine-wave approach. To complement the stable isotope data, a detailed baseflow geochemical analysis was conducted. Isotope ratios in precipitation resulted in the establishment of a regional meteoric water line of $\delta^2\text{H} = 7.42 \cdot \delta^{18}\text{O} + 0.88$ (n = 316; r^2 = 0.97) for the inland PNW. Isotope compositions showed a clear temperature-dependent seasonality: enriched values occurred during late spring and summer rains (April-September), while depleted values were observed throughout fall and winter (November-March) seasons. Low *d*-excess values in precipitation, particularly during the summer, revealed the incorporation of local recycled water vapor into the air mass and potential secondary evaporation of rainfall during small rain events. Despite the observed seasonal variation in precipitation, the annual stream δ^{18}O variation was very small except for one large snowmelt event. A highly significant power regression ($\tau = 0.11D^{-1.89}$; r^2 = 0.83) was found between relative MTT and the damping ratio, indicating greater subsurface travel times as the damping ratio decreased. Baseflow MTT ranged from 0.42 − 0.62 years (human-altered and basalt-

dominated landscape), 0.73 – 1.7 years (mining-altered and predominantly sedimentary rocks), and 0.67 − 3.2 years (forested and granitic-dominated watersheds). The best fits between observed and $\delta^{18}O$ ratios were obtained with the exponential and dispersion weighting functions. Baseflow geochemical data supported the relative water age estimates. Greater residence times were represented by more homogenous water chemistry whereas smaller residence times resulted in more dynamic compositions. The stable isotope and geochemical data presented provide an essential baseline for future water resources assessments and modeling efforts in the inland PNW.

Keywords: Natural and human-altered watersheds; isotope hydrology; mean transit times; baseflow geochemistry; watershed management.

1. Introduction

In the Pacific Northwest (PNW) region of the United States rapid population growth expected from ~15 million today to ~85−100 million by 2100 (Lackey, 2013) has led to an increasing debate over competing water supplies and diverse interests (i.e. ecological, agricultural, socio-economical, cultural) (Callahan et al., 1999; Miles et al., 2000, Mote et al., 2003; Hamlet, 2011; Chang et al., 2012; Wu et al., 2012; Sánchez-Murillo et al., 2013; Rudestam, 2014). The PNW includes the states of Washington, Oregon, Idaho, and western Montana. The central pillar of this debate relies on the scientific recognition of the PNW as a particularly sensitive region to climate variability (Mote et al., 2003; Stewart et al., 2005; McCabe et al., 2005; Van Kirk and Naman, 2008; Miles et al., 2000; Elsner et al., 2010, Mayer, 2012, Wu et al., 2012) which may result in significant hydrologic and stream temperature regime alterations. Overall, future climate scenarios for the PNW project a warming of 0.1°C to 0.6°C per decade in the 21st century (Mote and Salathé, 2010).

The inland PNW is bounded by the Cascades Mountains on the west and the Rocky Mountains on the east. This area comprises a variety of semi-arid and snow-dominated landscapes across Washington and Idaho that exhibit intrinsic hydrological feedbacks. For example, lower elevation areas that may experience more evapotranspiration in the future depend on the water supply from higher elevation snow-dominated watersheds which, at the same time, may be potentially shifting from snow to rainfall domains coupled with earlier spring runoff events in a warmer climate (Stewart et al., 2005). Consequently, future hydro-climate scenarios in the inland PNW may affect: *a)* the demand of groundwater supplies, electricity generation, clean drinking water, and recreation activities which may converge in individual and inter-state water rights debates, *b)* current water quality criteria under baseflow conditions, *c)* disruption of ecological assemblages (e.g. high water temperatures, low dissolved oxygen concentrations) along summer flows which are critical to many ecosystems such as salmon rearing habitats. Hence, one imperative need that emerges from the above mentioned scenarios is to improve our

understanding of the hydrological connectivity between the semi-arid and snow-dominated landscapes in the inland PNW.

To our knowledge, no comprehensive isotope hydrology assessments of precipitation and surface waters in the inland PNW of Washington and Idaho have been undertaken; rather isotopic research has been limited and site-specific (Larson et al., 2000; Lyn et al., 2004; Godwin, 2006; Koeniger et al., 2008; Moravec et al., 2010, Moxley, 2012). Stable isotope and geochemical data are needed to create a baseline for future water resources assessments and modeling efforts in the inland PNW. The objectives of this study, therefore, were to use the stable isotopes of water to: a) establish foundational regional and local meteoric water lines in the inland PNW; b) describe spatial and temporal isotopic variations in precipitation and surface waters; and c) evaluate differences in mean transit times and transit time distribution functions at variable catchment scales (10^0 – 10^2 km^2), land uses (i.e. agricultural-urban, mining, and forested), climatic gradients, and main underlying geology (i.e. basalt, granitic, metamorphic, and sedimentary). Mean transit time input-output relationships were constructed from $\delta^{18}O$ ratios in precipitation and surface waters over a sampling period of two years in most of the selected watersheds. The stable isotope data were complemented by a baseflow geochemical analysis conducted in five natural and human-altered watersheds to evaluate water quality conditions in these systems during the critical summer months.

1.1. Stable isotope basics

The use of stable isotopes of water, both deuterium (δ^2H) and oxygen-18 ($\delta^{18}O$) has provided novel insights into the understanding of subsurface water movement, storage, and mixing processes (Kendall and McDonnell, 1998). The development of new instrumentation based on laser spectroscopy in recent years has improved the temporal resolution of isotopic data, reduced the analytical uncertainty and analysis timeframe (Berden et al., 2000; Lis et al., 2008; Wen et al., 2008; Gupta et al., 2009; Munksgaard et al., 2012), and has provided new research avenues of

the atmospheric water cycle (i.e. ^{17}O-excess; Berman et al., 2013). Particularly, these naturally-occurring tracers have been recognized as a useful technique to study solute transport from column and plot studies (Koeniger et al., 2010), to watershed mean transit times (Frederickson and Criss, 1999; McGuire et al., 2002; Rodgers et al., 2005; Uchida et al., 2006; Tezlaff et al., 2011, Asano and Uchida, 2012), and widely to elucidate atmospheric moisture sources and their implications in the hydrological cycle (Dansgaard, 1964; Merlivat and Jouzel, 1979; Rozanski et al., 1992; Araguas-Araguas et al., 2000; Bowen and Revenaugh, 2003; Aggarwal et al., 2012; Sanchez-Murillo et al., 2013).

The global relationship between δ^2H and $\delta^{18}O$ in natural meteoric waters (i.e. continental precipitation that has not experienced evaporation), recognized by Craig (1961) and later known as the Global Meteoric Water Line (GMWL: $\delta^2H = 8 \cdot \delta^{18}O + 10$) serves as a foundational reference to determine regional or local deviations (i.e. Local Meteoric Water Line, LMWL) from equilibrium processes. Other factors such as the trajectory of air masses, latitude, altitude, precipitation amount, and distance to the coast may also affect the spatial and temporal variations of δ^2H and $\delta^{18}O$ in precipitation (Dansgaard, 1964). The GMWL slope of 8 is determined by the ratio between the equilibrium fractionation effects of hydrogen (δ^2H/δ^1H) and oxygen ($\delta^{18}O/\delta^{16}O$), while the intercept 10 is controlled by the kinetic fractionation occurring during non-equilibrium processes such as evaporation (Craig, 1961; Jouzel et al., 2000; Cappa et al., 2003; Wen et al., 2008). Water losses due to evaporation, the incorporation of recycled atmospheric moisture or mixing between isotopically-distinct reservoirs leave a unique water fingerprint that can be used to understand rainfall-runoff processes (Birkel et al., 2012), complex water flow paths (McGlynn et al., 2002), and groundwater to surface water connectivity (Tetzlaff and Soulsby, 2008; Speed et al., 2010; Wassenaar et al., 2011). In temperate regions, isotopic variations in precipitation have been frequently correlated to mean surface air temperature at the sampling site (Dansgaard, 1964; Rosanski et al., 1993; Araguás-Araguás et al., 2000; Wassenaar et al., 2011). In contrast, the deuterium excess or *d*-excess ($d = \delta^2H - 8 \cdot \delta^{18}O$) (Dansgaard, 1964) (i.e. a measure of the relative proportions of δ^2H

and $\delta^{18}O$ in meteoric waters) is correlated with the physical conditions (i.e. relative humidity and sea surface temperature) of the oceanic source area (Froehlich et al., 2002); therefore, the combination of $\delta^{2}H$, $\delta^{18}O$, and *d*-excess can be used to understand hydrological processes from the origin of atmospheric moisture to evapotranspiration fluxes, runoff mechanisms, and groundwater recharge pathways.

1.2. Mean transit time theory

The mean transit time (MTT) or the time a water molecule or tracer spends traveling along subsurface flow pathways to the stream network is a fundamental hydraulic descriptor that provides useful information about water sources and mixing processes, potential flow pathways, and storage capabilities within a particular catchment control volume (McGuire et al., 2002; Dunn et al., 2007; Soulsby et al., 2009; McDonnell et al, 2010; Stewart et al., 2012; Sanghyun and Sungwon, 2014). The conjugation of the MTT and the transit time distribution (TTD) characterizes the average discharge behavior of a catchment (Godsey et al., 2010; Hrachowitz et al., 2010; van der Velde et al., 2012; Hrachowitz et al., 2013), and consequently, describes how groundwater systems hold and release water, which is a key component of contaminant transport assessments and water resources management. While an unified criteria of catchment controls on MTT and the shape of TTD is unrealistic due the inherent complexity of water flowpaths and geomorphologic heterogeneities across landscapes, several studies have found significant correlations between MTT and catchment characteristics such as flow path depth (e.g. mountainous catchment, Central Japan, Asano and Uchida, 2012), storage within the unsaturated zone (e.g. humid catchment, New Zeeland; Dunn et al., 2007), slope direction and exposure (e.g. Redondo Peak, New Mexico; Broxton et al., 2009), soil cover (e.g. Cairngorm mountains, Scotland; Soulsby et al., 2006), and topography (e.g. mountainous catchments, Oregon; McGuire et al., 2005).

The MTT is usually estimated from the input-output dynamic of conservative tracers such as $\delta^{2}H$, $\delta^{18}O$, and chloride (Frederickson and Criss, 1999; Asano et al.,

2002; Rodgers et al., 2005; Viville et al., 2006; Katsuyama et al., 2010; Capell et al., 2012; Heidbüchel et al., 2013), which involves fitting an average TTD (i.e. assumed to be time-invariant) using inverse modeling approaches with lumped convolution integral models (Maloszewiski and Zuber, 1982, 1996; McGuire and McDonnell, 2006; Soulsby et al., 2011, Hrachowitz et al., 2010). The transport of the conservative tracer through a catchment can be described by the convolution integral (Eq. 1):

$$\delta_{out}(t) = \int_0^{\infty} g(\tau)\delta_{in}(t - \tau)d\tau = g(t) * \delta_{in}(t) \quad (1)$$

where $\delta_{in}(t)$ and $\delta_{out}(t)$ are the tracer output and input compositions at any time *t*, τ is the turnover time, and *g(t)* is the weighting function describing the shape of the TTD. The weighting function of the tracer is equal to the weighted function of the water infiltrated into the system if: (i) the tracer is conservative; (ii) the tracer is injected and measured proportionally to the volumetric flow rate; or (iii) there are no stagnant waters in the system (Zuber, 1986). In the case of steady flow, the MTT is defined by (Zuber, 1986):

$$\tau = \int_0^{\infty} tg(t)dt = \frac{V}{Q} \quad (2)$$

where V (L^3) is the volume of mobile water in the system, Q ($L^3\ T^{-1}$) is the volumetric flow rate through the system, *t* is the time variable and *g(t)* is the weighting function. Maloszewiski and Zuber (1982) proposed several models types (Table 1 and Fig.1) to describe the TTD function. The Piston Flow Model (PFM) is the simplest and less reliable distribution representation. This model assumes that water travels at equal velocities along all flowpaths which is never true in a catchment (i.e. hydrodynamic dispersion and diffusion are negligible); this mechanism is represented by a single pulse. The Exponential Model (EM) assumes that the tracer transport occurs in a system where flowpaths are distributed exponentially (i.e. equivalent to the response function of a well-mixed reservoir). The Dispersion Model (DM) can take several forms depending on the dispersion parameter *Dp.* The Exponential Piston Model (EPM) describes a system that is exponentially distributed but is delayed in time.

2. Study area

The study watersheds are located within the inland PNW in three areas of particular hydrological interest: Palouse Region, Silver Valley, and Priest River (Fig. 2). The study sites include a variety of climatic gradients, geologic features, and natural and human-altered watersheds. A summary of hydrogeological characteristics in each study area is presented herein. Additional information in five selected watersheds is presented in the Supplemental materials (Tables S1 and S2).

2.1. Palouse Region

The Palouse Region is located on the western slopes of the Saint Joe and Clearwater National Forests (Fig. 2A) covering roughly 9,000 km^2 of which 60% correspond to croplands (i.e. wheat and legumes) (Hall et al., 1999; Brooks et al., 2012) throughout Washington's Whitman County and Idaho's Latah County. The Palouse River Basin (PRB) is part of the eastern Columbia Plateau and its geology is divided in three main features: a) pre-tertiary crystalline basement rock, b) Miocene basalt flows and associated sedimentary interbeds of the Latah Formation, and c) thick Quaternary loess deposits (Murray et al., 2003). Mean annual precipitation ranges from 462 mm in the east to 1,188 mm in the west (Brooks et al., 2012). In recent years, drinking water availability has been a matter of concern in the area due to the steady decline in groundwater levels on the order of 30 cm per year (PBAC, 2012).

Stable isotope hydrology was studied in three nested watersheds within the Palouse Basin: Palouse River (Hooper, WA), North and South forks of the Palouse River (Colfax, WA) (Fig.2A). These watersheds were selected to determine the spatial and temporal (i.e. monthly) isotopic varialibility in surface waters at meso (~10^2 km^2) and large scales (~10^3 km^2). Isotopic variations at a finer time resolution (i.e. weekly and storm basis) and baseflow geochemistry were studied in two watersheds: South Fork of the Palouse River (Pullman, WA) and Crumarine Creek (Moscow, ID) (Fig.2A).

The South Fork of the Palouse River (Pullman, WA) comprises a drainage area of 342 km^2 over agricultural and urban areas (Moscow, Idaho and Pullman, Washington). Basalts of the Columbia River group covered by deposits of clayey silt loess compose the main bedrock geology feature (64.7%). Mean watershed slope is 12%. Total stream length corresponds to 586 km. Mean annual temperature is 8.22°C. Mean annual precipitation and discharge are 670 mm/yr and 97 mm/yr, respectively. Crumarine Creek is a small forested (i.e. coniferous) watershed with a drainage area of 6.35 km^2. Mean landscape slope is 28.4% with a total stream length of 8 km. Mean annual temperature is 7.27°C. Mean annual precipitation and discharge are 790 mm/yr and 230 mm/yr, respectively. The watershed is entirely composed of granitic rock producing stream beds of weathered granite.

2.2. Silver Valley

The Silver Valley also known as the Coeur d'Alene (CDA) mining district is a narrow valley (~64 km long) in the panhandle of northern Idaho (Fig. 2B) affected since the 1880s by mineral exploration and ore processing (i.e. 90 historical mines of silver, zinc, cooper, antimony, gold, and lead). The Silver Valley contains the largest underground mine in the United States (i.e. Bunker Hill Mine, with over 150 miles of workings), the deepest mine (i.e. Star-Morning, which is over 26 km deep), and the richest silver mine (i.e. Sunshine, which has produced over 10,000 metric tons of silver) (Mitchell et al., 2011). Until late 1968, when tailing ponds were established, most of the heavy metal-enriched wastes (~2,200 metric ton/day) were transported via the South Fork of the CDA River to Lake CDA (Horowitz and Elrick, 1993).

Stable isotope hydrology and baseflow geochemistry were studied in two mining-altered watersheds (i.e. Pine Creek and Canyon Creek) located within the Silver Valley (Fig.2.2). Pine Creek comprises 190 km^2 of snow dominated forested landscape with a mean watershed slope of 46.5%. Mean annual precipitation and discharge are 1,225 mm/yr and 703 mm/yr, respectively. Mean annual temperature is 5.46°C. Main underlying geology units are metamorphic (63.1%) and sedimentary

(36.9%). Pine Creek flows into the South Fork of the CDA River near the city of Pinehurst, Idaho. The Canyon Creek drainage hosted over 30 lead and silver mines and 8 mills by 1978 (Silver Valley Natural Resource Trustees, 2000). Historical lead concentrations in floodplain sediments range from 3,540 mg/kg to 136,000 mg/kg (Silver Valley Natural Resource Trustees, 2000). Canyon Creek drainage area is 60 km^2 with an average catchment slope of 46.3%. Mean annual precipitation and discharge are 1,313 mm/yr and 754 mm/yr, respectively. Mean annual temperature is 3.81°C. Canyon Creek geology is mainly metamorphic (66.1%), sedimentary (17.8%), and alluvial deposits (12.9%). Canyon Creek flows into the South Fork of the CDA River above the city of Wallace, Idaho.

2.3. Priest River area

The Priest River functions as hydrological connection between Priest Lake and the Pend Oreille River (Fig. 2C). Priest River's regional geology is mainly composed of an igneous and metamorphic culmination complex (Dougthy and Price, 1999). The Priest River Experimental Forest (PREF) is located on the western slopes of the Selkirk Mountains in northern Idaho with 90% of the land area in pristine coniferous forest. Elevation ranges from 626 m to 1,883 m. Three main drainages within the PREF are tributaries of the Priest River: Benton Creek, Canyon Creek, and Fox Creek. Stable isotope hydrology and baseflow geochemistry was studied in Benton Creek with drainage area of 7.24 km^2 (Fig. 2C). Mean watershed slope is 34.7%. Mean annual temperature is 5.67°C. Mean annual precipitation and discharge are 847 mm/yr and 240 mm/yr, respectively. Main bedrock geology is composed of granite (64.6%) and metamorphic (32.2%) features. Additionally, stable isotope samples were collected in Priest River near the city of Priest River, Idaho.

3. Methods and materials

3.1. Stable isotopes analyses

Precipitation was collected through passive collectors composed of a Buchner funnel (11.0 cm, diameter) (Fischer Scientific, USA) coupled with a fabric filter mesh (3 mm, diameter) to prevent sample contamination (e.g. dust, pollen, insects, debris). The funnel was connected to a 4L high density polyethylene container (HDPE) using silicone tubing (1 cm, diameter). A 2 cm thick mineral oil (Aspen Veterinary Resources Ltd., USA) layer was added to prevent fractionation according to standard sampling protocols (Kendall and McDonnell, 1998). Mineral oil was separated using a 500 mL glass separatory funnel (Fischer Scientific, USA). Samples were stored upside down at 5°C in 30 mL glass E-C borosilicate bottles with TFE-lined caps (Wheaton Science Products, USA). Bottles were filled with no head space and covered with parafilm (Thermo Scientific, USA) to avoid exchange with atmospheric moisture. Snow samples were collected using a snow sampler Model 3600 (4.13 cm, diameter) (Rickly Hydrological Company, USA). Snow cores were melted in sealed plastic bags. Samples were immediately transferred and stored upside down at 5°C in 30 mL glass E-C borosilicate bottles with TFE-lined caps (Wheaton Science Products, USA).

Surface water samples were collected using an automated sampler ISCO 3700 (Teledyne ISCO, USA) on a weekly basis at fixed times (1500 Pacific Standard Time) in each monitoring station. Storm sampling was conducted using a pressure transducer PT12 (INW, USA) connected to the automated sampler through a data logger CR10X (Campbell Scientific, USA). A 2 cm thick mineral oil (Aspen Veterinary Resources Ltd., USA) layer was added to 1L HDPE bottles to prevent evaporation during storage (Kendall and McDonnell, 1998). Mineral oil was separated using a 250 mL glass separatory funnel (Fischer Scientific, USA). Manual samples were collected in 30 mL glass E-C borosilicate bottles with TFE-lined caps (Wheaton Science Products, USA). Bottles were filled with no head space and covered with parafilm

(Thermo Scientific, USA) to prevent exchange with external moisture sources. All samples were stored upside down at 5°C until analysis. Supplementary materials (Table S3 and S4) present a summary of surface water and precipitation sampling locations in the inland PNW, including site identification, geographic coordinates, station elevation, period of record, number of samples, and sampling frequency.

Stable isotope analyses were conducted at the Idaho Stable Isotope Laboratory, University of Idaho (Idaho, USA) using a Cavity Ring Down Spectroscopy (CRDS) water isotope analyzer L1120-i (Picarro, CA) following the methods described by Lis et al. (2008). Laboratory standards, previously calibrated to the VSMOW2-SLAP2 reference waters, were EAG (δ^2H= −255.0‰, δ^{18}O= −30.8‰), CAS (δ^2H= −64.2.3‰, δ^{18}O = −8.3‰), and DDI (δ^2H= −15.4‰, δ^{18}O= −125.5‰). EAG and CAS were used to normalize the results to the VSMOW2-SLAP2 scale while DDI was a quality control standard. The laboratory precision on average was ±0.5‰ (1σ) for δ^2H and ±0.1‰ (1σ) for δ^{18}O. The *d*-excess analytical uncertainty was ±0.6‰ (1σ).

Periodic regression analysis (DeWalle et al., 1997) was used to fit a seasonal sine-wave model to δ^{18}O fluctuations as:

$$\delta 18O_p = \delta 18\bar{O} + A[\cos(ct - \theta)] \quad (3)$$

where $\delta^{18}O_p$ is the predicted δ^{18}O in ‰, $\delta^{18}\bar{O}$ is the annual mean δ^{18}O value in ‰, *A* is δ^{18}O annual amplitude in ‰, *c* is the radial frequency of annual fluctuations or 0.017214 rad d^{-1}, *t* is time in days after the beginning of the sampling, and θ is the phase lag or time of annual peak δ^{18}O in radians. The damping ratio (*D*) of the precipitation isotopic signal in the observed stream isotopic response was calculated as the ratio of the standard deviation of stream water isotopic composition (i.e. all data points) (SD_s) to the standard deviation of precipitation isotopic composition (SD_p) (McGuire, 2004):

$$D = \frac{SD_s}{SD_p} \quad (4)$$

Additionally, a preliminary estimation of MTTs was conducted using the exponential well-mixed model (Maloszewski et al., 1982):

$$\tau = c^{-1}[(D)^{-2} - 1]^{0.5} \quad (5)$$

where τ is the MTT in days, c is the radial frequency of annual fluctuations or 0.017214 rad d^{-1}, $\delta^{18}O_s$ and $\delta^{18}O_p$ correspond to the $\delta^{18}O$ amplitudes in the stream and precipitation, respectively.

3.2. Baseflow mean transit time simulations

Baseflow MTTs were estimated using the lumped parameter computer program FLOWPC 3.2 (http://www-naweb.iaea.org/napc/ih/IHS_resources_sampling.html) (Maloszewiski and Zuber, 1996) in five selected watersheds (i.e. SF Palouse River, Crumarine Creek, Pine Creek, Canyon Creek, and Benton Creek). Stream $\delta^{18}O$ values during runoff events were excluded, thus, the convolution age estimates were limited by the sample size of baseflow observations. FLOWPC has been widely applied to estimate MTT in a several hydrologic applications (Maloszewiski, 2000; Zuber et al., 2004; Katz et al., 2004; Viville et al., 2006; Einsiedl et al., 2009). Model parameters (τ, η, *D/vx*) for the different models (EM, EPM, DM) were obtained by trial and error in order to fit measured output isotope ratios. In FLOWPC, the goodness of the fit is determined as:

$$\sigma = \frac{\sqrt{\sum_{i=0}^{n}(C_m - C_p)^2}}{n} \quad (6)$$

where C_m and C_p are the measured and predicted tracer compositions, n is the number of observations. In order to complement the evaluation of the simulations in FLOWPC, other authors (Viville et al., 2006; Stumpp et al., 2009) have suggested the incorporation of the following goodness of fit criteria (Table 2): index of agreement *d* (Willmot, 1981), root mean square error *RMSE*, and the mean absolute error *MAE*. The index of agreement *d* proposed first by Willmot (1981) intends to overcome the insensitivity of the coefficient of determination r^2 to differences in the observed and predicted means and variances (Legates and McCabe, 1999). The index of agreement *d* ranges from 0 (i.e. no correlation) to 1 (i.e. perfect fit). The *MAE* and *RMSE* add the errors provide the absolute mean deviation from the measurements.

3.3. Aqueous geochemistry

A baseflow geochemical characterization was conducted during the 2013 summer (i.e. from May, 29 to September, 17, 2013) in five watersheds (i.e. Crumarine Creek, South Fork Palouse River, Canyon Creek, Pine Creek, and Benton Creek, Fig.2). Six manual samples were collected every three weeks in 125 mL high density polyethylene (HDPE) bottles. Extended alkalinity (i.e. total alkalinity, HCO_3^-, CO_3^{2-}, OH^-), pH, major anions (i.e. F^-, Cl^-, Br^-, NO_2^-, NO_3^-, PO_4^{3-}, and SO_4^{2-}), and dissolved metals (i.e. Ba, Ca, Cd, Co, Cr, Cu, Fe, K, Mg, Mn, Mo, Na, Ni, V, Zn) were analyzed at the Analytical Sciences Laboratory, University of Idaho, USA. Additionally, dissolved Pb was analyzed in two mining-altered watersheds (i.e. Pine Creek and Canyon Creek, Silver Valley, Fig. 2.3). Extended alkalinity samples were collected with no head space and immediately covered with Parafilm (Thermo Scientific, USA) to prevent atmospheric CO_2 exchange. Extended alkalinity was conducted by a tritimetric method (Method 310.1, USEPA, 1978). The reporting limit averages 3 mg/L $CaCO_3$. Determination of inorganic anions was conducted by ion chromatography (Method 300, USEPA, 1993) using a Dionex DX-100 Ion Chromatograph. Reporting limits average 0.15 mg/L (F^-), 0.2 mg/L (Cl^-), 0.05 mg/L (NO_2-N), 0.1 mg/L (Br^-), 0.05 mg/L (NO_3-N), 0.1 mg/L (PO_4-P), and 0.2 mg/L (SO_4^{2-}). Dissolved metal samples were acidified in situ (i.e. pH~2) to avoid precipitates. Samples were analyzed using Inductively Coupled Plasma Optical Emission Spectroscopy (Method 200.7, USEPA, 2001). Dissolved Pb was analyzed by Inductively Coupled Plasma Mass Spectrometry (Method 200.8, USEPA, 2007) (reporting limit 0.0025 μg/mL).

4. Results and discussion

4.1. δ^2H and δ^{18}O in precipitation

The δ^2H and δ^{18}O values of 316 precipitation samples collected in the Palouse Region (*n* = 203), Silver Valley (*n* = 87), and Priest River area (*n* = 26) between September 2011 and January 2014 are presented in Fig. 3. The precipitation isotope data are presented in the Supplemental materials (Table S5). The δ^2H and δ^{18}O ratios of precipitation in the Palouse Region ranged from −207.1‰ to −32.6‰ and −27.7‰ to −4.5‰, respectively. A least squares regression of the precipitation isotope data resulted in highly significant Palouse Region meteoric water line (PMWL); $\delta^2H = 7.45 \cdot \delta^{18}O + 1.78$ (r^2 = 0.97, Fig. 3). The simulated mean annual δ^{18}O composition of precipitation in the Palouse Region was −14.7‰, with extremes ranging from −17.2‰ up to −9.8‰. The δ^2H and δ^{18}O ratios in the Silver Valley ranged from −170.0‰ to −56.6‰ and −22.7‰ to −6.7‰, respectively. A least squares regression of the precipitation isotope data resulted in a significant Silver Valley meteoric water line (SVMWL); $\delta^2H = 7.28 \cdot \delta^{18}O - 1.75$ (r^2 = 0.96, Fig. 3). The simulated mean annual δ^{18}O composition of precipitation in the Silver Valley was −14.5‰, with δ^{18}O values ranging from −17.0‰ up to −10.5‰. The δ^2H and δ^{18}O ratios in the Priest River area ranged from −181.3‰ to −78.2‰ and −24.4‰ to −9.7‰, respectively. A least squares regression of the precipitation isotope data resulted in a significant Priest River area meteoric water line (PRMWL); $\delta^2H = 7.42 \cdot \delta^{18}O + 0.67$ (r^2 = 0.99, Fig. 3). The simulated mean annual δ^{18}O composition of precipitation in the Priest River area was −16.2‰, with δ^{18}O values ranging from −18.5‰ up to −11.5‰.

A Kruskall–Wallis non-parametric test revealed there was no significant difference (*p* = 0.086) in the hydrogen and oxygen isotope data collected in the three study areas; therefore, an inland PNW meteoric water line based on all the precipitation samples can be described as: $\delta^2H = 7.42 \cdot \delta^{18}O + 0.88$ (*n* = 316; r^2 = 0.97). Long-term isotopic records (> 2 years) in precipitation within the inland PNW

are scarce. Indeed, no stations are reported in the Global Network of Isotopes in Precipitation (GNIP, 2006) data base of the International Atomic Nuclear Agency (IAEA) and the World Meteorological Organization (WMO). Previous site-specific studies in the inland PNW have reported few meteoric water lines that also presented lower slopes and intercepts values: $\delta^2H = 7.1 \cdot \delta^{18}O - 5$ (Palouse region, Koeniger et al., 2008) and $\delta^2H = 6.9 \cdot \delta^{18}O - 18.5$ (Palouse region, Larson et al., 2000). A 10-yr LMWL was reported by Peng et al. (2004) for Calgary, Canada (i.e. close to the Canada-US border above northern Idaho): $\delta^2H = 7.68 \cdot \delta^{18}O - 0.21$.

Lower slopes and intercepts are usually attributed to convective recycling processes (Wassenaar et al., 2011); especially in semi-arid regions where soil and surface water evaporation losses (i.e. moisture enriched in δ^2H and $\delta^{18}O$) can mix with air masses resulting in lower values. Overall, δ^2H and $\delta^{18}O$ values in the inland PNW showed a temperature-dependent seasonality (Fig. 4A). Enriched or more positive values occurred during late spring and summer rains (May-October) whereas lower or more negative values were observed throughout the winter (November-April).

4.2 Deuterium excess and temperature correlation

The *d*-excess value of precipitation in the Palouse Region, Silver Valley, and Priest River areas ranged from −7.8‰ to +20.9‰ (mean = +9.8‰), −10.5‰ to +21.0 (mean = +8.7‰), −0.4‰ to +14.8 (mean = +10.0‰) (Fig. 4B), respectively, compared to the global mean *d*-excess +10.0‰ (Araguas-Araguas et al., 2000). Positive deviations (+10‰ to +30‰) in *d*-excess values indicate enhanced moisture recycling whereas negative deviations (−10‰ to +10‰) correspond to an indication of mixing of evaporation losses (Froehlich et al., 2002). Overall, *d-excess* values in the Priest River area were less variable and reflect less influence of recycling moisture or secondary evaporation process than observed in the Palouse Region and Silver Valley areas.

The lowest *d*-excess values were observed during the summer months and early fall whereas greater values were observed in the winter seasons (Fig. 4B). Low *d*-excess values for precipitation in the inland PNW, particularly during the summer, revealed the incorporation of local recycled water vapor into the air mass and potential secondary evaporation of rainfall during small rain events. In semi-arid regions, summer rainfalls from thunderstorms that obtain moisture mainly from local evapotranspiration are known to produce more negative *d*-excess values (Peng et al., 2004; Wassenaar et al., 2011). Basically, water drops below the cloud base may become isotopically more enriched in the heavy isotopes δ^2H and δ^{18}O by kinetic isotope effects during evaporation as they fall towards the ground surface (Miyake et al., 1968; Steward 1975; Jouzel, 1986). The greater *d*-excess values observed (+14.9‰ to +21‰) during the winter are correlated with non-equilibrium conditions during the formation of snow (Jouzel and Merlivat 1984) (Fig. 4B).

The δ^{18}O values of precipitation in the Palouse Region (2011-2014) and the average ground air temperature (T) during the sampling period are presented in Fig. 4C. The significant relationship ($p < 0.001$) between δ^{18}O values and average air temperature was $\delta^{18}O = 0.30 \cdot T - 15.9$ ($r^2 = 0.32$) (Fig. 4C). Lower air temperatures resulted in depleted δ^{18}O values whereas greater temperatures are correlated with enriched δ^{18}O compositions, supporting the seasonal behavior presented in Fig. 4A. This correlation was first observed by Dansgaard (1964) ($\delta^{18}O = 0.69 \cdot T - 13.9$ ‰). In the Calgary area, close to the northern Idaho US-Canada border Peng et al. (2004) ($\delta^{18}O = 0.46 \cdot T - 19.35$ ‰) and Wassenaar et al. (2011) ($\delta^{18}O = 0.33 \cdot T - 16.6$ ‰) reported similar correlations.

4.3. δ^2H and δ^{18}O in surface waters

The relationship of δ^2H and δ^{18}O values in surface waters in the inland PNW is presented in Fig. 5 along with the inland PNW meteoric water line as reference. The surface water isotope data are presented in the Supplemental materials (Table S6). As expected for a semi-arid region, meteoric water lines of surface waters exhibit low

slopes ranging from 3.99 to 6.09 and negative intercepts ranging from −18.02‰ to −50.1‰ indicating evaporation enrichment. In the Palouse Basin, the combination of low elevations, flat landscapes, and large surface travel times facilitate the evaporation enrichment along the stream networks as observed in Fig. 5A and 5B (i.e. scattering below the LMWL). The isotopic composition of surface waters in mountainous watersheds is less variable, which is represented by a tight cluster of data points close to the mean annual isotopic composition of precipitation (Fig. 5C and 5D).

Figure 6 shows the seasonal stream $\delta^{18}O$ variations compared to the volumetric discharge for all sampled streams. Stream $\delta^{18}O$ values in Crumarine Creek and the South Fork of the Palouse River (Pullman, WA) ranged from −13.7‰ to −17.7‰ (mean = −15.2‰) and −12.9‰ to −17.7‰ (mean = −15.0‰) (Fig. 6A and 6B), respectively. In the lower section of the Palouse Basin, $\delta^{18}O$ ratios in the South Fork and North Fork of the Palouse River (Colfax, WA) varied from −11.5‰ to −18.0‰ (mean = −14.5‰) and −10.6‰ to −16.8‰ (mean = −14.3‰), respectively. By the outlet of the Palouse River (Hooper, WA), $\delta^{18}O$ composition ranged from −12.5‰ to −17.8‰ (mean = −14.1‰) (Fig. 6C). In the Silver Valley, stream $\delta^{18}O$ values in Canyon Creek and Pine Creek ranged from −14.2‰ to −17.0‰ (mean = −15.8‰) and −14.5‰ to −16.2‰ (mean = −15.3‰) (Fig. 6D and 6E), respectively. In the Priest River area, $\delta^{18}O$ composition in Benton Creek and Priest River varied from −14.7‰ to −15.6‰ (mean = −15.5‰) and −15.2‰ to −15.7‰ (mean = −15.5‰) (Fig. 6F and 6G), respectively.

Despite the observed seasonal variation in precipitation in the inland PNW, seasonal stream $\delta^{18}O$ variations were very small. Standard deviations (1σ) of $\delta^{18}O$ values among all streams ranged from 0.13‰ (Priest River) up to 1.44‰ (North Fork of the Palouse River) compared to the range of standard deviations in precipitation (3.52‰, Palouse Region; 3.04‰, Silver Valley; 3.39‰, Priest River area). However, a large snowmelt event (March, 26th, 2012) produced a considerable depletion in the isotopic composition of stream waters up to −18‰ $\delta^{18}O$ (Fig.6). This snowmelt event was caused by a rapid warming up to 18°C resulting in a large depleted runoff

contribution. In the 2013 water year, snowmelt runoff was gradual resulting in less depleted runoff inputs to stream waters. Overall, $\delta^{18}O$ values during summer baseflow periods exhibited a closer composition to the mean annual $\delta^{18}O$ of precipitation whereas more depleted values were observed during winter and spring runoff events caused by depleted rains and snowmelt inputs. In the lower section of the Palouse Basin, a clear seasonal trend was observed with isotopic enrichment occurring in the summer time and depletion during the winter season (Fig. 6C).

4.4. $\delta^{18}O$ damping ratios and mean transit times

The relative age differences among the study watersheds can be shown by the damping ratio of the observed isotopic composition of precipitation in the observed stream water isotopic signal. Since the standard deviation of $\delta^{18}O$ in precipitation is quite similar across the inland PNW (3.04‰ up to 3.39‰), the damping ratio highly depends on the stream $\delta^{18}O$ variability. Streams with a high groundwater contribution such as those found in forested watersheds tend to exhibit a fairly constant isotopic composition (Fig. 6D, 6E, 6F) whereas human altered watersheds where runoff is a dominant process tend to have a more variable $\delta^{18}O$ composition (Fig. 6B). The damping ratios in the agricultural and urban altered watersheds of Crumarine Creek and the South Fork of the Palouse River (Pullman, WA) were 0.20 and 0.25, respectively. In the Silver Valley area, the mining-altered watersheds of Canyon Creek and Pine Creek exhibited a damping ratio of 0.12 and 0.09, respectively. In the Priest River area, the damping ratio of the pristine forested watershed of Benton Creek was 0.05.

Table 3 shows the baseflow mean transit times (bMTT) and goodness of fit metrics for each selected watershed. In Crumarine Creek (6.35 km^2, 100% granitic, forested watershed), the best model fit (r^2 = 0.41; σ = 0.056 ‰) with the observed $\delta^{18}O$ values was exhibited by the EM which resulted in a bMTT of 1.0 year. Likewise, in Benton Creek (7.4 km^2, 65% granitic, forested watershed), the best TTD was described by EM (r^2 = 0.25; σ = 0.045 ‰) which translates in a bMTT of 3.2 years.

The baseflow discharge behavior within the mining-altered watersheds dominated by sedimentary (66 % – 63 %) and metamorphic (17% − 37%) basement rocks was better described by the DM (D_p = 0.6). The bMTT were 1.5 and 0.73 years in Pine Creek (r^2 = 0.34; σ = 0.042 ‰) and Canyon Creek (r^2 = 0.27; σ = 0.034 ‰), respectively. The human-altered watershed, South Fork of the Palouse River, as expressed in a high damping ratio (D = 0.25, Fig. 7) was poorly correlated (Table 3) with all the weighting functions. Return flows such as irrigation or wastewater treatment plant outflow, especially during the summer season, could result in isotopic disturbances that may bias the $\delta^{18}O$ input-output relationship. In the South Fork of the Palouse River, bMTT ranged from 0.42 up to 0.62 years. A high discrepancy was found between the evaluation of model simulations between the index of agreement d and the coefficient of determination r^2 (Table 4). Relative high d values (i.e. indicating strong data fits) usually over 0.65 have been reported as a disadvantage of this method (Krause et al., 2005). In general, *MAE* (0.10 ‰ up to 0.62 ‰) and *RSME* (0.13 ‰ up to 0.74 ‰) indicated a low to moderate deviation from the $\delta^{18}O$ measurements.

A highly significant power regression ($\tau = 0.11D^{-1.09}$; r^2 = 0.83) was found between the bMTT and the damping ratio. A significant linear regression ($\tau = -10.9D + 2.93$; r^2 = 0.65, not shown in Fig. 7) was also found. McGuire (2004) reported a similar relationship ($\tau = -26.2D + 3.63$; r^2 = 0.82) in small catchments in the Western Cascades of Oregon. Overall, the relative MTT estimated by the sine-wave and periodic regression approach were slightly greater than the bMTT obtained with the lumped-parameter models. The relationship between the MTT and bMTT can be described as: bMTT = 1.03·MTT – 0.197; r^2 = 0.93. Although, the sine-wave method is computationally simple, it does not allow for the evaluation of multiple TDD, since an exponential behavior is assumed (See Eq.5). McGuire (2004) and DeWalle et al. (1997) have reported that the sine-wave can be used to estimate the potential maximum MTT that models are capable of simulating; nevertheless, the use $\delta^{18}O$ input-output time series and damping ratios can be used to depict potential MTT

bounds, which in turn are useful to evaluate contaminant degradation and transport times.

4.4 Baseflow geochemistry

Figure 8 shows the geochemical composition of major ions in surface waters of five selected watersheds (Crumarine Creek, South Fork of the Palouse River, Pine Creek, Canyon Creek, and Benton Creek) during the 2013 baseflow period. Additional geochemical information is presented in the Supplemental materials (Table S7). In line with the relative age estimates aforementioned, the urban and agricultural altered watersheds within the upper Palouse Basin presented a more dynamic geochemical composition over the recession period (Fig.8), whereas mountainous watersheds (Pine Creek, Canyon Creek, and Benton Creek) with greater mean transit times presented a more homogenous geochemical composition.

The baseflow geochemistry of the South Fork of the Palouse River (Pullman, WA) was dominated by Na−HCO_3 type water (i.e. Na > Ca > Mg > K and HCO_3 > Cl > SO_4 > NO_3 > F > PO_4) (See Table S5) with electrical conductivities ranging from 411 μS/cm up to 731 μS/cm and slightly basic pH (7.4−8.1). Total alkalinity ranged from 120 mg/L up to 170 mg/L $CaCO_3$. As shown in Fig. 8, the geochemical composition of the South Fork of the Palouse River evolved towards greater Na and Cl concentrations over the baseflow recession, which may be an indication of irrigation return flows rather than reflecting a natural groundwater signal. In Crumarine Creek, the dominant type water was described by Ca− HCO_3 system (Ca > Mg > K and HCO_3 > SO_4 > Cl), which comprised ~80% of the total ion composition (Fig. 8). Total alkalinity ranged from 20 mg/L up to 26 mg/L $CaCO_3$. Electrical conductivity ranging from 32 μS/cm up to 50 μS/cm coupled with near neutral pH (7.1−7.5) may indicate relative short flow paths and infiltrated snowmelt contributions, which also presented a fairly constant isotopic composition compared to the South Fork of the Palouse River.

In the mining-altered watersheds of the Silver Valley area baseflow geochemical compositions were dominated by Ca/Mg− HCO_3 type water. Greater transit times (i.e. longer water-rock contact time) compared to those in the Palouse Region are depicted by a more homogenous geochemical composition over the baseflow recession and a legacy of unique trace element fingerprints from the mining activity. In Canyon Creek and Pine Creek, total alkalinity ranged from 16−42 mg/L $CaCO_3$ and 11−14 mg/L $CaCO_3$, respectively. Canyon Creek presented greater electrical conductivities (36−123 μS/cm) than Pine Creek (16−35 μS/cm). Stream pH values were relatively similar with values ranging from 6.9−7.2 and 7.3−7.7 in Pine Creek and Canyon Creek, respectively. Sulfate constituted the second major anion with concentrations ranging from 4.8 mg/L up to 15.5 mg/L in Canyon Creek and 2.1 mg/L up to 5.4 mg/L in Pine Creek. Several heavy metals were detected in both streams (Ba, Cu, Mn, Zn, and Pb). Figure 9 shows the Zn and Pb total loads over the baseflow recession in Canyon Creek and Pine Creek. Zinc loads averaged 10 kg/d and 88 kg/d in Pine Creek and Canyon Creek, respectively. Zinc loads determined during the baseflow periods of 1994 and 1995 were 39.5 kg/d and 157 kg/d (Silver Valley Natural Resource Trustees, 2000) in Pine Creek and Canyon Creek, respectively. Lead loads averaged 55 g/d and 2.1 kg/d in Pine Creek and Canyon Creek, correspondingly. Lead loads determined during the baseflow periods of 1994 and 1995 were 363 g/d and 2.5 kg/d (Silver Valley Natural Resource Trustees, 2000) in Pine Creek and Canyon Creek, respectively. Even though significant reduction in the heavy metal transport has occurred in the study watersheds due to the absence of current explorations, the mining legacy is still an issue in the Silver Valley area, particularly during the summer months. The relatively large transit times (1.29 years to 1.71 years) found in the area could facilitate the adsorption of heavy metals in the soil matrix, but also, due to massive mining alteration, could enhance the water-rock interaction bringing contaminant solute to the surface water system.

The geochemical composition of Benton Creek was mostly dominated by Ca/Mg−HCO_3 type water (Ca > Mg and HCO_3 > SO_4 > Cl). Electrical conductivity ranged from 35 μS/cm up to 50 μS/cm and slightly acid pH (6.7−7.3). Total alkalinity ranged from 18 mg/L up to 24 mg/L $CaCO_3$. Nutrients (i.e. NO_3 and PO_4) and heavy

metals were not detected. Overall, the geochemistry data in Benton Creek during the baseflow period indicated contribution of infiltrated snowmelt with relatively low ion composition.

5. Conclusions

Isotope ratios in the inland PNW showed a temperature-dependent seasonality with a regional meteoric water line of $\delta^2H = 7.42 \cdot \delta^{18}O + 0.88$ ($n = 316$; $r^2 = 0.97$). Low *d*-excess values for precipitation in the inland PNW revealed the incorporation of local recycled water vapor into the traveling air masses and secondary basin scale evaporation processes. Despite the observed seasonal variation in precipitation, the seasonal stream $\delta^{18}O$ variation was very small. However, a significant depletion in surface waters was observed during the 2012 spring due to a large snowmelt event. Overall, the human-altered watershed showed greater isotopic variability, especially during the summer flows. Isotopic differences found in stream $\delta^{18}O$ time series across the study watersheds highlighted the relative contributions of depleted groundwater reservoirs in the streamflow regime.

A highly significant power regression ($\tau = 0.11D^{-1.89}$; $r^2 = 0.83$) was found between the MTT and the damping ratio, indicating greater subsurface travel times as the observed damping ratio decreased. Natural watersheds exhibited a lower damping ratio whereas human-altered watersheds presented greater variability. Relative MTT (i.e. sine-wave approach and damping ratio) and bMTT were greater in watersheds composed mainly of metamorphic and sedimentary basement rocks while watersheds in basalt formation presented smaller travel times. Baseflow mean transit times ranged from 0.42 − 0.62 years (human-altered and basalt-dominated landscape), 0.73 – 1.7 years (mining-altered and predominantly sedimentary rocks), and 0.67 − 3.2 years (forested and granitic-dominated watersheds). Baseflow geochemical data supported the relative water age estimates. Greater residence times were represented by more homogenous water chemistry whereas smaller residence times resulted in more dynamic compositions.

6. References

Aggarwal, P.K., Alduchov, O.A., Froehlich, K.O., Araguas-Araguas, L.J., Sturchio, N.C., Kurita, N. 2012. Stable isotopes in global precipitation: a unified interpretation based on atmospheric moisture residence time. *Geophysical Research Letters*, 39, L11705, doi:10.1029/2012GL051937.

Araguás-Araguás, L., Froehlich, K., and Rozanski, K. 2000. Deuterium and oxygen-18 isotope composition of precipitation and atmospheric moisture. *Hydrol. Process.*, 14: 1341-1355.

Asano, Y., Uchida, T., and Ohte, N. 2002. Residence times and flow paths of water in steep unchannelled catchments, Tanakami, Japan. Hydrology, 261: 173-192. http://dx.doi.org/10.1016/S0022-1694(02)00005-7

Asano Y., and Uchida T. 2012. Flow path depth is the main controller of mean base flow transit times in a mountainous catchment. *Water Resources Research,* 48, W03512, doi:10.1029/2011WR010906.

Berden G., Peeters R., and Meijer G. 2000. Cavity ring-down spectroscopy: Experimental schemes and applications. *Int. Reviews in Physical Chemistry*, 19 (4): 565-607.

Bernan E.S.F., Levin N.E., Landais A., Li S., and Owano T. 2013. Measurement of δ18O, δ17O, and 17O-excess in Water by Off-Axis Integrated Cavity Output Spectroscopy and Isotope Ratio Mass Spectrometry. *Analytical Chemistry,* (85):10392−10398, dx.doi.org/10.1021/ac402366t.

Birkel C., Soulsby C., Tezlaff D., Dunn S., and Spezia L. 2012. High-frequency storm event isotope sampling reveals time-variant transit time distributions and influence of diurnal cycles. *Hydrol. Process.* 26, 308–316, doi: 10.1002/hyp.8210.

Bowen, G., and Revenaugh, J. 2003. Interpolating the isotopic composition of modern meteoric precipitation. *Water Resources Research,* 39 (10) 1299, doi:10.1029/2003WR002086.

Brooks, E.S., Boll, J., McDaniel, P.A., 2012. Hydropedology in Seasonally Dry Landscapes: The Palouse Region of the Pacific Northwest USA. In: Lin, H. (Ed.), Hydropedology: Synergistic Integration of Soil Science and Hydrology. Academic Press, Elsevier B.V., pp. 329–350.

Broxton, P.D., Troch, P.A., and Lyon, S.W. 2009. On the role of aspect to quantify water transit times in small mountainous catchments. *Water Resources Research,* 45, W08427, doi:10.1029/2008WR007438.

Callahan B., Miles E., and Fluharty D. 1999. Policy implications of climate forecasts for water resources management in the Pacific Northwest. *Policy Sciences*, 32 (3): 269-293.

Capell, R., Tetzlaff, D., Hartley, A.J., and Soulsby, C. 2012. Linking metrics of hydrological function and transit times to landscape controls in a heterogeneous mesoscale catchment. *Hydrological Processes*, 26: 405-420. doi: 10.1002/hyp.8139

Cappa, C.D., Hendricks, M.B., DePaolo, D.J., Cohen, R.C., 2003. Isotopic fractionation of water during evaporation. *J. Geophys. Res.,* 108, 4525–4534.

Chang H., Jung I. W., Steele M., and Gannett M. 2012. Spatial patterns of March and September streamflow trends in Pacific Northwest streams, 1958–2008. *Geographical Analysis,* 44: 177–201. doi: 10.1111/j.1538-4632.2012.00847.x
Craig H. 1961. Isotopic variations in meteoric waters. *Science, 133:*1702-1703.

Dansgaard, W. 1964. Stable isotopes in precipitation. *Tellus*, 16, 436–468, doi:10.1111/j.2153-3490.1964.tb00181.x.

DeWalle, D.R., Edwards, P.J., Swistock, B.R., Aravena, R., Drimie, R.J. 1997. Seasonal isotope hydrology of three Appalachian forest catchments. *Hydro. Process.,* 11:1895-1906.

Dougthy P.T., and Price R. 1999. Tectonic evolution of the Priest River complex, northern Idaho and Washington- A reappraisal of the Newport fault with new insights on metamorphic core complex formation. *Tectonics,* 18(3):375-393.

Dunn, S.M., McDonnell, J.J., and Vaché, K.B. 2007. Factors influencing the residence time of catchment waters: A virtual experiment approach *Water Resources Research,* 43, W06408, doi:10.1029/2006WR005393.

Einsiedl, F., Maloszewski, F., and Stichler, W. 2009. Multiple isotope approach to the determination of the natural attenuation potential of a high-alpine karst system. Hydrology, 365:113–121. doi:10.1016/j.jhydrol.2008.11.042

Elsner M.M., Cuo L., Voisin N., Deems J.S., Hamlet A.F., Vano J.A., Mickelson K., Lee S., Lettenmaier D.P. 2010. Implications of 21st century climate change for the hydrology of Washington State. *Climatic Change,* 102: 225–260, doi:10.1007/s10584-010-9855-0.

Frederickson, G.C., and Criss, R.E. 1999. Isotope hydrology and residence times of the unimpounded Meramec River Basin, Missouri. *Chemical Geology,* 157:303-317.

Froehlich, K., Gibson, J.J., and Aggarwal, P. 2002. Deuterium excess in precipitation and its climatological significance. *Study of environmental change using isotope techniques*, C&S Papers Series 13/P, pp. 54-65, International Atomic Energy Agency, Vienna, Austria, ISBN 92-0-116402-5.

GNIP. 2006. Global Network of Isotopes in Precipitation. Available at http:// www naweb.iaea.org/napc/ih/IHS_resources_gnip.html (IAEA Isotope Hydrology, Vienna, Austria). Accessed January 15, 2014.

Godsey, S.E., Aas, W., Clair, T.A., de Wit, H.A., Fernandez, I.J., Kahl, S.J., Malcolm, I.A., Neal, C., Neal, M., Nelson, S.J., Norton, S.A., Palucis, M.C., Skjelkvåle, B.L., Soulsby, C., Tetzlaff, D., and Kirchner, J.W. 2010. Generality of fractal 1/f scaling in catchment tracer time series, and its implications for catchment travel time distributions. *Hydrological Processes,* 24: 1660–1671. doi: 10.1002/hyp.7677

Goodwin A.J. 2006. Oxygen-18 in surface and soil waters in a dry land agricultural setting, eastern Washington: flow processes and mean residence times at various watersheds scales. Masters Thesis. Washington State University. Pullman, Washington. 142 pp.

Gupta, P., Noone, D., Galewsky, J., Sweeney, C., and Vaughn, B.H. 2009. Demonstration of high-precision continuous measurements of water vapor isotopologues in laboratory and remote field deployments using wavelength-scanned cavity ring-down spectroscopy (WS-CRDS) technology. *Rapid Com. in Mass Spectrometry, 23(16): 2534-2542.* doi: 10.1002/rcm.4100.

Hall M., Young D.L., Walker D.J. 1999. Agriculture in the Palouse: a portrait of diversity. University of Idaho, Moscow, Idaho. Agricultural Communications, Bulletin 794. 20 pp.

Hamlet A.F. 2011. Assessing water resources adaptive capacity to climate change impacts in the Pacific Northwest Region of North America. *Hydrol. Earth Syst. Sci.,* 15: 1427–1443. doi:10.5194/hess-15-1427-2011.

Heidbüchel, I., Troch, P.A., Lyon, S.W. 2013. Separating physical and meteorological controls of variable transit times in zero-order catchments. *Water Resources Research,* 49, 7644–7657, doi:10.1002/2012WR013149

Horowitz A.J., and Elrick K. 1993. Effect of mining and related activities on the sediment trace element geochemistry of Lake Coeur D'Alene, Idaho, USA. Part I: surface sediments. *Hydrological Processes*, 7:403-423.

Hrachowitz, H., Soulsby, C., Tetzlaff, D., Malcolm, A., and Schoups, G. 2010. Gamma distribution models for transit time estimation in catchments: Physical interpretation of parameters and implications for time-variant transit time assessment. *Water Resources Research,* 46, W10536. doi:10.1029/2010WR009148

Hrachowitz, M., Savenije, H., Bogaard, T.A., Tetzlaff, D, and Soulsby, C. 2013. What can flux tracking teach us about water age distribution patterns and their temporal dynamics? *Hydrological Earth Systems Sciences,* 17:533–564. doi:10.5194/hess-17-533-2013.

Jouzel, J. and Merlivat, L. 1984. Deuterium and oxygen-18 in precipitation: modelling of the isotopic effect during snow formation. *J.Geophys. Res.* 89, 11 749–11 757.

Jouzel, J. 1986. Isotopes in cloud physics: multiphase and multistage condensation processes. In: *Handbook of Environmental Isotope Geochemistry, Vol. 2 The Terrestrial Environment, B* (eds. P. Fritz and J.Ch. Fontes). Elsevier, Amsterdam, 61–105.

Jouzel, J., Hoffmann, G., Koster, R.D., Masson, V., 2000. Water isotopes in precipitation: data/model comparison for present day and past climates. *Quat. Sci. Rev.,* 19, 363–379.

Katsuyama, M., Tani, M., and Nishimoto, S. 2010. Connection between streamwater mean residence time and bedrock groundwater recharge/discharge dynamics in weathered granite catchments. *Hydrological Processes,* 24, 2287–2299. doi: 10.1002/hyp.7741

Katz, B.G., Chelette, A.R., and Pratt, T.R. 2004. Use of chemical and isotopic tracers to assess nitrate contamination and ground-water age, Woodville Karst Plain, USA. Hydrology, 289: 36–61. doi:10.1016/j.jhydrol.2003.11.001

Kendall, C., and McDonnell, J.J (Eds). 1998. Isotope tracers in catchment hydrology. Elselvier. Amsterdam, Netherlands. 839 pp.

Krause, P., Boyle, D.P., and Bäse, F. 2005. Comparison of different efficiency criteria for hydrological model assessment. *Advances in Geosciences*, 5, 89–97. doi:10.5194/adgeo-5-89-2005

Koeniger, P., Hubbart, J. A. Link, T., and Marshall, J.D. 2008. Isotopic variation of snow cover and streamflow in response to changes in canopy structure in a snow-dominated mountain catchment. *Hydrol. Process*. 22:557–566.

Koeniger P., Leibundgut C., Link T., and Marshall J. 2010. Stable isotopes applied as water tracers in column and field studies. *Organic Geochemistry*, 41: 31–40, doi:10.1016/j.orggeochem.2009.07.006.

Lackey R.T. 2013. Providing ecosystems services for an additional 50+ million PNW residents: the challenge to natural resource and environmental agencies. Pacific Northwest 2100 project. Oregon State University, USA. http://fw.oregonstate.edu/system/files/u2937/2013p%20-%20Pacific%20Northwest%202100%20Project%20-%20Web%20Description%20-%202013.pdf.

Larson, K.R., Keller, C.K., Larson, P.B., and Allen-King, R.M., 2000. Water resource implications of 18O and 2H distributions in a basalt aquifer system. *Groundwater,* 38:947– 953.

Legates, D. R. and McCabe Jr., G. J. 1999. Evaluating the use of “goodness-of-fit” measures in hydrologic and hydroclimatic model validation. Water Resources Research, 35, 1, 233–241. doi:10.1029/1998WR900018

Lis, G.P., L.I. Wassenaar, and M.J. Hendry. 2008. High-precision laser spectroscopy D/H and 18O/16O measurements of microliter natural water samples, *Anal. Chem.,* 80(1), 287–293, doi:10.1021/ac701716q.

Lyn B., Knobel L., Hall L.F., DeWayne C., and Green J. 2004. Development of a local meteoric water line for Southeastern Idaho, Western Wyoming, and South-central

Montana. U.S. Geological Survey Scientific Investigations Report 2004-5126. Prepared in cooperation with the U.S. Department of Energy. Idaho Falls, Idaho, USA. 23pp.

Maloszewski, P. and Zuber, A. 1982. Determining the turnover time of groundwater systems with the aid of environmental tracers, I. Models and their applicability. *Hydrology,* 57: 207–231.

Maloszewski, P., and Zuber, A. 1996. Lumped parameter models for the interpretation of environmental tracer data. Manual on Mathematical Models in Isotope Hydrology, IAEA-TECDOC 910, 9–58, IAEA, Vienna.

Maloszewski, P. 2000. Lumped-parameter models as a tool for determining the hydrological parameters of some groundwater systems based on isotope data. *Tracers and Modeling in Hydrogeology* (Proceedings of the TraM'2000 Conference held at Liège, Belgium, May 2000). IAHS Publ. no. 262: 271-276.

Mayer T.D. 2012. Controls of summer stream temperature in the Pacific Northwest. *Hydrology*, 475: 323–335. http://dx.doi.org/10.1016/j.jhydrol.2012.10.012.

McCabe, G.J., and Clark, M.P. 2005. Trends and variability in snowmelt runoff in the Western United States. *Hydrometeorology,* 6 (4):476-482. doi: http://dx.doi.org/10.1175/JHM428.1.

McGuire, K.J., DeWalle, D.R., and Gburek, D.J. 2002. Evaluation of mean residence in subsurface waters using oxygen-18 fluctuations during drought conditions in the mid-Appalachians. *Hydrology*, 261: 132-149. http://dx.doi.org/10.1016/S0022-1694(02)00006-9

McGuire, K.J. 2004. Water residence time and runoff generation in the western Cascades of Oregon. Oregon State University. Corvallis, Oregon. 239 pp.

McGuire, K.J., McDonnell, J.J., Weiler, M., Kendall, C., McGlynn, B.L., Welker, J.M., Seibert J. 2005. The role of topography on catchment-scale water residence time. *Water Resources Research*, 41. doi: 10.1029/2004WR003657.

McGuire, K.J., and McDonell, J.J. 2006. A review and evaluation of catchment transit time modeling. *Hydrology,* 330, 543-563. doi:10.1016/j.jhydrol.2006.04.020

McGlynn B., McDonnel J.J., and Brammer D.D. 2002. A review of the evolving perceptual model of hillslope flowpaths at the Maimai catchments, New Zealand. *Hydrology*, *257*:1-26.

Merlivat L., and Jouzel J. 1979. Global climatic interpretation of the deuterium-oxygen 18 relationship for precipitation. *Geophysical Research,* 84:4918-4922.

Miles E.L. Snover A.K., Hamlet A.F., Callahan B., Fluharty, D. 2000. Pacific Northwest Regional Assessment: The impacts of climate variability and climate change on the water resources of the Columbia River Basin. *Journal of American Water Resources Association*, 36 (2): 399-420, doi: 10.1111/j.1752-1688.2000.tb04277.x.

Mitchell, V., Reed L., and Larsen J. 2011. Geology of northern Idaho and the Silver Valley. Idaho Geological Survey. Idaho State University. Accessed on January 15, 2014. http://geology.isu.edu/Digital_Geology_Idaho/Module7/mod7.htm

Miyake, Y., Matsubaya, O. and Nishihara, C. 1968. An isotopic study on meteoric precipitation. *Pap. Meteor. Geophys.* 19, 243–266.

Moravec, B C., Keller, K.C., Smith, J.L., Allen-King, R-M., Goodwin, A.J., Fairley, J.P., and Larson, P.B. 2010. Oxygen-18 dynamics in precipitation and streamflow in a semi-arid agricultural watershed, Eastern Washington, USA . *Hydrol. Process.,* 24:446–460.

Mote P. W. 2003. Trends in snow water equivalent in the Pacific Northwest and their climatic causes. *Geophys. Res. Lett.,* 30:1601, doi:10.1029/2003GL017258.

Mote P.W., and Salathé E.P. 2010. Future climate in the Pacific Northwest. *Climatic Change.* doi:10.1007/s10584-010-9848-z.

Moxley, N. 2012. Stable isotope analysis of surface water and precipitation in the Palouse Basin: hydrologic tracers of aquifer recharge. Masters Thesis.Washington State University. Pullman, Washington. 120 pp.

Munksgaard, N.C., Wurster, C.M., Bass, A., Bird, M.I. 2012. Extreme short-term stable isotope variability revealed by continuous rainwater analysis. *Hydrol. Process.,* 26, 3630–3634, doi: 10.1002/hyp.9505.

Murray, J., O'Green A.T., and McDaniel P.A. 2003. Development of a GIS database for ground-water recharge assessment of the Palouse Basin. Soil Science, 168(11): 759-768.

Palouse Basin Aquifer Committee (PBAC). 2012. Palouse ground water basin water use report. Pullman-Moscow Area. 20 pp. http://www.webpages.uidaho.edu/pbac/.

Peng, H., Mayer B., Harris S., and Krouse H.R. 2004. A 10-yr record of stable isotope ratios of hydrogen and oxygen in precipitation at Calgary, Alberta, Canada. *Tellus,* 56B, 147–159.

Rodgers, P., Soulsby, C., Waldron, S., Tezlaff, D. 2005. Using stables isotopes tracers to assess hydrological flow paths, residence times and landscape influence in a nested mesoscale catchment. *Hydrol. Earth Syst. Sci.,* 9:139-155.

Rozanski K., Araguas-Araguas L.J., Gonfiantini, R. 1992. Relation between long-term trends of oxygen-18 isotope composition of precipitation and climate. *Science,* 258: 981-985.

Rozanski K., Araguas-Araguas L.J., Gonfiantini, R. 1993. Isotopic patterns in modern global precipitation. In Climate Change in Continental Isotopic Records, Swart PK, Lohmann KC, McKenzie J Savin S (eds) Geophysical Monograph No 67. American Geophysical Union. Washington: 1-36.

Rudestam K. 2014. Loving water, resenting regulation: sense of place and water management in the Willamette watershed. *Society and Natural Resources: An International Journal,* 27:1, 20-35, doi: 10.1080/08941920.2013.840020.

Sánchez-Murillo, R., Brooks E.S., Sampson L., Boll J., Wilhelm F. 2013. Ecohydrological analysis of Steelhead (Oncorhynchus mykiss) habitat in an effluent dependent stream in the Pacific Northwest, USA. *Ecohydrology,* doi: 10.1002/eco.1376.

Sánchez-Murillo, R., G. Esquivel-Hernández, K. Welsh, E.S. Brooks, J. Boll, R. Alfaro-Solís, and J. Valdés-González, (2013), Spatial and temporal variation of stable isotopes in precipitation across Costa Rica: an analysis of historic GNIP records, *Modern Hydrology,* 3, 226-240, doi: 10.4236/ojmh.2013.34027.

Sanghyun, K, and Sungwon, J. 2014. Estimation of mean water transit time on a steep hillslope in South Korea using soil moisture measurements and deuterium excess. *Hydrological Processes,* 28: 1844-1857. doi: 10.1002/hyp.9722

Soulsby, C., Tetzlaff, D., Rodgers, P., Dunn, S.M., and Waldron, S. 2006. Runoff processes, stream water residence times and controlling landscape characteristics in a mesoscale catchment: an initial evaluation. *Hydrology*, 325: 197–221. http://dx.doi.org/10.1016/j.jhydrol.2005.10.024

Soulsby, C., Tetzlaff, D., and Hrachowitz, M. 2009. Tracers and transit times: windows for viewing catchment scale storage? *Hydrological Processes,* 23: 3503–3507. doi: 10.1002/hyp.7501.

Speed M., Tezlaff D., Soulsby C., Hrachowitz M., and Waldron S. 2010. Isotopic and geochemical tracers reveal similarities in transit times in contrasting mesoscale catchments. *Hydrol. Process.* 24:1211–1224. doi: 10.1002/hyp.7593.

Steward, M. K. 1975. Stable isotope fractionation due to evaporation and isotopic exchange of falling water drops: applications to the atmospheric processes and evaporation of lakes. *J. Geophys. Res.* 80, 1133–1146.

Stewart, I.T., Cayan, D.R., and Dettinger, M.D. 2005. Changes toward earlier streamflow timing across Western North America. *Climate*, 18:1136-1155, doi: http://dx.doi.org/10.1175/JCLI3321.1.

Stewart, M.K., Morgenstern, U., McDonnell, J.J., and Pfister, L. 2012. The 'hidden streamflow' challenge in catchment hydrology: a call to action for stream water transit time analysis. *Hydrological Processes,* 26, 2061–2066. doi: 10.1002/hyp.9262

Stumpp, C., Maloszewski, P., Stichler, W., and Fank, J. 2009. Environmental isotope ($\delta^{18}O$) and hydrological data to assess water flow in unsaturated soils planted with different crops: Case study lysimeter station ''Wagna" (Austria). *Hydrology,* 369: 198–208. doi:10.1016/j.jhydrol.2009.02.047

Sylver Valley Natural Resources Trustees. 2000. Canyon Creek response actions 1995-1999. Kellog, Idaho, USA. 28 pp.

Tezlaff D., and Soulsby C. 2008. Towards simple approaches for mean residence time estimation in ungauged basins using tracers and soil distributions. *J. Hydrology*, 363:60– 74, doi:10.1016/j.jhydrol.2008.10.001.

Tezlaff, D., Soulsby, C., Hrachowitz, M., Speed, M. 2011. Relative influence of upland and lowland headwaters on the isotope hydrology and transit time of larger catchments. *J.Hydrology*, 400:438-447.

Uchida, T., McDonell, J.J., and Asano, Y. 2006. Functional intercomparison of hillslopes and small catchments by examining water source, flowpath and mean residence time. Hydrology, 327:627-642.

USEPA. 1978. Methods for the Chemical Analysis of Water and Wastes (MCAWW) (EPA/600/4-79/020) EPA Method 310.1: alkalinity. https://www.nemi.gov/methods/method_summary/5230/

USEPA. 1993. Determination of inorganic ions by ion chromatography. EPA Method 300. Revision 2.1. http://water.epa.gov/scitech/methods/cwa/bioindicators/upload/2007_07_10_methods_method_300_0.pdf

USEPA. 2001. Trace elements in water, solids, and biosolids by inductively coupled plasma-atomic emission spectroscopy. EPA Method 200.7. Revision 4.4. http://water.epa.gov/scitech/methods/cwa/bioindicators/upload/2007_07_10_methods_method_200_7.pdf

USEPA. 2007. Trace elements in water, solids, and biosolids by inductively coupled plasma-mass spectroscopy. EPA Method 200.8. Revision 5.4. http://water.epa.gov/scitech/methods/cwa/bioindicators/upload/2007_07_10_methods_method_200_8.pdf

van der Velde, Torfs, P. J. J. F., van der Zee, S. E. A. T. M., and Uijlenhoet, R. 2012. Quantifying catchment-scale mixing and its effect on time-varying travel time distributions. *Water Resources Research,* 48, W06536, doi:10.1029/2011WR011310

van Kirk R.W., and Naman S.W. 2008. Relative effects of climate and water use on base-flow trends in the lower Klamath basin. *Journal American Water Resources Association,* 44(4): 1032-1052, doi: 10.1111/j.1752-1688.2008.00212.x.

Viville, D., Ladouche, B., Bariac, T. 2006. Isotope hydrological study of mean transit time in the granitic Strengbach catchment (Vosges massif, France): application of the FlowPC model with modified input function. *Hydrological Processes,* 20: 1737–1751. doi: 10.1002/hyp.5950.

Wassenaar L.I., P. Athanasopoulos, and Hendry M.J. 2011. Isotope hydrology of precipitation, surface and ground waters in the Okanagan Valley, British Columbia, Canada. *J. Hydrology*, 411: 37–48, doi:10.1016/j.jhydrol.2011.09.032.

Wen X.F., Sun X.M., Zhang S.C., Yu G.R., Sargent S.D., and Lee X. 2008. Continuous measurement of water vapor D/H and 18O/16O isotope ratios in the atmosphere. *J. Hydrology*, 349, 489– 500, doi:10.1016/j.jhydrol.2007.11.021.

Willmot, C. J. 1981. On the validation of models. Physical Geography, 2,184–194. doi:10.1080/02723646.1981.10642213

Wu H., Kimball J.S., Elsner M.M., Mantua N., Adler R., Stanford J. 2012. Projected climate change impacts on the hydrology and temperature of Pacific Northwest rivers. *Water Resources Research,* 48, W11530, doi:10.1029/2012WR012082.

Zuber, A., Weiseb, S.M., Motykac, J., Osenbrückd, K., and Różánski. 2004. Age and flow pattern of groundwater in a Jurassic limestone aquifer and related Tertiary sands derived from combined isotope, noble gas and chemical data. Hydrology, 286:87–112. doi:10.1016/j.jhydrol.2003.09.004

Table 1: Weighting functions proposed by Maloszewiski and Zuber (1982).

Model	*Weighting function g(t)	Parameters	Variance
Piston flow (PFM)	$\delta(t-\tau)$	τ	0
Exponential (EM)	$\tau^{-1}\exp\left(\frac{-t}{\tau}\right)$	τ	τ^2
Exponential and piston flow (EPM)	$\frac{\eta}{\tau}\exp\left(-\frac{\eta t}{\tau}+\eta-1\right)$ for $t \geq \tau(1-\eta^{-1})$ 0 for $< \tau(1-\eta^{-1})$	τ, η	$\left(\frac{\tau}{\eta}\right)^2$
Dispersion (DM)	$\left(\frac{4\pi D_p t}{\tau}\right)^{-\frac{1}{2}} t^{-1}\exp\left[-\left(1-\frac{t}{\tau}\right)^2\left(\frac{\tau}{4\pi D_p t}\right)\right]$	$\tau, D_p = \frac{D}{vx}$	$\tau^2\left(2\frac{D}{vx}\right)$

*τ is the MTT, D_p is the apparent dispersion parameter (D_p=D/vx, the reciprocal of the Péclet number, which describes the ratio of the dispersion to advection), η is the ratio of the total volume to the volume with the exponential distribution of transit times, and $(t-\tau)$ is the Dirac delta function.

Table 2: Description of goodness of fit metrics used to evaluate FLOWPC simulations.

Metric	*Function	Reference
Root mean square error, RMSE	$\sqrt{\frac{1}{n} \cdot \sum_{i=1}^{n} \left(C_p - C_m\right)^2}$	Stumpp et al., 2009
Index of agreement, *d*	$1 - \frac{\sum_{i=1}^{n} \left(C_m - C_p\right)^2}{\sum_{i=1}^{n} \left(\left\|C_p - \bar{C}\right\| + \left\|C_m - \bar{C}\right\|\right)}$	Willmot, 1981
Mean absolute error, *MAE*	$\frac{1}{n} \sum_{i=1}^{n} \left\|C_p - C_m\right\|$	Viville et al., 2006

*$C_m, C_p, and\ \bar{C}$ are the measured, predicted, and mean measured tracer compostions; n is the number of observations.

Table 3: Baseflow mean transit times τ (years), goodness of fit σ (‰), and coefficient of determination r^2 for the EM, EMP, and DP models. The best model results per study site are in bold.

Site	EM			EPM (η = 1.5)			DM (D_p= 0.6)			DM (D_p = 0.1)		
	τ (yr)	**σ (‰)**	**r^2**	**τ (yr)**	**σ (‰)**	**r^2**	**τ (yr)**	**σ (‰)**	**r^2**	**τ (yr)**	**σ (‰)**	**r^2**
Crumarine Creek	**1.0**	**0.056**	**0.41**	0.67	0.084	0.03	0.88	0.056	0.19	0.90	0.063	0.11
SF Palouse River	0.62	0.138	0.01	**0.42**	**0.141**	**0.08**	0.54	0.124	0.05	0.55	0.161	0.01
Pine Creek	1.7	0.054	0.01	1.2	0.076	0.22	**1.5**	**0.042**	**0.34**	1.5	0.061	0.25
Canyon Creek	1.3	0.042	0.01	0.84	0.045	0.02	**0.73**	**0.034**	**0.27**	1.1	0.034	0.02
Benton Creek	**3.2**	**0.045**	**0.25**	0.67	0.057	0.16	2.8	0.055	0.16	2.9	0.096	0.01

Table 4: Additional goodness of fit metrics for FLOWPC model simulations.

Site	EM			EPM (η = 1.5)			DM (D_p= 0.6)			DM (D_p = 0.1)		
	RMSE (‰)	MAE (‰)	*d*	RMSE (‰)	MAE (‰)	*d*	RMSE (‰)	MAE (‰)	*d*	RMSE (‰)	MAE (‰)	*d*
Crumarine Creek	0.26	0.21	0.85	0.39	0.36	0.69	0.35	0.30	0.86	0.32	0.29	0.80
SF Palouse River	0.63	0.52	0.45	0.65	0.53	0.29	0.57	0.47	0.41	0.74	0.62	0.33
Pine Creek	0.21	0.18	0.83	0.29	0.25	0.72	0.16	0.13	0.90	0.24	0.20	0.77
Canyon Creek	0.16	0.14	0.85	0.17	0.15	0.85	0.13	0.10	0.88	0.13	0.11	0.89
Benton Creek	0.17	0.13	0.87	0.21	0.16	0.76	0.21	0.16	0.78	0.36	0.33	0.71

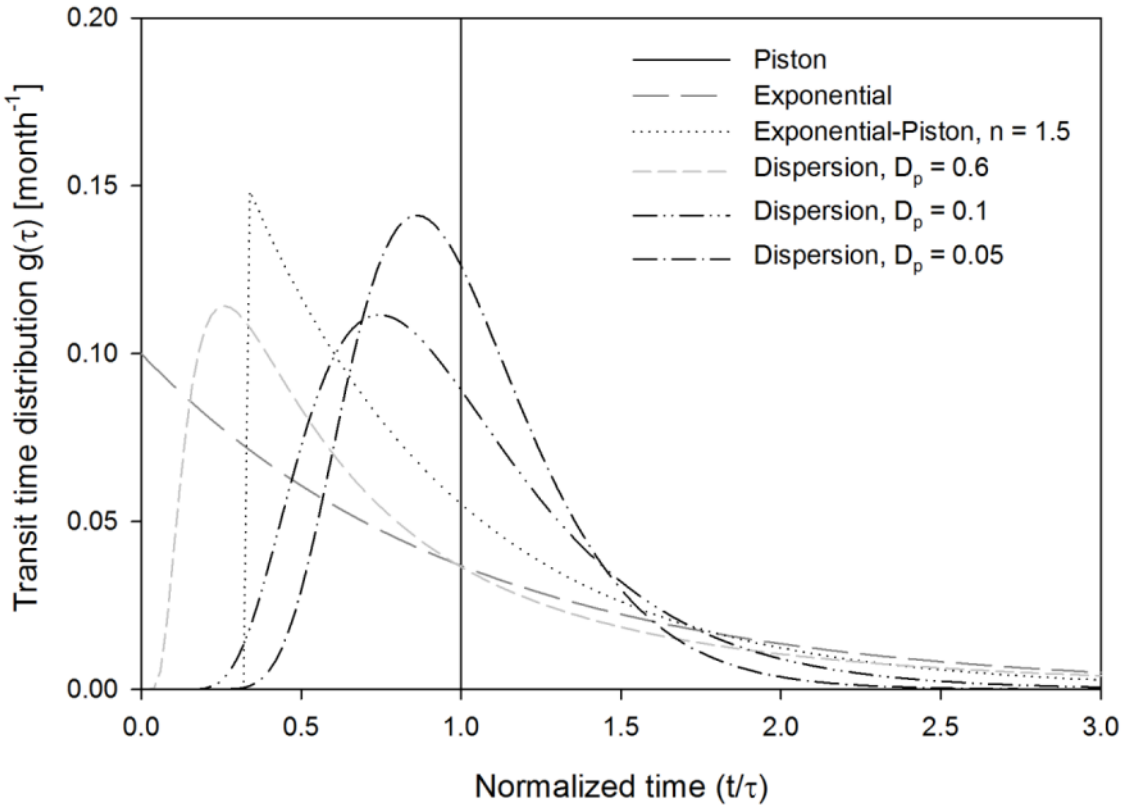

Figure 1: Examples of common mean transit time distribution functions (TTD) used in FLOWPC simulations.

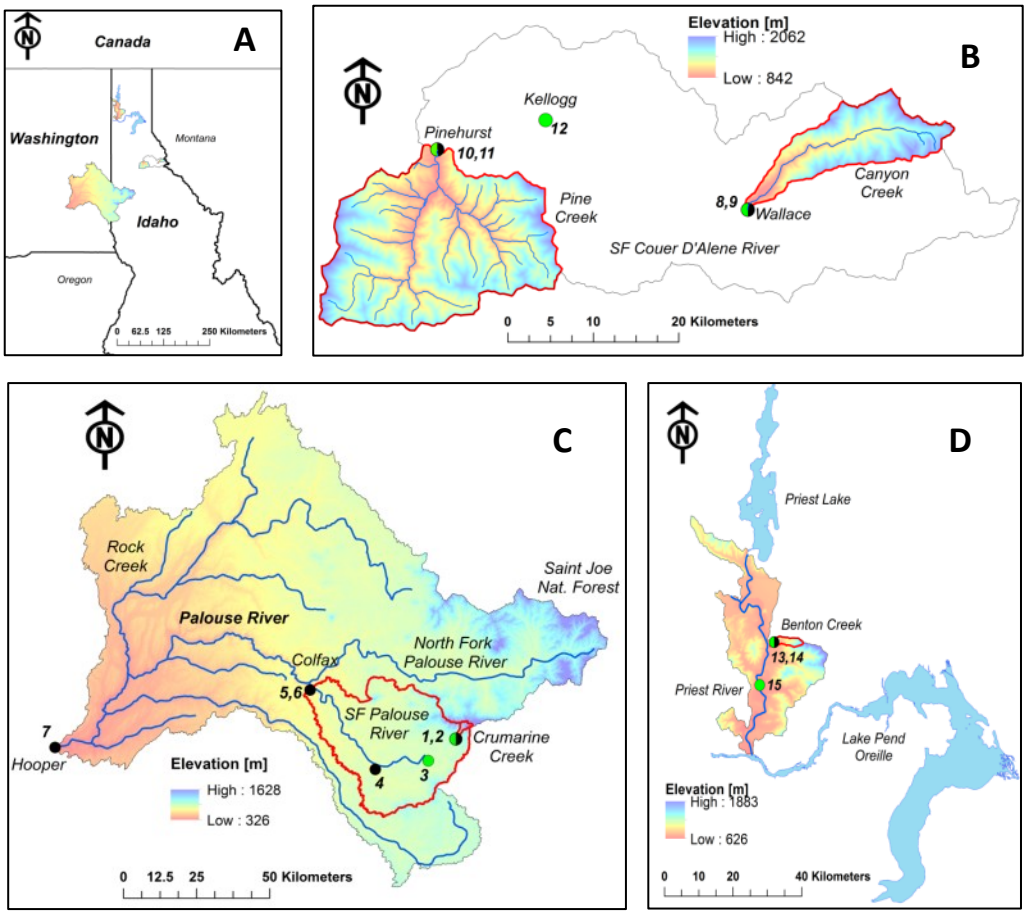

Figure 2: Study watersheds showing elevation [m], main locations and streams, and surface water (black circles) and precipitation (green circles) sampling stations. Semi-filled circles denote stations where both stream and precipitation samples were collected. The inset shows an overview of study area within the inland Pacific Northwest, USA. B) Pine Creek and Canyon Creek catchments comprise locations 8-9 (Wallace, ID), 10-11 (Pinehurst, ID), and 12 (Kellogg, ID). c) Palouse River basin includes sampling points 1-2 (Crumarine Creek), 3 (Moscow, ID), 4 (South Fork Palouse River, Pullman, WA), 5-6 (North and South tributaries of the Palouse River), and 7 (Hooper, WA). d) Lower Priest River watershed includes sampling points 12-14 (Benton Creek) and 5 (Priest River, ID).

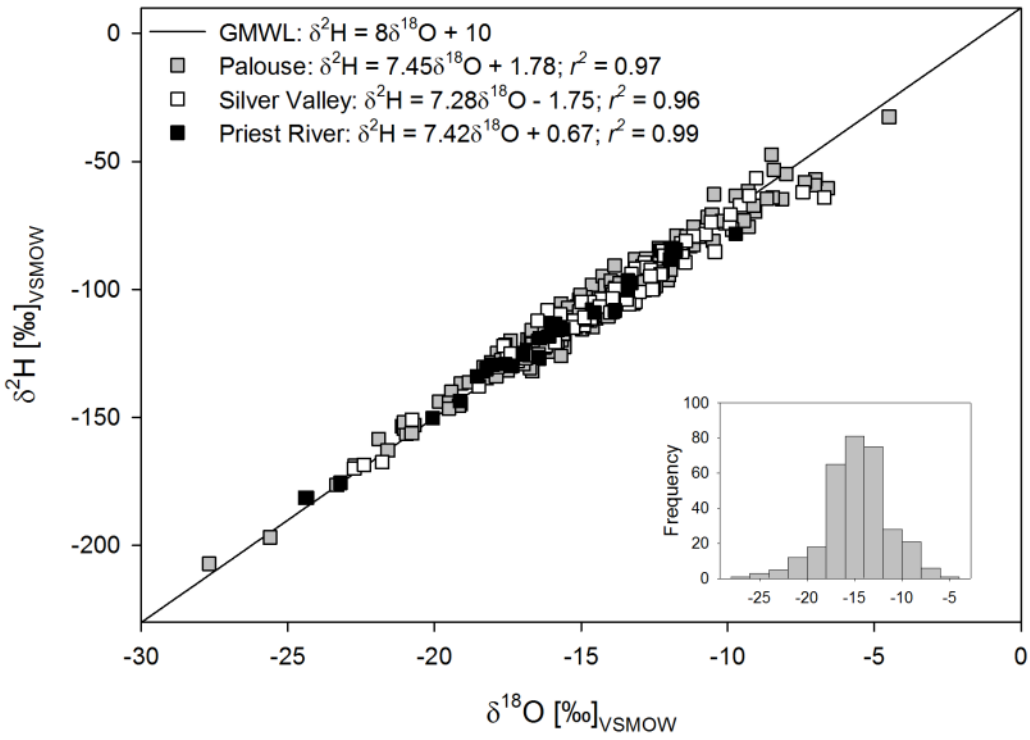

Figure 3: Isotopic composition of precipitation in the inland Pacific Northwest, USA. Grey squares represent the Palouse region meteoric water line (*n* = 203). Open squares correspond to the Silver Valley meteoric water line (*n* = 87). Black squares denote the Priest River meteoric water line (*n* = 26). Local meteoric water lines are compared to the Global Mateoric Water Line (GMWL). Inset shows a distribution of $\delta^{18}O$ values among all the sampling sites.

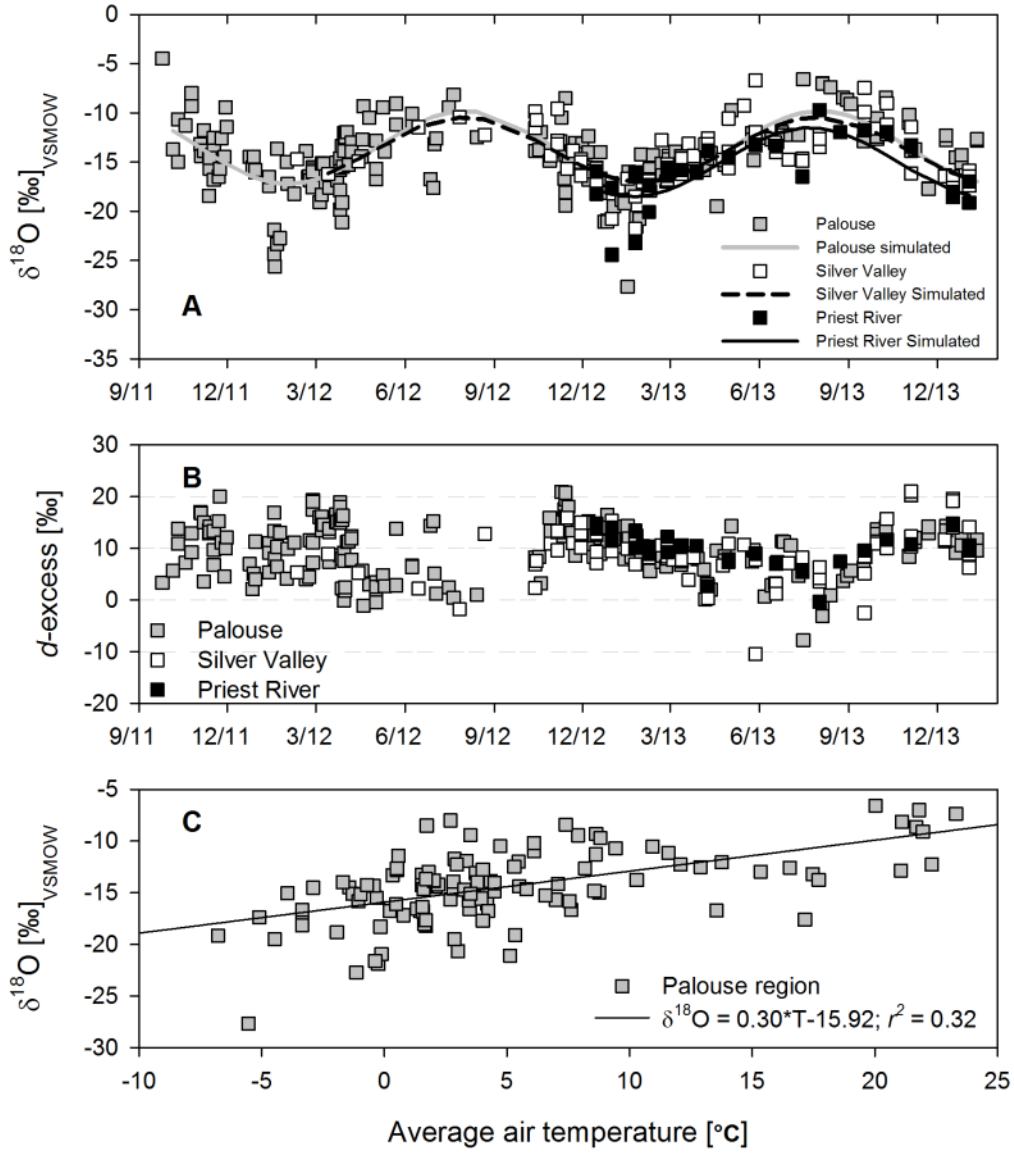

Figure 4: A) Time series of $\delta^{18}O$ [‰] in precipitation for the Palouse region (grey squares), Silver Valley (open squares), and Priest River (black squares). Isotope values show a clear seasonality effect where depleted ratios occurred during winter and enriched ratios throughout the summer and early fall. Sine-wave $\delta^{18}O$ simulations are shown (grey line, Palouse region; black dash line, Silver Valley; black line, Priest River). B) *d*-excess time series for Palouse region (grey squares), Silver Valley (open squares), and Priest River (black squares). The *d*-excess values were lowest in the summer and highest in the winter. C) Relationship of average air temperature [°C] and $\delta^{18}O$ values in the Palouse region (n = 203).

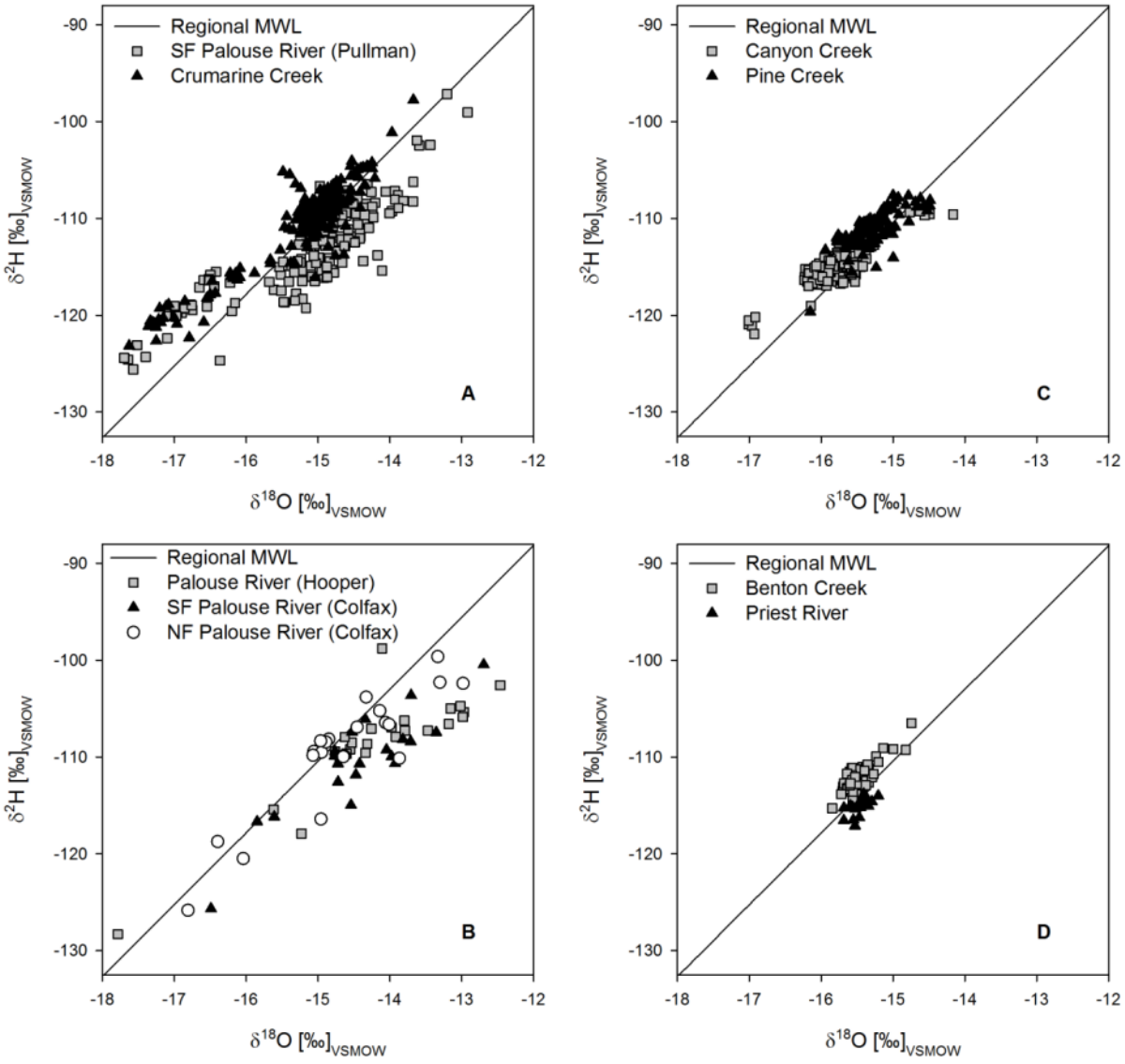

Figure 5: Isotopic composition of surface waters in the inland Pacific Northwest, USA. The regional meteoric water line is plotted as reference ($\delta^2H = 7.42 \cdot \delta^{18}O + 0.88$). A) SF Palouse River (Pullman, WA): $\delta^2H = 4.52 \cdot \delta^{18}O - 44.5$; $n = 195$, $r^2 = 0.73$. Crumarine Creek (Moscow, ID): $\delta^2H = 5.34 \cdot \delta^{18}O - 29.3$; $n = 245$, $r^2 = 0.85$. B) Palouse River (Hooper, WA): $\delta^2H = 4.47 \cdot \delta^{18}O - 45.2$; $n = 24$, $r^2 = 0.76$. SF Palouse River (Colfax, WA): $\delta^2H = 5.02 \cdot \delta^{18}O - 38.1$; $n = 23$, $r^2 = 0.88$. NF Palouse River (Colfax, WA): $\delta^2H = 4.88 \cdot \delta^{18}O - 38.2$; $n = 23$, $r^2 = 0.86$. C) Canyon Creek (Wallace, ID): $\delta^2H = 4.15 \cdot \delta^{18}O - 49.4$; $n = 158$, $r^2 = 0.71$. Pine Creek (Pinehusrt, ID): $\delta^2H = 3.99 \cdot \delta^{18}O - 50.1$; $n = 143$, $r^2 = 0.48$. D) Benton Creek (Priest River, ID): $\delta^2H = 6.09 \cdot \delta^{18}O - 18.02$; $n = 84$, $r^2 = 0.66$. Priest River (Priest River, ID): $\delta^2H = 4.57 \cdot \delta^{18}O - 44.5$; $n = 18$, $r^2 = 0.38$.

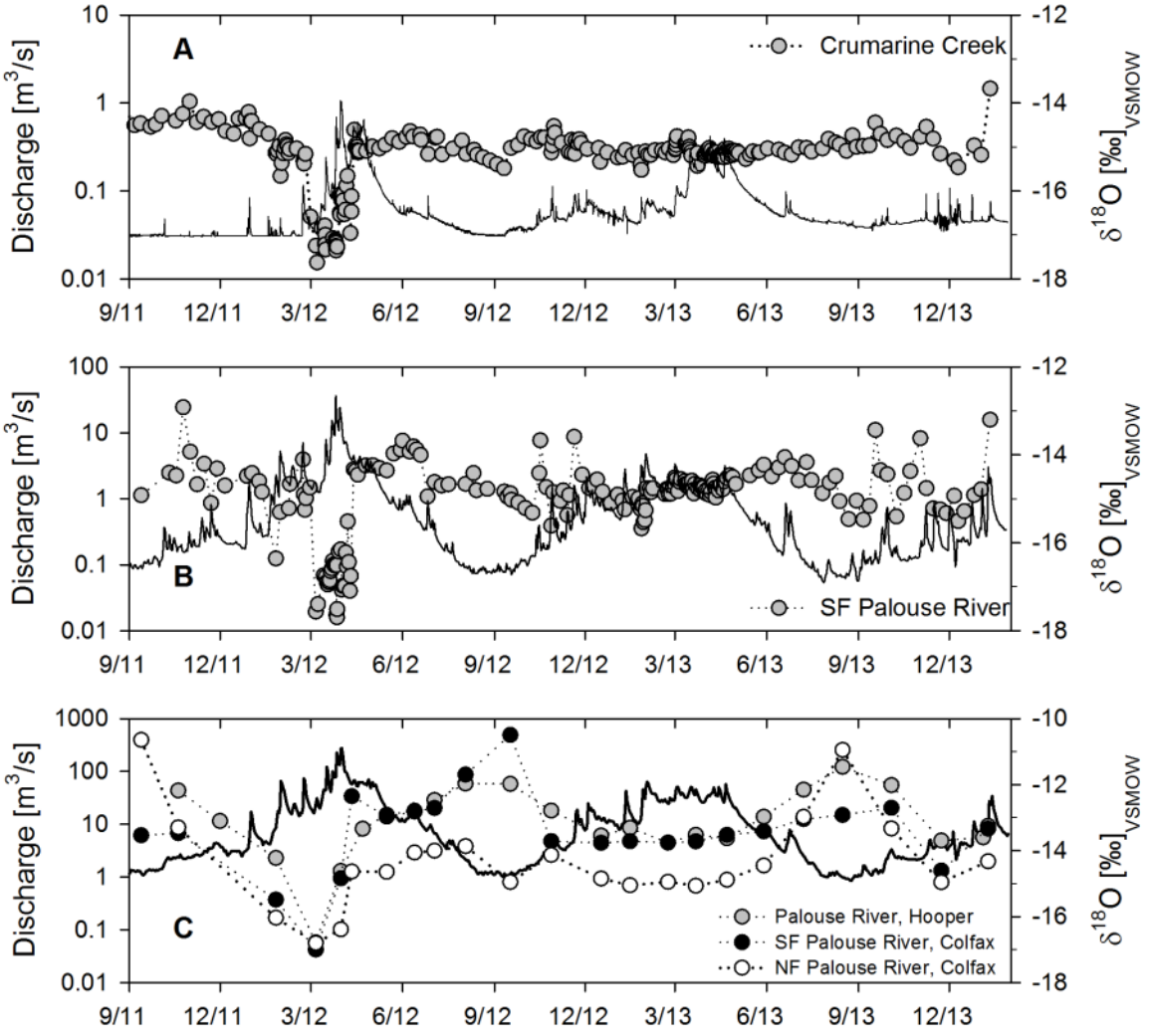

Figure 6: Time series of $\delta^{18}O$ [‰] for surface water compared to discharge [m^3 s^{-1}] at each outflow location (Fig.1). A) Crumarine Creek, Moscow Mountain, Idaho [A=6.35 km^2]. B) South Fork of the Palouse River, Pullman, Washington [A=342 km^2]. C). Palouse River (grey circles) [A=6,472 km^2], Hooper, Washington; South Fork of the Palouse River (black circles) [A=709 km^2], Colfax, Washington; North Fork of the Palouse River (open circles) [A=1,287 km^2], Colfax, Washington. Black line denotes the discharge of the Palouse River at Hooper, Washington.

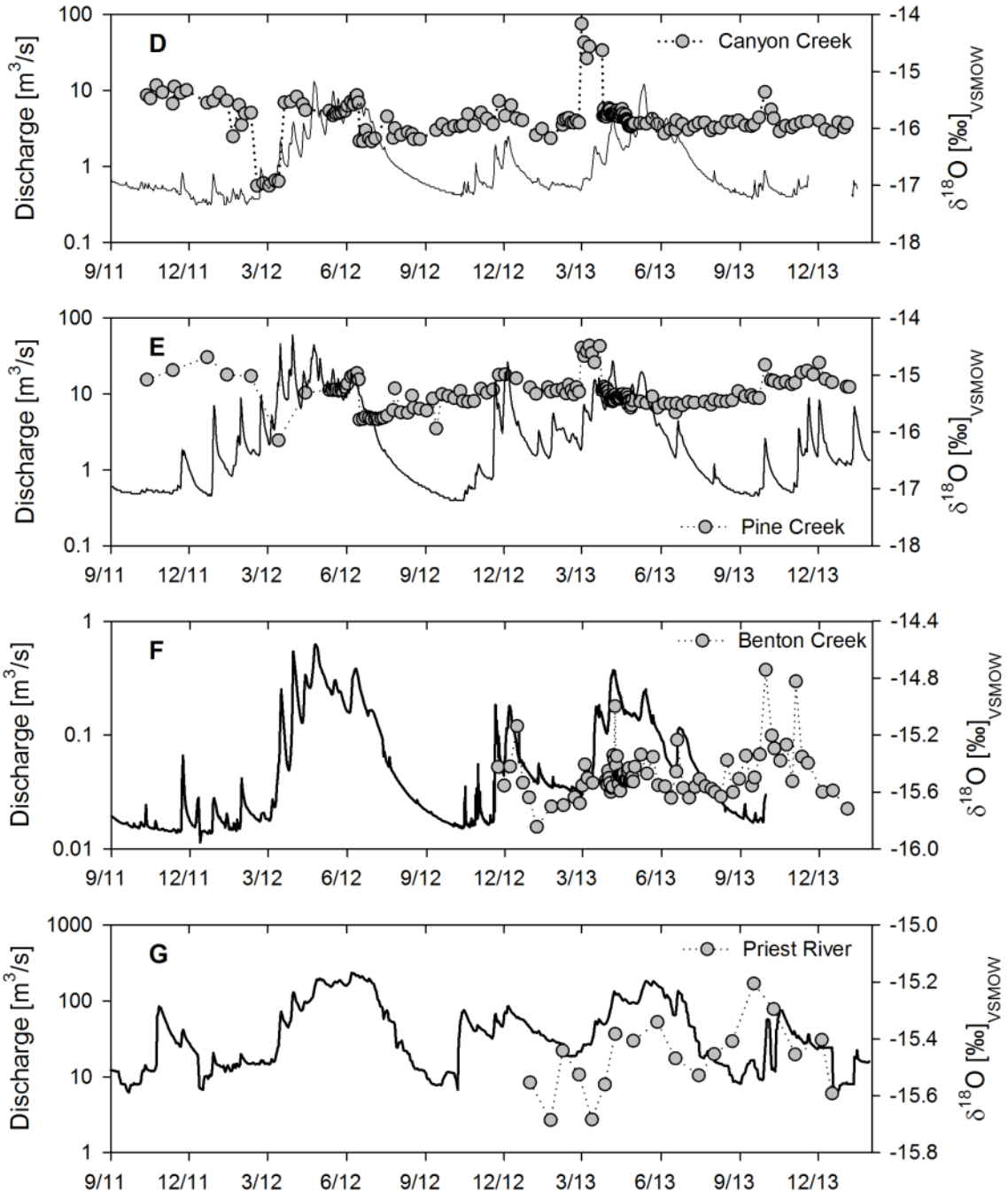

Figure 6 (continued): D) Canyon Creek [A=60 km^2], Wallace, Idaho. E) Pine creek [A=190 km^2], Pinehurst, Idaho. F) Benton Creek [A= 7.24 km^2], Priest River, Idaho. G) Lower Priest River [A=2,335 km^2], Priest River, Idaho.

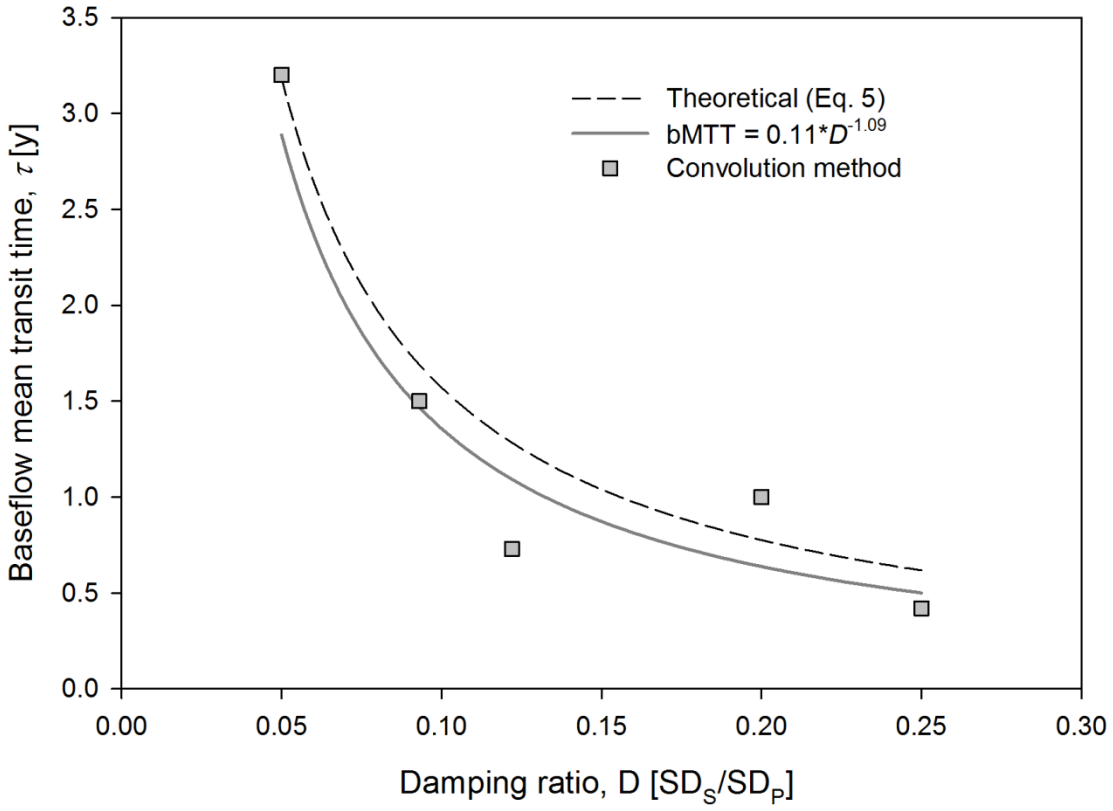

Figure 7: The relationship between baseflow mean transit time (τ) and the damping ratio of the standard deviations of $\delta^{18}O$ of stream water (SD_s) to precipitation (SD_p).

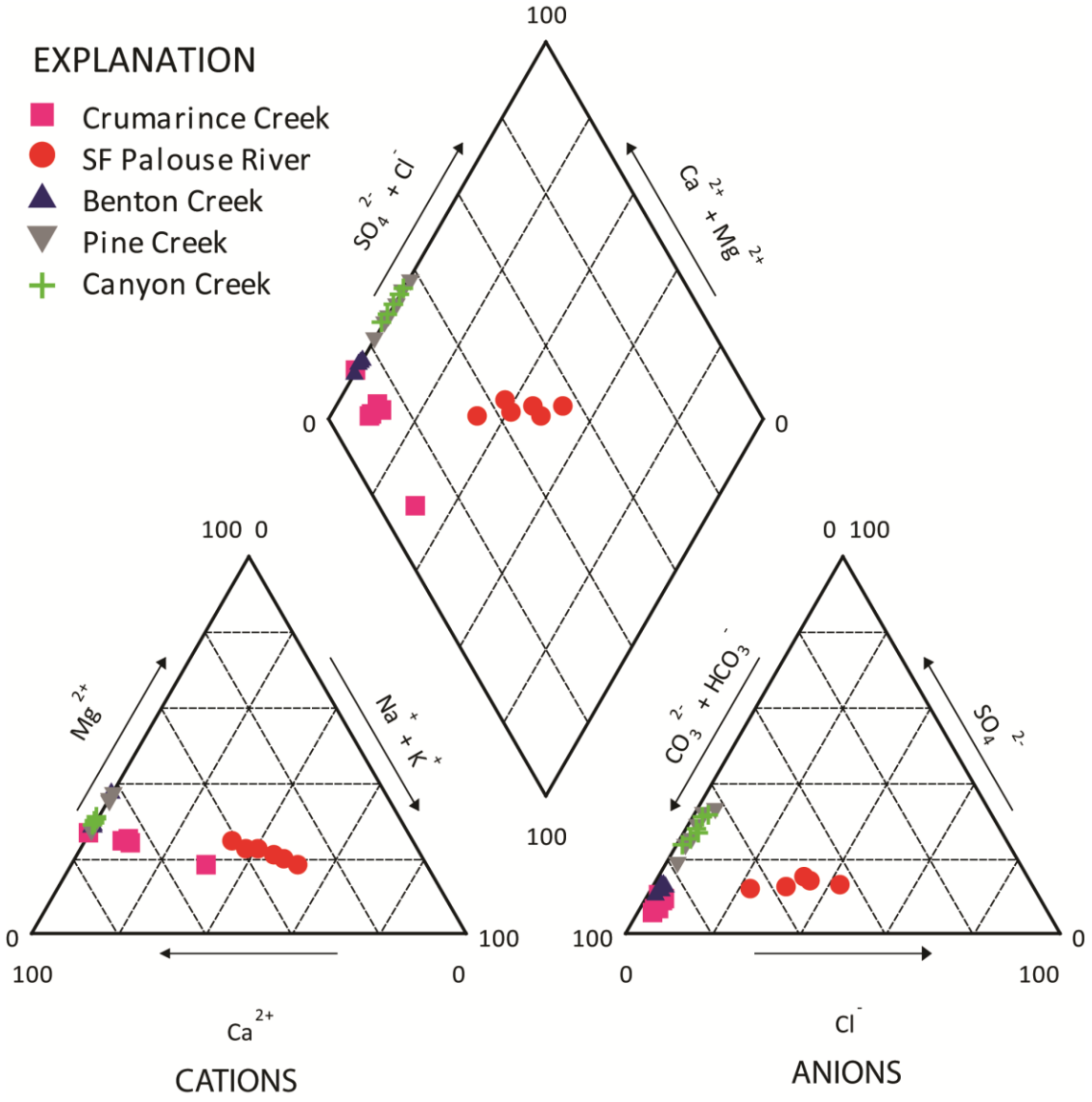

Figure 8: Piper diagram showing major ion composition in five watersheds in the inland Pacific Northwest throughout the baseflow summer period in 2013.

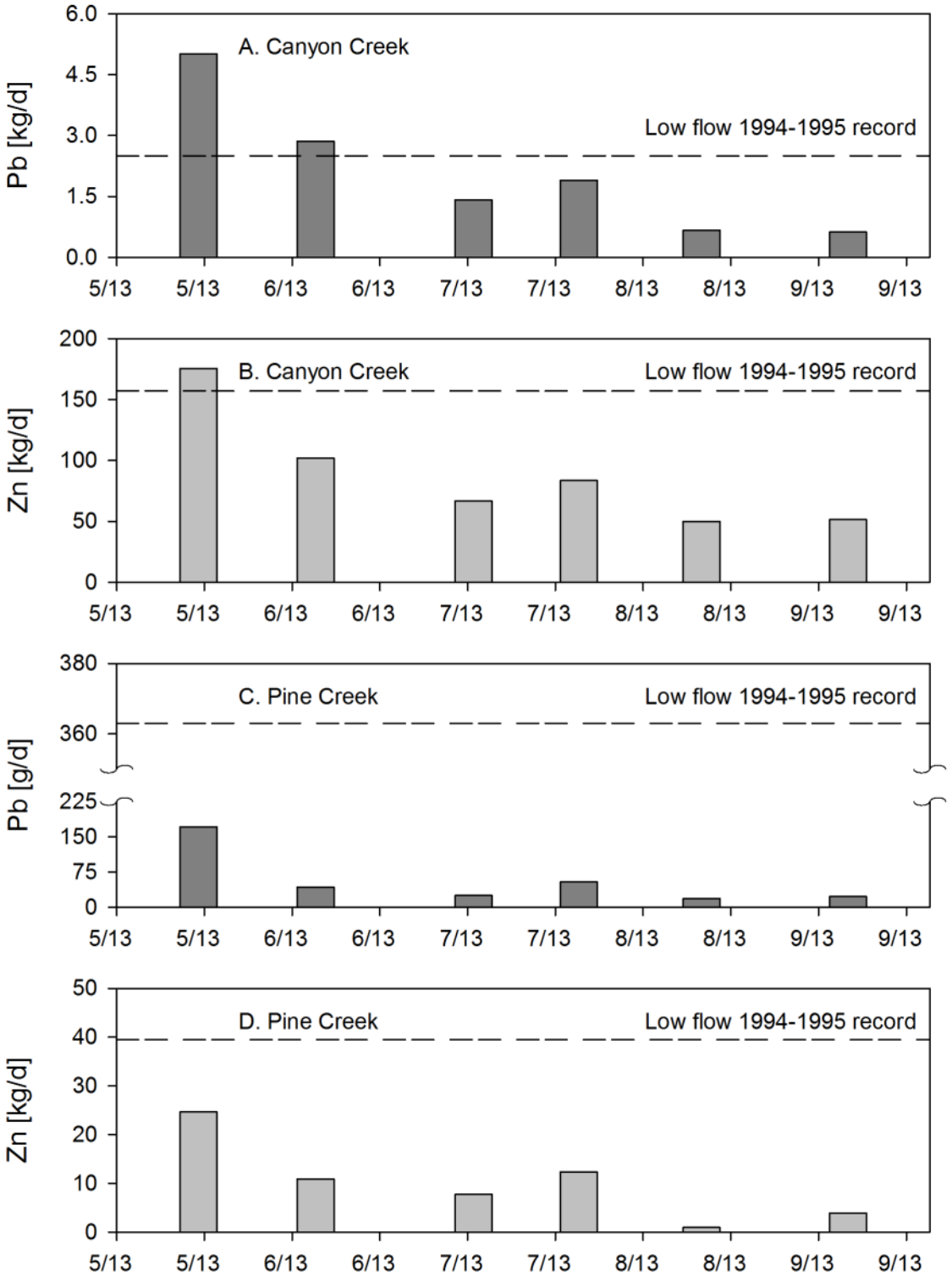

Figure 9: Zn and Pb stream loads in Canyon Creek and Pine Creek during the 2013 baseflow period. Dash lines denote historic Zn and Pb loads during the 1994-1995 baseflow recessions.

Supplemental tables

Table S1: Summary of geomorphic and climatic characteristics in five selected watersheds.

Watershed	Q [mm/yr]	ET [mm/yr]	P [mm/yr]	Mean temperature [˚C]	Mean slope [%]	Area [km^2]	Total stream length [km]
Pine Creek	703	522	1225	5.46	46.5	190	231
Canyon Creek	754	559	1313	3.81	46.3	60	64
Crumarine Creek	230	801	790	7.27	28.4	6.4	8
SF Palouse River	97	573	670	8.22	12.0	342	586
Benton Creek	240	607	847	5.67	34.7	7.2	6.5

Table S2: Summary of main geologic features in five selected watersheds.

Watershed	Percent of main geologic features				
	Alluvial	**Granitic**	**Basalt**	**Metamorphic**	**Sedimentary**
Pine Creek	0.0	0.0	0.0	63.1	36.9
Canyon Creek	12.9	3.2	0.0	66.1	17.8
Crumarine Creek	0.0	100	0.0	0.0	0.0
SF Palouse River	5.8	28.7	64.8	0.7	0.0
Benton Creek	3.2	64.6	0.0	32.2	0.0

Table S3: Surface water sampling stations in the inland Pacific Northwest, USA. Station ID numbers are plotted in Fig. 2.

Station	ID	Longitude [dec.deg]	Latitude [dec.deg]	Elevation [m]	Period of record	N	Sampling frequency
Palouse region							
Crumarine Creek, Moscow, ID	1	46.7773	116.9158	847	June, 2011 – January, 2014	245	Weekly/storm basis
South Fork Palouse River, Pullman, WA	4	46.7324	117.1814	707	September,2011 – January, 2014	195	Weekly/storm basis
South Fork Palouse River, Colfax, WA	5	46.8894	117.3672	596	September,2011 – January, 2014	23	Monthly
North Fork Palouse River, Colfax, WA	6	46.8894	117.3672	596	September,2011 – January, 2014	23	Monthly
Palouse River, Hooper, WA	7	46.7584	118.1495	326	September,2011 – January, 2014	24	Monthly
Silver Valley							
Canyon Creek, Wallace, ID	8	47.3391	115.9153	828	October, 2011 – January, 2014	158	Weekly
Pine Creek, Pinehurst, ID	10	47.5143	116.2421	700	October, 2011 – January, 2014	143	Weekly
Priest River area							
Benton Creek, Priest River, ID	13	48.3503	116.8344	712	November, 2012 – January, 2014	84	Weekly
Priest River, Priest River, ID	15	48.2846	116.8720	665	December, 2012 – December, 2013	18	Every 3 weeks

Table S4: Precipitation sampling stations in the inland Pacific Northwest, USA. Station ID numbers are plotted in Fig. 2.

Station	ID	Longitude [dec.deg]	Latitude [dec.deg]	Elevation [m]	Period of record	N	Sampling Frequency
Palouse region							
Moscow, ID	3	46.7293	117.0209	789	November, 2011 January, 2014	91	Weekly
Moscow Mountain, ID	2	46.7918	116.9080	931	September,2011 January, 2014	112	Weekly
Silver Valley							
Wallace, ID	9	47.3391	115.9153	828	February, 2012 January, 2014	32	Every 3 weeks
Pinehurst, ID	11	47.5143	116.2421	700	October, 2012 January, 2014	28	Every 3 weeks
Kellogg, ID	12	47.5360	116.1227	706	September,2012 September, 2013	27	Biweekly
Priest river area							
Priest River, ID	14	48.3503	116.8344	712	November, 2012 January, 2014	26	Every 3 weeks

The following supplementary tables are provided in a digital format.

Table S5: Isotopic data in precipitation for the Palouse Region, Silver Valley, and Priest River area.

Table S6: Isotopic data in surface waters for the Palouse Region, Silver Valley, and Priest River area.

Table S7: Summary of baseflow geochemical data in five selected watersheds of the inland PNW.

CHAPTER III

Geochemical Evidence for Active Tropical Serpentinization in the Santa Elena Ophiolite, Costa Rica: An Analogue of a Humid Early Earth?

R. Sánchez-Murillo., E. Gazel., E. Schwarzenbach., M. Crespo-Medina., M. O. Schrenk, J. Boll, and B. C. Gill.

In press. Submitted to Geochemistry, Geophysics, Geosystems on December 20th, 2013. Revised on April 5th, 2014. Accepted April 14th, 2014.

Abstract

Serpentinization is a planetary process that has important consequences on geochemical cycles, supporting microbial activity through the formation of H_2 and CH_4 and having the potential to sequester atmospheric CO_2. We present geochemical evidence of active serpentinization in the Santa Elena Ophiolite, Costa Rica which is sustained by peridotites with a degree of serpentinization less than 50% with no evidence of an internal heat source. Average spring water temperatures are 29.1°C. Two hyperalkaline spring systems were discovered, with a spring fluid pH up to 11.18. The fluids are characterized by low Mg (1.0-5.9 mg/L) and K (1.0-5.5 mg/L) and relative high Ca (29-167 mg/L), Na (16-27 mg/L), Cl (26-29 mg/L), hydroxide (41-63 mg/L), and carbonate (31-49 mg/L). Active CH_4 (24.3% v/v) vents coupled with carbonate deposits ($\delta^{13}C_{CO2}$= -27 to -14 ‰; $\delta^{18}O_{CO2}$= -17 to -6 ‰) also provide evidence for active serpentinization and carbonation. Isotope ratios of the alkaline fluids ($\delta^{18}O$= -7.9‰, $\delta^{2}H$= -51.4‰) and groundwater ($\delta^{18}O$= -7.6‰; $\delta^{2}H$= -48.0‰) suggests that, during baseflow recession, springs are fed by groundwater circulation. Methanogenic Archaea, which comprises a relatively high percentage of the RNA tag sequences, suggests that biological methanogenesis may play a

significant role in the system. Santa Elena's extreme varying weather results in a scenario that could be of significant importance for a) improving the knowledge of conditions on a humid early Earth or Mars that had periodic changes in water supply, b) revealing new insights on serpentinizing solute transport, and c) modeling hydrogeochemical responses as a function of recharge.

Keywords: Santa Elena Ophiolite; serpentinization; hyperalkaline fluids; baseflow hydrology; geobiology.

1. Introduction

1.1. Serpentinization

Serpentinization – the reaction of ultramafic rocks with fluids to form serpentine – is a planetary process (i.e., Earth-like planets, moons and undifferentiated bodies such as chondritic asteroids) that results in the formation of H_2 through oxidation of Fe^{2+} in the primary minerals and has been described in several systems both in seawater exposed mantle rocks along slow-spreading mid-ocean ridges and in ultramafic rocks emplaced on the continents [Frost, 1985; Allen and Seyfried, 2003; Bach et al., 2006; Frost and Beard, 2007; Alt et al., 2007; 2013; Schwarzenbach et al., 2013a].

The presence of H_2 and CH_4, the latter formed through abiotic reduction of CO_2 [Proskurowski et al., 2008; Lang et al., 2012;], are major energy sources for microbial activity and have been shown to support prolific microbial communities in peridotite-hosted hydrothermal systems [Kelley et al., 2005; Brazelton et al.,2006; Brazelton et al., 2011; Suzuki et al., 2013; Brazelton et al., 2013]. Additionally, serpentinization of ultramafic rocks generally produces hyperalkaline fluids (pH>10) with high Ca^{2+}, low Mg^{2+} and low total carbon concentrations that also plays an important role in the abiogenic cycling of carbon [Barnes et al., 1967; Neal and Stanger, 1983; Kelley et al., 2001; Schwarzenbach et al., 2013a, 2013b; Schrenk et al., 2013].

Sections of mantle rocks exposed on the surface of our planet under sub-aerial conditions (named here continental serpentinization) provide natural laboratories to study present-day serpentinization [Blank et al., 2009; Szponar et al., 2012; Schwarzenbach et al., 2013b; Chavagnac et al., 2013; Morill et al., 2013; Etiope et al., 2013; Pirard et al., 2013] and potential geologic CO_2 sequestration [Matter et al., 2007; Kelemen and Matter, 2008; Kelemen et al., 2011; Paukert et al., 2012]. These laboratories serve as an analog to other terrestrial planets and moons that have an ultramafic and mafic crust and contain liquid water and thus can give new insights into the occurrence of “habitable environments in the universe.” Recent

mapping efforts of Mars' surface have reported the dominance of mafic to ultramafic rocks [Hoefen et al., 2003; Christensen et al., 2005]. Ongoing initiatives on mid-ocean ridges and in ophiolites have already provided insight into the importance of this process for the life on our planet [Schrenk et al., 2004; Brazelton et al., 2006; 2010; 2013; Schwarzenbach et al., 2013a]. However, the factors (e.g., H_2, CH_4 fluxes, water input, pH, temperature gradients, and nutrient availability) that control the occurrence of microbial communities in these systems are still unknown. The presence of H_2 and CH_4 in the fluid controls the occurrence of biological activity, and methane and sulfur metabolizing microorganisms were found at the Lost City hydrothermal field, a peridotite-hosted hydrothermal system along the Mid-Atlantic Ridge [Schrenk et al., 2004; Kelley et al., 2005; Brazelton et al., 2006]. These systems are thought to be similar to those found in early Earth, leading to an increased interest in studying the ability of such environments to not only host the most primitive life-forms on Earth, but also to have served as a birth place of life [Russell et al., 1989; 1994; Früh-Green et al., 2004; Holm et al., 2006; Schulte et al., 2006; Martin and Russell, 2007]. Given their composition, other planets, planetesimals or moons (such as Mars or Europa) hold the potential to host similar ecosystems [Russell and Hall, 1989; Hand et al., 2007; Russell and Kanik, 2010]. Presently mantle-derived ultramafic rocks are ubiquitously exposed on the seafloor, in the forearc regions of some intraoceanic arcs and on continents by tectonic processes [Cannat, 1993; Kelley et al., 2001; Cannat et al., 2013]. However, ultramafic volcanic rocks were significantly more abundant on Earth's surface during the Archean [Myers and Crowley, 2000; Nisbet and Sleep, 2001].

On land, interaction of meteoric water with peridotites results in Mg-HCO_3 waters, which in the absence of a CO_2 source, progressively evolve to hyperalkaline Ca^{2+}-OH waters [Bruni et al., 2002; Boschetti and Toscani, 2008; Marques et al., 2008]. Despite presumably low reaction temperatures in the basement (50-100 °C, as no heat source has been observed in any of the continental serpentinization sites), high methane and/or hydrogen concentrations were measured in the Voltri Massif, Italy [Cipolli et al., 2004], the Zambales Ophiolite, Philippines [Abrajano et al., 1988; Abrajano, 1990], in the Newfoundland Ophiolite, Canada [Szponar et al.,

2012], in the Samail Ophiolite, Oman [Neal and Stanger, 1983], and in the Othrys Ophiolite, Greece [Etiope et al., 2013]. The availability of hydrogen – and thus indirectly the availability of methane – as an energy source for microorganisms may strongly be regulated by water-rock ratios (i.e., fluid fluxes) that influence the rate of serpentinization. Additionally, the availability of inorganic carbon in the fluids controls the amount abiogenic of methane formed. Shervais et al. [2005] suggested that the production of hydrogen may, to some degree, be self-sustaining due to the increase in volume and potential mechanical fracturing, consequently, exposing new un-reacted mineral surface area to meteoric water and organisms. Despite the aforementioned models, the role – and importance – of new meteoric water and its subsurface transit time in continental serpentinization systems remains unclear both in temperate and tropical environments.

Interaction of the alkaline spring waters with atmospheric CO_2 results in the formation of carbonate deposits. Where Mg-HCO_3 waters discharge, magnesite is formed as the water gets oversaturated with respect to magnesite, while interaction of the Ca-OH fluids with atmospheric CO_2 results in the formation of calcite. Such calcite deposits usually precipitate at the exit sites of the alkaline spring waters, where they form carbonate crusts or travertines on the basement rock as abundantly observed in association with mantle rocks [e.g., Neil & Stanger, 1983; Clark and Fontes, 1990; Kelemen and Matter, 2008; Chavagnac et al., 2013; Schwarzenbach et al., 2013b]. Such carbonate deposits are typical features that indicate that the serpentinization process is occurring in the subsurface. At the same time, concentrations of other species that can serve as nutrients for microbial activity (e.g. DIC, SO_4) evolve as well, e.g., due to the interaction with sulfur- or carbon-bearing minerals in the peridotite (e.g. sulfide minerals, sulfate carbonates formed during seafloor serpentinization). Thus, the chemical evolution of the fluids is related to the subsurface serpentinization reactions that are controlled by the chemical composition of the primary peridotite, water input from the surface, or potential interlayered sediments when present. Methane in these systems may be derived from abiotic reduction of CO_2, in-situ microbial activity, or have a primary mantle origin. Therefore, the amount of H_2 that is generated is likely controlled by the primary mineralogy (i.e.,

the amount of unaltered peridotite available) and the rate of serpentinization, which in turn is primarily controlled by temperature and the water-to-rock ratio.

1.2. Climate and hydrogeological uniqueness of the Santa Elena Ophiolite

The main objective of this study is to present geochemical evidence of a new tropical active serpentinization end-member discovered early in 2013 within the Santa Elena Ophiolite, Costa Rica. Extreme varying climate conditions between dry and wet seasons result in a unique hydrogeological scenario that could be of significant importance for a) improving current knowledge of conditions on a humid early Earth or Mars that had periodic changes in water supply [Barron et al., 1989; Craddock and Howard, 2002; Paige, 2005; Fairén, 2010], b) revealing new insights on serpentinization processes and the natural release of hyperalkaline fluids as baseflow, and c) modeling hydrogeochemical responses as a function of meteoric water recharge and baseflow recession in present-day continental serpentinization environments.

Commonly, continental serpentinization and hyperalkaline spring studies have been conducted in temperate regions (e.g., Tablelands, Canada; Western Coastal Range, USA; Gruppo di Voltri, Italy; Othrys, Greece) and at subtropical sites (e.g., Samail, Oman). In these regions precipitation is mostly composed of snow events, meteoric recharge occurs in a short time during spring runoff or in relatively slow snowmelt rates. Coastal temperate sites might experience intermittent rainfall at relatively low intensities. Furthermore, in arid and semi-arid areas where precipitation events are scarce and isolated, infiltration is limited due to large evaporation losses. Contrary to the previous scenarios, in tropical environments precipitation amounts and rainfall intensities are usually greater and occur throughout several months, which facilitate infiltration, and thus, water-rock interaction, may be exacerbated. To our knowledge, this study constitutes the first comprehensive characterization of active serpentinization in a tropical environment and poses a novel opportunity to study the interplay between the hydrology, serpentinization, and life.

2. Study Area

2.1. Santa Elena Ophiolite and sampling locations

Geotectonically, Costa Rica is situated at the triple junction of the Cocos, Caribbean and Nazca plates. Along the Middle American Trench the subduction of the Cocos Plate underneath the Caribbean Plate results in an active volcanic front (Carr et al, 2007; Saginor et al, 2013). Along the Pacific side of Costa Rica several oceanic complexes have been accreted onto the Caribbean Plate (Hauff, et al. 2000; Denyer and Gazel 2009; Herzberg and Gazel 2009 and references therein). The Santa Elena Ophiolite is the northernmost of these oceanic complexes and comprises an area of 250 km^2 of mafic and ultramafic lithologies (Gazel, et al. 2006) located in the Santa Elena peninsula within the Area Conservación Guanacaste (ACG, i.e. Guanacaste Conservancy Area). The structure of the Santa Elena Peninsula includes an ultramafic complex at the hanging-wall and an igneous-sedimentary complex at the footwall – the Santa Rosa Acretionary complex (Baumgartner and Denyer 2006; Denyer and Gazel 2009). The ophiolite (Fig. 1) contains variably serpentinized peridotites, dunites, and locally layered gabbros. Various generations of pegmatitic gabbros and diabase dikes cut the peridotites. Some of these dikes do not preserve chilled margins, implying that they intruded into the mantle host when it was hot and plastic. A secondary mineralogy in the mafic lithologies composed of albite + epidote + actinolite + chlorite, and variable serpentinization in the peridotites is evidence of ocean floor metasomatism (Gazel, et al. 2006). The Santa Elena Ophiolite was correlated with other peridotites outcrops along the Costa Rica-Nicaragua border interpreted as E-W suture zone emplaced between different tectonic blocks (Tournon, et al. 1995). The fact that the Santa Elena complex is covered by Campanian-age rudists reef limestones suggest that the exhumation was active during the Upper Cretaceous (Gazel et al., 2006; Denyer and Gazel, 2009), nevertheless details studies are required to reconstruct the exhumation and tectonic history of this complex.

The ACG was included in the UNESCO World Heritage List in 1999 due to its unique terrestrial (i.e., presence of an ophiolite and the most important tropical dry forest in Mesoamerica) and marine-coastal environments. We conducted two field sampling campaigns in the Santa Elena Ophiolite (January and March 2013) during which we sampled groundwater (12 private and municipal wells outside of the ACG, 30-70 m depth), surface waters (27 locations), freshwater springs (10 sites), hyperalkaline springs (2 systems), mineral precipitates (17 samples), gas emissions (1 site), and microbial communities (2 sites) (Fig. 1, Table S1). A subset of water samples were selected for comprehensive geochemical analyses as shown in Tables S2 and S3.

Two main hyperalkaline systems were sampled within Murciélago and Potrero Grande rivers which constitute the most significant perennial streams in the area (Fig. 1). Potrero Grande River is characterized by a 10.3 km long floodplain and relatively steep tributaries (~33% slope). Active erosion processes resulted in the greater peridotite exposure among all watersheds in the Santa Elena peninsula. Vegetation (i.e., deciduous trees) is mostly located in riparian areas, whereas tropical dry forest grass is common on the upper part of the stream canyons. The hyperalkaline system within Potrero Grande is located in the headwaters about 121 m.a.s.l. Murciélago River is characterized by a relatively narrow valley and a greater presence of riparian vegetation. The hyperalkaline springs within Murciélago are located within the lower portion of the catchment (78 m.a.s.l.). Overall, field evidence suggests that hyperalkaline seepages are numerous and are active late in the baseflow period of perennial streams. Hyperalkaline springs often form shallow pools characterized by moderate turbidity, thin white films of carbonates, and extensive yellow-brown carbonate deposits (Figs. 2 and 3). Hyperalkaline fluids mixing with perennial receiving stream waters occurs at a low rate; therefore, dilution occurs rapidly. Sampling of hyperalkaline fluids was conducted directly at the spring outflow without the interference of stagnant or diluted stream waters.

2.2. Climate and hydrological singularities

The climate of Costa Rica is controlled by northeast trade-winds, the shifts of the Intertropical Convergence Zone (ITCZ) and indirect influence of Caribbean cyclones [Waylen et al., 1996]. These circulation processes produce two main seasons: The wet season (May-October) corresponds to the time when the ITCZ travels over Costa Rica, and precipitation is characterized by heavy convective rainstorms. The dry season (November - April) comprises of the months when the ITCZ is to the south of Costa Rica [Guswa et al., 2007]. The Santa Elena Peninsula receives on average 1,464 mm/yr of rainfall (based on 10 years of historical records at the Santa Rosa climatological station, Auxiliary Figure A1). La Niña phenomena produce a considerable rainfall increase up to 3,000 mm, while El Niño years are characterized by annual precipitation below 1,200 mm and a dry period usually spans 5–7 months. Seasonal temperature variation is low; mean annual maximum and minimum ambient temperatures are 31 °C and 23 °C, respectively. During the dry period, maximum temperatures can reach up to 40 °C. A summary of climate data for 2012 climatological water year conditions is presented in Figure 4 and additional years in Auxiliary Figure A1.

The Northwestern Pacific region of Costa Rica has estimated regional groundwater recharge rates of less than 300 mm/yr [Mulligan and Burke, 2005]. Baseflow recession starts in November and reaches its minimum in late April. Presumably, heavy convective storms produce flash runoff events. Most of the groundwater recharge in the peninsula occurs between July and October. Due to its UNESCO World Heritage status, the extent of hydrogeological research has been limited within ACG. Therefore, no hydraulic test and aquifer parameter information is available. Likewise, to our knowledge, long-term or current discharge data are not available for this area.

3. Sampling methods and analytical techniques

3.1. Water chemistry

A set of parameters (i.e. water temperature, pH, conductivity) were measured in situ with a portable probe (Model 99130, Hannah Instruments). This probe was

calibrated twice a day using pH standard and conductivity solutions (HI 7000 Series, Hannah Instruments). Hyperalkaline fluids were sampled directly from seepage sources into sterile Nalgene HDPE bottles. A set of blank bottles containing ultrapure water was treaded in the same manner as the samples. Samples were stored at 5°C, transported, and analyzed within one week of collection. Bottles for alkalinity analysis were filled completely (i.e., no head space) and covered with parafilm to avoid CO_2 exchange. Samples for determination of heavy and alkaline metals were acidified to a pH<2 to prevent precipitation during storage. Samples were filtered through 0.45 μm glass fiber filters (Millipore) immediately after arrival in the laboratories. Samples for stable isotope analysis were collected in 30 mL glass E-C borosilicate vials with TFE-lined caps (Wheaton Science Products). Vials were filled without head space and covered with parafilm (Thermo Scientific) to avoid interaction with atmospheric moisture or fractionation.

Expanded alkalinity was analyzed by potentiometric titration [Standard Method 2320b, Eaton et al., 1998]. The results obtained from the phenolphthalein and total alkalinities allowed the stoichiometric determination of bicarbonate, carbonate, and hydroxide, which concentrations are reported as mg/L of $CaCO_3$ equivalent. Major and trace elements were measured by inductively coupled plasma optical emission spectrometry (Thermo Trace Jarrel-ash 51-i) [Standard Method 3120b, Eaton et al., 1998]. Calibration was conducted using synthetic standards with a relative standard deviation (RSD) of 2% or better. Both expanded alkalinity major and trace elements analyses were conducted at the certified (INTE-ISO/IEC 17025:2005) Agrotec Analytical Laboratory (San José, Costa Rica). Ion concentrations were measured by ion chromatography (Model ICS-5000 Dual) with an electrical conductivity detector. Calibration was conducted using synthetic standards with a RSD of 3% or better. Stable isotope analysis were conducted at the Chemistry School of the National University of Costa Rica using a cavity ring down spectroscopy (CRDS) water isotope analyzer (L2120-i, Picarro Inc.) following the methods described by Lis et al. [2008]. Laboratory standards, previously calibrated to the VSMOW2-SLAP2 reference waters were EAG (δ^2H= -255.0‰, $\delta^{18}O$= -30.8‰), CAS (δ^2H= -64.2.3‰, $\delta^{18}O$= -8.3‰), and

DDI (δ^2H= -15.4‰, δ^{18}O= -125.5‰). EAG and CAS were used to normalize the results to the VSMOW2-SLAP2 scale, while DDI was a quality control standard. The laboratory precision for this analytical run was ±0.5‰ (1σ) for δ^2H and ±0.1‰ (1σ) for δ^{18}O.

3.2. Gas chemistry

Preliminary sampling revealed novel information about the presence of methane emissions within the Santa Elena Ophiolite. A gas vent located approximately 300 m upstream from the hyperalkaline system within the Murciélago River (Poza del General, Auxiliary Table A1) was sampled for methane determinations. Gas emission occurred in non-uniform time intervals at the bottom of a 4 m deep pool. The stream bed was surveyed to discard the presence of decomposing organic matter. Samples were collected using a 15.24 cm (diameter) HDPE funnel connected to a Supel-inert film gas sampling bag (3 mm thickness, Sigma-Aldrich) through a 6 m long vinyl tubing (0.64 cm diameter) with a push-lock valve. The funnel was placed at the streambed by a professional diver to trap gas emanations. Three replicates were collected with a collection time of 20 min each. Samples were analyzed within four days of collection at LAQAT Atmospheric Chemistry Laboratory (National University, Costa Rica) using a gas chromatographer (8610C, SRI Instruments) with a flame ionization detector; 1 mL of sample was injected with an automatic valve (Valco Instruments) into a 1 m column (Hayesep D, 0.32 cm diameter). Calibration was conducted with a methane standard (1% volume) (Scott Specialty Gases). Only methane was analyzed during these field explorations.

3.3. Carbonate mineral precipitates

Carbonate deposits and carbonate-bearing sediments underlying the deposits were collected at various locations within the riverbeds of the alkaline springs. At two springs (Murciélago and Potrero Grande, locations in Auxiliary Table A1), carbonate

precipitates floating on the river water were sampled. Carbonate-bearing sediments and carbonate travertine deposits were crushed with the agate mortar to prepare bulk rock samples, while for a few travertine deposits single carbonate layers of the deposit were extracted with a 5 mm drill with the aim to reveal isotopic heterogeneities between different carbonate layers. The carbonate precipitates from the rivers were dried for two days at 40°C. All carbonate samples were in a final step homogenized to produce a fine-grained powder

The mineralogy of the carbonate samples was determined by X-ray diffraction on a Rigaku MiniFlex XRD with powder diffraction analysis package PDXL at the Geosciences department at Virginia Tech. The carbon and oxygen isotope composition was analyzed on a MultiFlowGeo headspace sampler at Virginia Tech. Samples were prepared in septum vials, flushed with He, acidified with phosphoric acid and reacted for at least 3 hours before analyses, as no magnesite or dolomite was present in any of the analyzed samples. Reproducibility is better than ± 0.1‰ for $\delta^{13}C$ and better than ±0.3‰ for $\delta^{18}O$.

3.4. Microbiology

Fluid samples, ranging from 20-170 mL, were collected from the two alkaline springs at Río Murciélago (Spring 8 and Spring 9, Table A1) and from Quebrada Danta Spring and stored frozen until analyses. In the laboratory, samples were thawed and either preserved in 3.7% formaldehyde for cell counts and stored at 4°C, or filtered using sterile syringes through 0.2 µm Sterivex filter cartridges (Millipore) for DNA extraction. Fluids preserved for cell abundance enumeration were filtered through a 0.2 µm filter, and cells stained with 4',6-diamidino were filtered counted with an Olympus BX61 spinning disk epifluorescence confocal microscope according to published protocols [Hobbie et al., 1977; Schrenk et al., 2003]. DNA extraction followed described protocols in Huber et al. [2002] and Sogin et al. [2006]. DNA extracts were purified with the DNA Clean and Concentrator^{TM}-5 kit (Zymo Research) according to the manufacturer's instructions.

16S rRNA amplicons (tag) were generated at the Marine Biological Laboratory (Woods Hole, MA) using an Illumina MiSeq apparatus. This method produces ~250 nt reads targeting the Bacterial and Archaeal 16S rRNA v4v5 region. Additional amplification and sequencing methods are available at the VAMPS website (http://vamps.mbl.edu/resources/primers.php). Data processing, chimera detection, and taxonomic classification procedures have been previously described [Sogin et al., 2006; Huse et al., 2008; Huse et al., 2010].

4. Results

Auxiliary Table A1 presents a description of the sampling locations during both field expeditions (January and March, 2013). Locations are described by their local name, sampling date and time, type of discharge, geographic coordinates (decimal degrees), and altitude (m). Auxiliary Tables A2 and A3 contain physical parameters, stable isotopes, major ions, trace elements, and extended alkalinity composition of the surface, spring, and ground waters collected in both sampling campaigns. Table 1 presents percent of sequences related to hydrogen, methane and methanol metabolism in Río Murciélago springs 8 and 9, and Quebrada Danta spring (Auxiliary Table A1). Auxiliary Table A4 presents bacterial and Archaeal diversity by next-generation tag sequencing of the 16S rRNA gene. Auxiliary Tables A5 and A6 contain information on the taxonomic classification of Bacterial and Archaeal tag sequences, respectively, that accounted for 1% or more of the total sequences in a sample.

4.1. Hyperalkaline spring systems

Potential hydrogen (pH) of the springs ranged from 11.01 up to 11.18 (Fig. 5). Both spring systems, Murciélago and Potrero Grande (Fig. 1), are representative of Ca^{2+}-OH^{-} waters. Hydroxide and carbonate concentrations ranged from 41-63 mg/L

and 31-49 mg/L (reported as mg/L $CaCO_3$ equivalent), respectively. Maximum dissolved calcium concentrations of 167 mg/L were measured in Murciélago spring 9 (Supplementary Table S1). In addition, the springs are characterized by low Mg (1.0-5.9 mg/L) and K (1.0-5.2 mg/L) concentrations and relatively high Na (16-27 mg/L) and Cl (26-29 mg/L) (Fig. 5). Nickel (15.5 μg/L) and iron (0.24 mg/L) were also measured in minor concentrations. Sulfate was not detected in the analyzed fluids (detection limit = 0.33 mg/L). Average spring temperature was 29±2 (1σ) °C, which is 3°C higher than the average temperature of non-alkaline springs. Active gas vents with CH_4 concentrations of up to 24.3 % (v/v) were detected at the Río Murciélago site ~300 m upstream of the hyperalkaline spring system.

Hydrological connectivity between the groundwater system and hyperalkaline spring seepage was explored using stable isotopes in private and municipal wells. Isotope compositions of hyperalkaline fluids ($\delta^{18}O$= -7.9‰, $\delta^{2}H$= -51.4‰, Fig. 6, Auxiliary Table A3) is remarkably similar to the well signals ($\delta^{18}O$= -7.6‰; $\delta^{2}H$= -48.0‰) sampled within the Cuajiniquil and Murciélago watersheds. Isotopic baseflow composition generally represents the mean annual isotopic composition of meteoric waters. In Costa Rica, the annual weighted precipitation composition is $\delta^{18}O$= -7.4‰ and $\delta^{2}H$= -49‰ [Sánchez-Murillo et al., 2013] which corresponds to the isotopic signal found in the hyperalkaline fluids. Mean electrical conductivity (EC) in the hyperalkaline springs ranged from 487 up to 741 μS/cm.

4.2. Surface waters

Well-mixed surface waters within the Santa Elena Peninsula are of a dominant Mg-bicarbonate system which represents ~95% of the major ions composition. Bicarbonate concentration ranges from 218–288 mg/L (i.e. reported as mg/L $CaCO_3$ equivalent) with a mean of 246±20 (1σ) mg/L. Magnesium concentrations vary from 45–63 mg/L with a mean of 54±5 (1σ) mg/L. Inversely to the hyperalkaline fluids, these surface waters showed low Ca 4.6±5 mg/L (1σ), Na + K (1.4-9.8 mg/L), and chloride 2.5±1.4 (1σ) mg/L concentrations (Fig. 5). Mean surface water pH was

8.0±0.5 (1σ); nevertheless, pH values greater than 8.5 were consistently measured across the studied streams (Fig. 5). Electrical conductivity was on average 477±107 (1σ) uS/cm across the main four watersheds. Surface water temperature was fairly uniform with a mean of 26.8±1.4°C (1σ) across the studied streams. Mean isotope composition of surface waters ($\delta^{18}O$= -6.8‰, $\delta^{2}H$= -43.4‰) shows clear evaporation enrichment as travel time increases from headwaters to the lower reach of the catchments (Fig. 6).

4.3. Groundwater

Groundwater EC ranged from 504 to 1,084 uS/cm with a mean of 722±220 (1σ) uS/cm, which is 1.2 and 1.5 times greater than hyperalkaline springs and surface waters, respectively, which indicates a greater extent of water-rock interaction. Mean well water temperature was 30±2°C (1σ). One sample from well Aguas Calientes (Auxiliary Table A3) was analyzed for aqueous chemistry. Interestingly, this well is located outside the ophiolite; however, the headwaters of Cuajiniquil watershed are within the peridotite. Besides the pH (7.2), the composition of this well water shared similarities with alkaline fluids: high Ca (73 mg/L), sulfate (5.74 mg/L), Cl (41.3 mg/L), Na (16.2 mg/L), and low Mg (4.33 mg/L) and Fe (1.35 mg/L), which may indicate that deep percolation is also transferring the hyperalkaline signature to the groundwater system. As mentioned in section 4.1, groundwater isotope composition was remarkably similar to hyperalkaline fluids.

4.4. Carbonate deposits

Strongly ^{13}C and ^{18}O depleted calcite deposits suggest calcite precipitation by uptake of atmospheric CO_2 dominated by kinetic fractionation and are found in many continental serpentinization systems (Fig. 7) [Clark et al., 1992, O'Neil and Barnes, 1971, Schwarzenbach et al., 2013b, Quesnel et al., 2013]. These characteristically depleted isotope compositions are a result of the high pH and extremely low C_{total} of

the fluids, which causes immediate uptake of CO_2 upon interaction with the atmosphere. With continuous interaction of the fluids with the atmospheric CO_2 the formed carbonates get less negative in their isotopic composition resulting in the linear trend seen in Figure 6. This process has been described in detail for ^{13}C and ^{18}O depleted calcite deposits in the Voltri Massif, Italy [Schwarzenbach et al., 2013b] (Fig. 7).

4.5. Microbiology

Quebrada Danta spring had the highest cell density (1.51 x 10^5 cells/ml). Cell densities at Río Murciélago Spring 8 and Spring 9 were 7.93 x 10^4 and 2.0 x 10^4 cells/mL, respectively. These values reflect low biomass, which is consistent with other serpentinizing systems. Bacterial and Archaeal diversity were estimated by next-generation tag sequencing of the 16S rRNA gene (Auxiliary Table A4).

Evidence of microorganisms involved in hydrogen oxidation, methane and methanol oxidation, as well as methananogenesis can be deduced from our sequencing results (Table 1). Sequences related to methanotrophs belonging to the families Methylococcaceae, Methylobacteriaceae, and Methylocystaceae were found in all samples, being more abundant at Río Murciélago Spring 8. The bacterial community in this spring was highly dominated by the genus of methylotrophic bacteria Methylibium (50% of the total sequences in this sample). Although to a lesser extent, sequences related to several genera within the family of methanol oxidizers Methylophilaceae were identified in Río Murciélago Spring 9 and Quebrada Danta sample (Supplementary Table S1). Two genera dominated the community in Murciélago Spring 9; the alkaliphilic genera Silanimonas and the H_2-oxidizing genus Hydrogenophaga. Representatives of these genera have been previously detected at other surveys from other continental serpentinite springs [Brazelton et al., 2013; Susuki et al., 2013]. Hydrogenophaga sequences were identified in all samples, as well as other hydrogen oxidizing bacteria from the families Hydrogenophilaceae, Hyphomicrobiaceae, Pseudonocardiaceae and Rhodobacteraceae.

Signatures of methanogenic archaea from the orders Methanobacteriales, Methanocellales and Methanomicrobiales were detected in all samples (Table 1) suggesting methanogenesis as an important process at this system, as has been suggested for other serpentinizing environments [Blank et al., 2009; Brazelton et al., 2012; Susuki et al., 2013]. This initial community composition analyses indicate the presence of microorganisms typically associated with other serpentinizing environments; however, additional sequence data as well as activity and transcriptomic data would further expand our knowledge of the microbial communities thriving this system and their metabolism.

5. Discussion

5.1 Serpentinization and hydrology: The role of a tropical environment

In the tropics, baseflow can be seen as the cumulative outflow from all upstream riparian areas (i.e., adjacent areas along the stream channel) and deep aquifers during rainless periods; its discharge (e.g., spring seepage or gaining streams) regulates stream chemistry and water temperature during critical dry months. The natural release of water as baseflow can be seen as a function of the hydraulic properties within the underlying geology and climatic conditions (Brutsaert, 2005). From a hydrological perspective, underlying geologic features are invariant with time (decades to hundreds of years) and significant climate effects can be distinguished only over large timeframes. However, hydrological processes in ophiolites, particularly, infiltration and groundwater flow are permanently altered due to active serpentinization resulting in constant volume changes in the altered materials [Macdonald and Fyfe, 1985; Shervais et al., 2005; Schrenk et al., 2013]; these transformations may play a key role in the overall subsurface flow paths distribution.

This novel hydro-geological system invokes three fundamental questions: a) To what extent can serpentinization and microbial life be facilitated in a humid

environment under high infiltration rates during the rainy season? b) How do subsurface water-rock interaction pathways and mean transit time influence spring water geochemistry? and c) What are the effects on the system effective porosity and hydraulic conductivity and overall solute transport by carbonate precipitates related with the serpentinization process? A humid serpentinizing environment with high meteoric water infiltration -as expected in the Santa Elena Ophiolite- may stimulate the growth of microbial communities by replenishing oxidants and nutrients (i.e. including carbon) in the shallow subsurface flow paths while benefiting from accelerated rates of water-rock reaction and associated hydrogen and methane evolution. The mean transit time or (MTT) the time a water molecule or solute spends traveling along subsurface flow pathways to the stream network is a fundamental hydraulic descriptor that provides useful information about water sources and mixing processes, potential flow pathways, and storage capabilities within a particular catchment control volume (McGuire et al., 2002; Dunn et al., 2007; Soulsby et al., 2009; Stewart et al., 2012; Sanghyun and Sungwon, 2014). However, despite its relevance, mean transit time has been poorly investigated in continental serpentinization studies (Dewandel et al., 2005). Detailed description of MTT coupled with geochemical data from alkaline seepage could provide a quantitative descriptor of water-rock contact time. Likewise, the dissolution and precipitation of minerals along the subsurface flowpaths could alter the aquifer effective porosity, and consequently, the hydraulic conductivity of the system. In the case of the Santa Elena Ophiolite, the high variability of precipitation events during the wet season (May-November) (Fig. 4) may concatenate changes in hydraulic conductivity (i.e., horizontal and vertical anisotropy) across a geological setting with mostly less than 50% degree of serpentinization.

Figure 8 shows a schematic rationale of water flow paths coupled with baseflow geochemical evidence. In the Santa Elena Ophiolite, baseflow conditions comprise approximately 4-5 months of the streamflow regime in which the minimum discharge occurs late in April or the beginning of May; it is clear that the peridotite-aquifer storativity is large enough to maintain baseflow in Potrero Grande and Murciélago after prolonged dry periods.

Due to the absence of a well-developed soil profile (less than 20 cm), infiltration of meteoric water occurs directly through the ultramafic rocks. Consequently, infiltrated water is modified by the serpentinization process before discharging at a topographic low (Fig. 8). Once at the surface, hyperalkaline fluid chemistry is modified by evaporation, precipitation, and mixing processes. Meteoric water can also flow through fully serpertinized macropores (e.g., faults) preserving a near neutral pH (~7.2) and freshwater-type chemistry characteristics if the system is open in respect to CO_2. Near neutral pH values may also correspond to short residence times in some of these springs. This type of spring is common and can be found in the proximity of hyperalkaline seepages, which supports the hypothesis of an intricate anisotropic subsurface matrix. Perennial surface waters exhibited slightly alkaline conditions (pH 8.0-8.7) due to the potential mixing with serpentinizing fluids along the stream reach (Fig. 8) such as diffuse bank sources. Despite high surface runoff and evapotranspiration amounts, rivers such as the Potrero Grande, Cuajiniquil, and Murciélago (Fig. 1) are perennial in most of their main sections. Perennial discharge suggests a large water storativity in the mantle peridotite and a higher hydraulic head in the peridotite than in the perennial streams. . The groundwater system is most likely an unconfined aquifer underlain by a basalt impermeable layer at the base of the ophiolite overthrust or between basaltic sills as observed during the field expeditions. Based on the Mulligan and Burke [2005] regionalized hydrological model, recharge may represent 18% of the available precipitation, whereas runoff may reach as much as 21%.

Dewandel et al. [2003; 2004; and 2005] studied the baseflow response within a similar ultramafic formation in Oman. Although Oman is located in a subtropical arid region with precipitation amounts of approximately 250 mm/yr, the hydraulic peridotite properties may share strong similarities. The authors found that in ophiolite rocks, groundwater circulation takes place mostly in the fissures close to the surface horizon (~50 m), and, to a lesser degree, in the tectonic fractures. In a water year of 250 mm available precipitation, Dewandel et al. [2005] estimated that only 8% (20 mm/yr) contributed to groundwater recharge, 12% runoff (30 mm/yr), and 80% evapotranspiration (200 mm/yr). Hydraulic conductivity of the fissured horizon was

estimated at 10^{-5} to 10^{-6} m/s for gabbro and diabase, and 10^{-7} m/s for peridotite. In general, the authors concluded that despite low annual rainfall, a relatively low hydraulic conductivity and a significant storage coefficient explain the perennial behavior of the streams within the peridotite. Dewandel et al. [2005] also illustrated a deep circulation (~500 m deep) with a residence time up to 25 years as a common subsurface flow mode, requiring high potential energy to allow for deep-circulation flow paths; resulting in spring flow near or in mountain areas. Another study conducted by Matter et al. [2006] also provided valuable hydraulic information of the Samail Ophiolite. For instance, the authors reported transmissivities ranging from 8×10^{-5} to 1×10^{-4} m^2/s and an average storage coefficient of 8×10^{-4} within fractured and weathered peridotites. Matter et al. [2006] also suggested that fracturing during tectonic emplacement and consequently weathering produced an increase of near-surface porosity.

Water supply during the wet season sets the Santa Elena Ophiolite apart from the hydrological scenarios observed in temperate or semi-arid regions. The potential of meteoric recharge can be analyzed from two perspectives: annual rainfall amounts and individual storm size. In Santa Elena, daily rainfall amounts can reach up to 211 mm (based on 10 years of historical records at the Santa Rosa climatological station, Auxiliary Figure A1); this is approximately equal to the annual precipitation in Oman (Auxiliary Figure A2). In Newfoundland, Canada and Genoa, Italy daily precipitation amounts (based on 20 years of historical records, National Climatic Data Center, NOAA, USA, Auxiliary Figure A2) can reach up to 94 mm and 154 mm, respectively. Although mean annual precipitation amounts in Genoa, Italy (1,135 mm) and Newfoundland, Canada (1,108 mm) are close to Santa Elena's annual precipitation (1,434 mm); what makes Santa Elena so unique is that the water supply is received in only 6 months rather than intermittent rainfall activity or snowpack accumulation. For example, meteoric recharge in Santa Elena is on average 10 times greater than those reported in Oman [Dewandel et al., 2005]; that being the case, it is plausible to expect that fissuring and constant development of macropores flow or active lateral flow pathways may increase to a great extent the permeability (i.e., vertically and

horizontally) in the peridotite resulting in greater water-rock interaction during the wet season and hyperalkaline fluid seepage throughout the baseflow period.

5.2. Hyperalkaline fluid chemistry comparison with other ultramafic systems

Figure 9 shows a comparison of hyperalkaline fluid composition in multiple ultramafic systems in temperate (Gruppo di Voltri, Italy; Cabeço de Vide, Portugal; Tablelands, Canada; Cazadero, USA; Kulasi, Bosnia), subtropical (Samail, Oman), and tropical environments (Le Coulee, New Caledonia; Santa Elena, Costa Rica, this study). As expected in a tropical setting, Santa Elena's hyperalkaline fluids exhibited the highest water temperature (29.0-30.7 °C) compared to the other sites. Recently, Chavagnac et al. [2013] reported temperatures ranging from 33-40°C in the Oman Ophiolite, yet these high temperatures are mostly the result of radiative heating of the surface waters. The lowest spring temperatures (below 18°C) correspond to the Gruppo di Voltri, Italy and Cabeço de Vide, Portugal. Overall, spring temperatures among all sites support the idea of an internal heat source related to present-day continental serpentinization. Calcium concentrations appear to be consistently between 5.1 mg/L and 60 mg/L; however, in this study, spring 9 in the Murciélago River has a maximum value of 167 mg/L, which may be evidence of active serpentinization rate versus a low CO_2 uptake. Palandri and Reed [2004] reported that serpentinizing waters may export high dissolved Ca concentrations out of the system, thus, if this solute transport process is slower than the CO_2 uptake (i.e. in a system that is closed in respect to CO_2) [Bruni et al., 2001] then Ca can accumulates in the hyperalkaline seepage pools. All ultramafic systems are consistently depleted in Mg concentrations. Depletion of Mg can be explained by formation of serpentine and/or brucite as suggested by Bruni et al. [2001]:

(R1) Mg^{2+} (aq) + 2 OH^- = $Mg(OH)_2$ (s)

(R2) 3 Mg^{2+} (aq) + 2$SiO_{2(}$aq) + 5H_2O = 2$Mg_3Si_2O_5(OH)_4$(s) + H^+

Other element chemistry such as Na, K, and Cl are within very similar ranges, except for the springs in the Oman Ophiolite where saltier conditions result in greater concentrations.

6. Conclusions

Field explorations in the Santa Elena Ophiolite provide strong evidence of active serpentinization in the area. In the hyperalkaline fluids, Mg was highly depleted probably due to serpentine formation and brucite precipitation in the subsurface, whereas Ca was abundant along with high concentrations of hydroxide, carbonates, and chloride. Further, the combination of active methane vents and extensive carbonate deposits also provide evidence of active serpentinization, though, methane may also form through methanogenic organisms. Signatures of methanogenic archaea from the orders Methanobacteriales, Methanocellales and Methanomicrobiales detected in the hyperalkaline fluids suggest that methanogenesis is an important process at this system. Further evidence for active serpentinization could give the possible presence of H_2 in the spring waters, which will be considered in future studies.

Natural well-mixed surface waters were characterized by a dominant Mg-HCO_3^- system, which represents ~95% of the major ions composition. Stable isotope data shows notable groundwater to surface water connectivity in the main perennial rivers where the hyperalkaline fluids were discovered. Most importantly, spring seepage temperature and isotopic composition (i.e. plotted on the local meteoric water line) strongly suggest no isotopic enrichment or any external heat source such as hydrothermal activity.

Overall, the long rainy season coupled with high rainfall intensity mainly controlled by coastal convective storms position the Santa Elena Ophiolite as an analogue of an early humid Earth where meteoric water inputs were abundant and mainly dominated by changes in the global circulation and sea surface temperature regimes. Given the distribution of mafic-ultramafic rocks on other planetary environments (e.g. Mars), the unique Santa Elena's environment will serve as a natural laboratory to better and fully characterize the planetary conditions that can support life. Likewise, variations in the carbonate mineralogy of veins or layered deposits can give insight into changing fluid compositions and element transport that might be a result of seasonal changes in the hydrological cycle.

Future work on the of carbonate deposits formed by discharge of the hyperalkaline springs will serve to refine the search criterion for the surface expression of these systems which could be used to identify both active and inactive serpentinization systems on other planetary bodies. Further evaluations will require continuous physical-chemical monitoring (i.e. resolution of minutes to hours) coupled with sampling of hyperalkaline fluids on an event basis (i.e. single storm responses) to determine the role of rapid meteoric recharge in serpentinization rates and chemosynthetic organisms as well as depicting the evolution of the hyperalkaline fluids composition throughout the baseflow recession regime.

7. Acknowledgments

The authors wish to thank the valuable collaboration from the ACG personnel, especially, Roger Blanco Segura (Research Program Coordinator), M. Marta Chavarría (Biodiversity especialist), and J. Calvo (field assistant). Field assistance by P. Madrigal and P. Denyer was also fundamental for field expeditions. We would like to thank the laboratory assistance of H. Hernández at Agrotec Analytical Laboratory and G. Esquivel, R. Alfaro, and J. Valdés at the Chemistry School of the National University, Costa Rica as well as figures design by A. Alcocer at University of Idaho. Santa Rosa weather data were kindly provided by the ACG. We thank W. Bach and an anonymous reviewers for helpful comments. This project was supported by the National Science Foundation grant No.EAR-1019327 to EG.

8. References

Abrajano, T.A., N.C. Sturchio, J.K. Bohlke, G.L. Lyon, R.J. Poreda, and C.M. Stevens (1988), Methane-hydrogen gas seeps, Zambales ophiolite, Philippines: Deep or shallow origin? *Chem. Geol.* 71, 211-222, doi: 10.1016/0009-2541(88)90116-7.

Abrajano, T.A., N.C. Sturchio, B.M. Kennedy, and G.L. Lyon (1990), Geochemistry of reduced gas related to serpentinization of the Zambales ophiolite, Philippines, *Appl. Geochem.* 5, 625-630, http://dx.doi.org/10.1016/0883-2927(90)90060-I

Allen, D. E. and W.E.J. Seyfried (2003), Compositional controls on vent fluids from ultramafic-hosted hydrothermal systems at mid-ocean ridges: An experimental study at 400°C, 500 bars, *Geochim. Cosmochim. Acta.* 67, 1531-1542, http://dx.doi.org/10.1016/S0016-7037(02)01173-0

Alt, J. C., E. M. Schwarzenbach, G. L. Früh-Green, W. C. Shanks, S. M. Bernasconi, C. J. Garrido, L. Crispini, L. Gaggero, J. A. Padrón-Navarta, and C. Marchesi (2013), The role of serpentinites in cycling of carbon and sulfur: Seafloor serpentinization and subdurction metamorphism, *Lithos,* 178(15), 40-54, http://dx.doi.org/10.1016/j.lithos.2012.12.006

Alt, J. C., W.C. Shanks, W. Bach, H. Paulick, C. J. Garrido, and G. Beaudoin (2007), Hydrothermal alteration and microbial sulfate reduction in peridotite and gabbro exposed by detachment faulting at the Mid-Atlantic Ridge, 15°20'N (ODP Leg 209): A sulfur and oxygen isotope study, *Geochem. Geophys. Geosyst.* 8(8), Q08002, doi:10.1029/2007GC001617.

Bach, W., H. Paulick, C.J. Garrido, B. Ildefonse, W.P. Meurer, and S.E. Humphris (2006), Unraveling the sequence of serpentinization reactions: petrography, mineral chemistry, and petrophysics of serpentinites from MAR 15°N (ODP Leg 209, Site 1274), *Geophys. Res. Lett.* 33, *L13306, doi:*10.1029/2006GL025681.

Barnes, I., V.C. LaMarceh, and G. Himmelberg (1967), Geochemical evidence of present-day serpentinization, *Science.* 156, 830-832.

Barnes I., J.R. O'Neil, and J.J. Trescases (1978), Present day serpentinization in New Caledonia, Oman and Yugoslavia, *Geochim. Cosmochim. Acta*. 42, 144-145.

Barron, E.J., W.W. Hay, and S. Thompson (1989), The hydrologic cycle: A major variable during Earth history, *Global and Planetary Change*, 1(3): 157-174, http://dx.doi.org/10.1016/0031-0182(89)90175-2

Baumgartner, P.O., and Denyer, P (2006), Evidence for middle Cretaceous accretion at Santa Elena Peninsula (Santa Rosa Accretionary Complex), Costa Rica. *Geologica Acta*, 4(1-2):179-191.

Blank, J.G., S.J. Green, D. Blake, J.W. Valley, N.T. Kita, A. Treiman, and P.F. Dobson (2009), An alkaline spring system within the Del Puerto Ophiolite (California, USA): A Mars analog site, *Planetary and Space Science,* 57, 533–540, doi:10.1016/j.pss.2008.11.018.

Boschetti, T., and L. Toscani (2008), Springs and streams of the Taro-ceno valleys (northern Apennine, Italy): Reaction path modeling of waters interacting with serpentinized ultramafic rocks, *Chem. Geol.,* 257, 76-91, doi:10.1016/j.chemgeo.2008.08.017

Brazelton, W.J., M.O. Schrenk, D.S. Kelley, and J.A. Baross (2006), Methane- and sulfur-metabolizing microbial communities dominate the Lost City hydrothermal field ecosystem, *Appl. Environ. Microbiol.* 72(9), 6257-6270, doi: 10.1128/AEM.00574-06

Brazelton, W.J., M.L. Sogin, and J.A. Baross (2010), Multiple scales of diversification within natural populations of archaea in hydrothermal chimney biofilms, *Environ. Microbiol. Rep.* 2(2), 236-242, doi: 10.1111/j.1758-2229.2009.00097.x

Brazelton, W.J., B. Nelson, and M.O. Schrenk (2012), Metagenomic evidence for H_2 oxidation and H_2 production by serpentinite-hosted subsurface microbial communities, *Frontiers in microbiology,* 2, 268. doi:10.3389/fmicb.2011.00268

Brazelton, W. J., P. L. Morrill, N. Szponar, and M.O.Schrenk (2013), Bacterial Communities Associated with Subsurface Geochemical Processes in Continental Serpentinite Springs, *Appl. Environ. Microbiology,* 79(13), 3906–3916, doi: 10.1128/AEM.00330-13.

Bruni, J., M. Canepa, G. Chiodini, R. Cioni, F. Cipolli, A. Longinelli, L. Marini, G. Ottonello, and M.V. Zuccolini (2002), Irreversible water- rock mass transfer accompanying the generation of the neutral, Mg-HCO3 and high-pH, Ca-OH spring waters of the Genova province, Italy, *Appl. Geochem.* 17, 455-474, http://dx.doi.org/10.1016/S0883-2927(01)00113-5.

Brutsaert, W (2005) Hydrology: an introduction. Cambridge University Press. Cambrigde, United Kingdom. 605 pp.

Cannat, M. (1993), Emplacement of mantle rocks in the sea-floor at mid-ocean ridges, *J. Geophys. Res.* 98(B3), 4163-4172, doi:10.1029/92JB02221.

Cannat, M., F. Fontaine, and J. Escartín (2013), Serpentinization and Associated Hydrogen And Methane Fluxes at Slow Spreading Ridges, in Diversity of Hydrothermal Systems on Slow Spreading Ocean Ridges (eds P. A. Rona, C. W. Devey, J. Dyment and B. J. Murton), American Geophysical Union, Washington, D. C., doi: 10.1029/2008GM000760.

Carr, M. J., Saginor, I., Alvarado, G. E., Bolge, L. L., Lindsay, F. N., Milidakis, K., Turrin, B.D., Feigenson, M.D., and Swisher, C. C. (2007), Element fluxes from the volcanic front of Nicaragua and Costa Rica, *Geochemistry Geophysics Geosystems*, *8*(6). doi: 10.1029/2006GC001396

Chavagnac, V., C. Monnin, G. Ceuleneer, C. Boulart, and G. Hoareau (2013), Characterization of hyperalkaline fluids produced by low-temperature serpentinization of mantle peridotites in the Oman and Liguria ophiolites, *Geochemistry, Geophysics, Geosystems, G3.* 14(00), 1-27, doi:10-1002/ggge.20147.

Christensen, P.R., Jr.H.Y. McSween, J.L. Bandfield, S.W. Ruff, A.D. Rogers, V.E. Hamilton, N. Gorelick, M.B. Wyatt, B.M. Jakosky, H.H. Kieffer, M.C. Malin, and J.E. Moersch (2005), Evidence for magmatic evolution and diversity on Mars from infrared observations, *Nature.* 436, 504–509, doi:10.1038/nature03639.

Cipolli, F., B. Gambardella, L. Marini, G. Ottonello, and M.V. Zuccolini (2004), Geochemistry of high-pH waters from serpentinites of the Gruppo di Voltri (Genova, Italy) and reaction path modeling of CO_2 sequestration in serpentinite aquifers, *Appl. Geochem.* 19, 787-802, doi:10.1016/j.apgeochem.2003.10.007

Clark, I. D., and J. C. Fontes (1990), Paleoclimatic reconstrution in the nothern Oman based on carbaontes from hyperalkaline groundwaters, *Quaternary Research,* 33(3), 320-336, http://dx.doi.org/10.1016/0033-5894(90)90059-T

Craddock, R., and A. Howard (2002), The case for rainfall on a warm, wet early Mars, *Geophysical Research,* 17, NO. E11, 5111, doi:10.1029/2001JE001505.

Denyer, P., and E. Gazel (2009), The Costa Rican Jurassic to Miocene oceanic complexes: Origin, tectonics and relations. *J. South Am Earth Sci.*, 28(4), 429-442, http://dx.doi.org/10.1016/j.jsames.2009.04.010

Dewandel, B., P. Lachassagne, and A. Qatan (2004), Spatial measurements of stream baseflow, a relevant method for aquifer characterization and permeability

evaluation. Application to a hard-rock aquifer, the Oman ophiolite, *Hydrological Processes,* 18, 3391–3400, doi: 10.1002/hyp.1502.

Dewandel, B., P. Lachassagne, F. Boudier, S. Al-Hattali, B. Ladouche, J.L. Pinault, and Z. Al-Suleimani (2005), A conceptual hydrogeological model of ophiolite hard-rock aquifers in Oman based on a multiscale and a multidisciplinary approach, *Hydrogeology*, 13, 708–726, doi: 10.1007/s10040-005-0449.

Dewandel, B., P. Lachassagne, M. Bakalowicz, P. Weng., and A. Al-Malki (2003), Evaluation of aquifer thickness by analyzing recession hydrographs. Application to the Oman ophiolite hard-rock aquifer, *Hydrology,* 274, 248-269, doi:10.1016/S0022-1694(02)00418-3.

Dunn, S.M., McDonnell, J.J., and Vaché, K.B. 2007. Factors influencing the residence time of catchment waters: A virtual experiment approach *Water Resources Research,* 43, W06408, doi:10.1029/2006WR005393.

Eaton, A. D., L. S. Clesceri, A.E.Greenberg, and M.A.H. Franson (1998), American Public Health Association., American Water Works Association., and Water Environment Federation. *Standard methods for the examination of water and wastewater*. Washington, DC: American Public Health Association.

Etiope, G., B. Tsikouras, S. Kordella, E. Ifandi, D. Christodoulou, G. Papatheodorou (2013), Methane flux and origin in the Othrys ophiolite hyperalkaline springs, Greece, *Chemical Geology*, 347 (2013) 161–174, http://dx.doi.org/10.1016/j.chemgeo.2013.04.003

Fairén, A. (2010), A cold and wet Mars, *Icarus*, 208: 165-175, http://dx.doi.org/10.1016/j.icarus.2010.01.006

Foustoukos, D. I., and W.E.J. Seyfried (2004), Hydrocarbons in hydrothermal vent fluids: The role of chromium-bearing catalysts, *Science*, 304, 1002-1005, *doi:*10.1126/science.1096033

Frost, B. R. (1985), On the stability of sulfides, oxides, and native metals in serpentinite. *J. Petrol.* 26, 31-63, doi:10.1093/petrology/26.1.31.

Frost, B. R., and J. S. Beard (2007), On silica activity and serpentinization, *J. Petrol.* 48, 1351-1368, doi: 10.1093/petrology/egm021.

Früh-Green, G.L., J.A. Connelly, A. Plas, D.S. Kelley, and B. Grobéty (2004), Serpentinization of oceanic peridotites: Implications for geochemical cycles and biological activity. In: the subseafloor biospere at Mid-Ocean Ridges, 2004. The Subseafloor Biosphere at Mid-Ocean Ridges, 144. American Geophysical Union, Washington D.C.

Früh-Green, G.L., E.M. Schwarzenbach, S. Méhay, M.D. Lilley, S.M. Bernasconi, M. Molinari, and L. Marini (2009), Alkaline fluids and reduced volatiles in modern serpentinizing environments, American Geophysical Union, Fall Meeting 2009, abstract #V43B-2256.

Gazel, E., P. Denyer, and P.O. Baumgartner (2006), Magmatic and geotectonic significance of Santa Elena Peninsula, Costa Rica, *Geologica Acta.* 4(1-2), 193-202, doi:10.1344/105.000000365.

Guswa, A.J., A. Rhodes, and S.E. Newell (2007), Importance of orographic precipitation to the water resources of Monteverde, Costa Rica, *Advances in Water Resources.* 30, 2098–2112, http://dx.doi.org/10.1016/j.advwatres.2006.07.008.

Hand, K.P., R.W. Carlson, and C.F. Chyba (2007), Energy, chemical disequilibrium, and geological constraints on Europa, *Astrobiology.* 7, 1006–1022, doi:10.1089/ast.2007.0156.

Hauff, F., Hoernle, K., Van den Bogaard, P., Alvarado, G.E., Garbe-Schönber, D (2000), Age and geochemistry of basaltic complexes in western Costa Rica: Contributions to the geotectonic evolution of Central America. *Geochemistry, Geophysics, Geosystems,* 1(5). doi: 10.1029/1999GC000020

Herzberg, C., and Gazel, E (2009), Petrological evidence for secular cooling in the mantle plumes. *Nature*, 458(7238):619-622.

Hobbie, J.E., R.J. Daley, and S. Jasper (1977), Use of nucleopore filters for counting bacteria by fluorescence microscopy, *Appl. Environ. Microbiol.* 33, 1225-1228, PMC170856.

Hoefen, T.M., R.N. Clark, J.L. Bandfield, M.D. Smith, J.C. Pearl, P.R. Christensen (2003), Discovery of olivine in the Nili Fossae region of Mars, *Science.* 302, 627-630, doi:10.1126/science.1089647.

Holm, N.G., M. Dumont, M. Ivarsson, and C. Konn (2006), Alkaline fluid circulation in ultramafic rocks and formation of nucleotide constituents: a hypothesis, *Geochem. Trans.* 7(7), doi:10.1186/1467-4866-7-7.

Huber, J.A., D.A. Butterfield, and J.A. Barros (2002), Temporal changes in archaeal diversity and chemistry in a mid-ocean ridge subseafloor habitat, *Appl. Environ. Microbiol.* 68, 1585-1594, doi: 10.1128/AEM.68.4.1585-1594.2002.

Huse, S.M., L. Dethlefsen, J.A. Huber, D.M. Welch, D.A. Relman, and M.L. Sogin (2008), Exploring microbial diversity and taxonomy using SSU rRNA hypervariable tag sequencing, *PLoS Gent*., 4:e1000255.doi:10.1371/journal.pgen.1000255

Huse, S.M., D.M. Welch, H.G. Morrison, and M.L. Sogin (2010), Ironing out the wrinkles in the rare biosphere through improved OUT clustering, *Environ.Microbiol.,* 12, 1889-1898, doi: 10.1111/j.1462-2920.2010.02193.x.

Jedryseck, M.O., and M. Sachanbiski (1994), Stable isotope and trace element studies of vein ophicarbonates at Gogolow-Jordanow serpentinite massif (Poland): A contribution to the origin of phiaragonite and ophimagnesite, *Geochemical,* 28, 341-350.

Kelemen, P., and J. Matter, (2008), In situ carbonation of peridotite for CO2 storage, *PNAS*, 105(45): 17295–17300, doi:10.1073/pnas.0805794105

Kelemen, P.B., Matter, Juerg, Streit, Elisabeth E., Rudge, John F., Curry, William B. and Blusztajn, Jerzy (2011) Rates and mechanisms of mineral carbonation in peridotite: natural processes and recipes for enhanced, in situ CO2 capture and storage, *Annual Review of Earth and Planetary Sciences*, 39, (1), 545-576, doi:10.1146/annurev-earth-092010-152509.

Kelley, D.S., J.A. Karson, G.L. Früh-Green, D.R.Yoerger, T.M. Shank, D.A. Butterfield, J.M. Hayes, M.O. Schrenk, E.J. Olson, G. Proskurowski, M. Jakuba, A. Bradley, B. Larson, K.A. Ludwig, D. Glickson, K. Buckman, A.S. Bradley, W.J. Brazelton, K. Roe, M.J. Elend, A. Delacour, S.M. Bernasconi, D.M. Lilley, J.A. Baross, R.E. Summons, and S.P. Sylva (2005), A serpentinite-hosted ecosystem: The lost city hydrothermal field, *Science.* 307, 1428 – 1434, doi:10.1126/science.1102556

Kelley, S.D., J.A. Karson, D.K. Blackman, G.L. Früh-Green, D.A. Butterfield, D.M. Lilley, E.J. Olson, M.O. Schrenk, K.K. Roell, G.T. Lebon, P. Rivizzigno, and the AT3-

60 Shipboard Party. (2001), An off-axis hydrothermal vent field near the Mid-Atlantic Ridge at 30° N, *Nature.* 412, 145-149, doi:10.1038/35084000

Lang, S.Q., Früh-Green, G.L., Bernasconi, S.M., Lilley, M.D., Proskurowski, G., Mehay, S., Butterfield, D.A. Microbial utilization of abiogenic carbon and hydrogen in a serpentinite-hosted system. *Geochimica and Cosmochimica Acta, 92: 82-99.* http://dx.doi.org/10.1016/j.gca.2012.06.006

Lis, G.P., L.I. Wassenaar, and M.J. Hendry (2008), High-precision laser spectroscopy D/H and 18O/16O measurements of microliter natural water samples, *Anal. Chem.,* 80(1), 287–293, doi:10.1021/ac701716q

Matter, J., H. N. Waber , S. Loew, and A. Matter, (2006), Recharge areas and geochemical evolution of groundwater in an alluvial aquifer system in the Sultanate of Oman, *Hydrogeology Journal*, 14: 203–224, DOI 10.1007/s10040-004-0425-2

Matter, J., T. Takahashi, and D. Goldberg, (2007), Experimental evaluation of in situ CO2-water-rock reactions during CO2 injection in basaltic rocks: Implications for geological CO2 sequestration, *Geochemistry, Geophysics, Geosystems,* 8(2), doi:10.1029/2006GC001427

Macdonald, A.H. and W.S. Fyfe (1985), Rate of serpentinization in seafloor environments, *Tectonophysics*, 116, 123-135, http://dx.doi.org/10.1016/0040-1951(85)90225-2

McGuire, K.J., DeWalle, D.R., and Gburek, D.J. 2002. Evaluation of mean residence in subsurface waters using oxygen-18 fluctuations during drought conditions in the mid-Appalachians. Hydrology, 261: 132-149. http://dx.doi.org/10.1016/S0022-1694(02)00006-9

Marques, J.M., P.M. Carreira, M.R. Carvalho, M.J. Jatias, F.E. Goff, M.J. Basto, R.C. Graca, L. Aires-Barros, and L.Rocha (2008), Origins of high pH mineral waters from ultramafic rocks, Central Portugal, *Appl. Geochem.,* 23, 3278 – 3289, doi:10.1016/j.apgeochem.2008.06.029

Martin, W., and M. J. Russell (2007), On the origin of biochemistry at an alkaline hydrothermal vent, *Philos. Trans. R. Soc. B-Biol. Sci.*, 362, 1887-1925, doi: 10.1098/rstb.2006.1881

Morrill, P.L., J.G. Kuenen, O.J. Johnson, S. Suzuki, A. Rietze, A.L. Sessions, M.L. Fogel, and K.H. Nealson (2013), Geochemistry and geobiology of a present-day serpentinization site in California: The Cedars, *Geochimica et Cosmochimica Acta*, (109), 222–240, http://dx.doi.org/10.1016/j.gca.2013.01.043

Mayhew, L. E., E. T. Ellison, T. M. McCollom, T. P. Trainor, and A. S. Tempelton (2013), Hydrogen generation from low-temperature water-rock reactions, *Nat. Geosci.,* 6, 478-484, doi:10.1038/ngeo1825

Myers, J. S., and J. L. Crowley (2000), Vestiges of life in the oldest Greenland rocks? A review of early Archean geology in the Godthabsfjord region, and reappraisal of field evidence for >3850 Ma life on Akilia, *Precambrian Res.* 103, 101-124.

Mulligan, M. and S.M. Burke (2005), Fog Interception for the enhancement of streamflow in tropical Areas (90 m resolution hydrological model). Data base accessed on September 30, 2013. http://www.ambiotek.com/fiesta

National Climatic Data Center. Climate data online: search tool. National Oceanic and Atmospheric Administration. http://www.ncdc.noaa.gov/cdo-web/search. Accesed on: November, 25, 2013.

Neal, C., and G. Stanger (1983), Hydrogen generation from mantle source rocks in Oman, *Earth Planet. Sci. Lett.* 66, 315-320, http://dx.doi.org/10.1016/0012-821X(83)90144-9

Neubeck, A., N.T. Duc, D. Bastviken, P. Crill, and N. G. Holm (2011), Formation of H_2 and CH_4 by weathering of olivine at temperatures between 30 and 70°C, *Geochem. Trans.* 12(6), doi:10.1186/1467-4866-12-6

Nisbet, E.G., and N.H. Sleep (2001), The habitat and nature of early life, *Nature,* 409, 1083-1091, doi:10.1038/35059210

O'Neil, J. R., and I. Barnes (1971), C13 and O18 compositions in some fresh-water carbonates associated with ultramafic rocks and serpentinites: Western United States, *Geochim. Cosmochim. Acta,* 35, 687-697.

Palandri, J.L., and M.H. Reed (2004), Geochemical models of metasomatism in ultramafic systems: Serpertinization, rodingitization, and sea floor carnonate chimmey precipitation, *Geochim. Cosmochim. Acta,* 68(5), 1115-1133, doi:10.1016/j.gca.2003.08.006

Paige, D (2005), Ancient Mars: Wet in Many Places, *Science,* 307: 1575-1576, doi*:* 10.1126/science.1110530

Paukert, A.N., M. Jürg, P.B. Kelemen, E.L. Shock, and J.R Havig (2012), Reaction path modeling of enhanced in situ CO2 mineralization for carbon sequestration in the peridotite of the Samail Ophiolite, Sultanate of Oman, Chemical Geology, 330-331, 86-100, doi:10.1016/j.chemgeo.2012.08.013

Pirard, C., J. Hermann, and H.St.C. O'Neill (2013), Petrology and geochemistry of the crust-mantle boundary in a nascent arc, Massif du Sud Ophiolite, New Caledonia, SW Pacific, *Petrology*, 54(9): 1759-1792, doi:10.1093/petrology/egt030

Proskurowski, G., Lilley, M.D., Seewald, J.S., Frueh-Green, G.L., Olson, E.J.. Lupton, J.E., Sylva, S.P., and Kelley, D.S. Abiogenic hydrocarbon production at Lost City Hydrothermal Field. *Science,* 319: 604–607. *doi:* 10.1126/science.1151194

Quesnel, B., P. Gautier, P. Boulvais, M. Cathelineau, P. Maurizot, D. Cluzel, M. Ulrich, S. Guillot, S. Lesimple, and C. Couteau, (2013), Syn-tectonic, meteoric water–derived carbonation of the New Caledonia peridotite nappe, *Geology,* 41(10), 1063–1066, doi:10.1130/G34531.1

Russell, M.J., and I. Kanik (2010), Why does life start, what Does it do, where might it be, how might we find it? *J. Cosmol.,* 5, 1008–1039.

Russell, M.J., A.J. Hall, and D. Turner (1989), In vitro growth of iron sulphide chimneys: possible culture chambers for origin-of-life experiments, *Terra Nova*, 1, 238–241, doi: 10.1111/j.1365-3121.1989.tb00364.x

Russell, M.J., R.M. Daniel, A.J. Hall, and J. Sherringham (1994), A hydrothermally precipitated catalytic iron sulphide membrane as a first step toward life, *J. Mol. Evol.,* 39, 231–243.

Saginor, I., Gazel, E., Condie, C., and Carr, M.J (2013), Evolution of geochemical variations along the Central American volcanic front, *Geochemistry, Geophysics, Geosystems*, *14*(10), 4504-4522.

Sanghyun, K, and Sungwon, J. 2014. Estimation of mean water transit time on a steep hillslope in South Korea using soil moisture measurements and deuterium excess. *Hydrological Processes*, 28: 1844-1857. doi: 10.1002/hyp.9722

Sánchez-Murillo, R., G. Esquivel-Hernández, K. Welsh, E.S. Brooks, J. Boll, R. Alfaro-Solís, and J. Valdés-González, (2013), Spatial and temporal variation of stable isotopes in precipitation across Costa Rica: an analysis of historic GNIP records, *Modern Hydrology,* 3, 226-240, doi: 10.4236/ojmh.2013.34027

Schrenk, M.O., D.S. Kelley, J.R. Delaney, and J.A. Baross (2003), Incidence and diversity of microorganisms within the walls of an active deep-sea sulfide chimney, *Appl. Environ. Microbiol.* 69, 3580-3592, doi: 10.1128/AEM.69.6.3580-3592.2003

Schrenk, M.O., D.S. Kelley, S.A. Bolton, and J.A. Baross (2004), Low archaeal diversity linked to subseafloor geochemical processes at the Lost City Hydrothermal Field, Mid-Atlantic Ridge, *Environ. Microbiol.,* 6(10), 1086-1095, doi:10.1111/j.1462-2920.2004.00650.x

Schrenk, M.O., W.J. Brazelton, and S.Q. Lang (2013), Serpentinization, Carbon, and Deep Life. Mineralogical Society of America, *Reviews in Mineralogy and Geochemistry*, 75: 575-606, doi: 10.2138/rmg.2013.75.18

Schulte, M., D. Blake, T. Hoehler, and T. McCollom (2006), Serpentinization and its implications for life on the early Earth and Mars, *Astrobiology*. 6, 364-376, doi: 10.1130/focus102010.1

Schwarzenbach, E.M., G.L. Früh-Green, S.M. Bernasconi, J.C. Alt, and A. Plas (2013a), Serpentinization and the incorporation of carbon: A study of two ancient peridotite-hosted hydrothermal systems, *Chemical Geology*, 351, 115-133, doi:10.1016/j.chemgeo.2013.05.016

Schwarzenbach, E.M., S.Q. Lang, G.L. Früh-Green, M.D. Lilley, S.M. Bernasconi, and S. Méhay (2013b), Sources and cycling of carbon in continental, serpentinite-hosted alkaline springs in the Voltri Massif, Italy, *Lithos,* 177, 226-244, doi:10.1016/j.lithos.2013.07.009

Shervais, J.W., P. Kolesar, and K. Andreasen (2005), A field and chemical study of serpentinization—Stonyford, California: chemical fluxes and mass balance, *Int. Geol. Rev.* 47, 1–23, doi:10.2747/0020-6814.47.1.1

Sogin, M.L, H.G. Morrison, J.A. Huber, D.M. Welch, S.M. Huse, P.R. Neal, J.M. Arrieta, and G.J. Herndl (2006), Microbial diversity in the deep sea and the underexplored “rare biosphere”, *Proc. Natl. Acad. Sci. U.S.A.,* 103:12115-12120, doi:10.1073/pnas.0605127103

Soulsby, C., Tetzlaff, D., and Hrachowitz, M. 2009. Tracers and transit times: windows for viewing catchment scale storage? *Hydrological Processes,* 23: 3503–3507. doi: 10.1002/hyp.7501.

Stewart, M.K., Morgenstern, U., McDonnell, J.J., and Pfister, L. 2012. The 'hidden streamflow' challenge in catchment hydrology: a call to action for stream water transit time analysis. *Hydrological Processes,* 26, 2061–2066. doi: 10.1002/hyp.9262

Szponar, N., W.J. Brazelton, M.O. Schrenk, D.M. Bower, A. Steele, and P.L. Morrill (2012), Geochemistry of a continental site of serpentinization, the Tablelands Ophiolite, Gros Morne National Park: A Mars analogue, *Icarus,* 224, 286–296, doi:10.1016/j.icarus.2012.07.004

Suzuki, S., S. Ishnii, A.Wu, A. Cheung, A. Tenney, G. Wanger, J.G. Kuenen, and K. Nealson (2013), Microbial diversity in The Cedars, and ultrabasic, ultrareducing, and low salinity serpentinizing ecosystem, *Proc Natl Acad Sci,* 110(38):15336-41, PMC3780913

Tournon, J., Seyler, M., Astorga, A (1995), Les peridotites du Rio San Juan (Nicaragua et Costa Rica); jalons possibles d'une suture ultrabasique E-W en Amerique Centrale meridionale. *Comptes Rendus de l'Academie des Sciences*, 320(8), 757-764.

Waylen, P., C.N. Caviedes, and M.E. Quesada (1996), Interannual variability of monthly precipitation in Costa Rica, *Climate*. 9, 2506-2613.

Table 1: Percent of sequences related to hydrogen, methane and methanol metabolism.

Division	Family;Genus	Metabolism	Murciélago Spring 8	Murciélago Spring 9	Danta Spring
Bacteria	Pseudonocardiaceae; Pseudonocardia	Hydrogen oxidation	0.00	0.00	0.01
Bacteria	Hyphomicrobiaceae; Xanthobacter	Hydrogen oxidation	0.00	0.00	0.01
Bacteria	Hydrogenophilaceae; Hydrogenophilus	Hydrogen oxidation	0.24	0.01	0.00
Bacteria	Hydrogenophilaceae; Tepidiphilus	Hydrogen oxidation	0.00	0.14	0.00
Bacteria	Hydrogenophilaceae; Thiobacillus	Hydrogen oxidation	0.02	0.00	0.00
Bacteria	Rhodobacteraceae; Paracoccus	Hydrogen oxidation	0.18	0.02	0.00
Bacteria	Comamonadaceae; Azohydromonas	Hydrogen oxidation	0.00	0.00	0.00
Bacteria	Comamonadaceae; Hydrogenophaga	Hydrogen oxidation	8.10	19.82	3.21
Bacteria	Methylococcaceae; Methylocaldum	Methane oxidation	0.00	0.00	0.00
Bacteria	Methylococcaceae; Methylomonas	Methane oxidation	0.02	0.01	0.00
Bacteria	Methylococcaceae; Methylosoma	Methane oxidation	0.01	0.00	0.00
Bacteria	Methylobacteriaceae; Meganema	Methane oxidation	0.12	0.00	0.00
Bacteria	Methylobacteriaceae; Methylobacterium	Methane oxidation	0.26	0.01	0.01
Bacteria	Methylocystaceae; Methylocystis	Methane oxidation	0.08	0.01	0.00
Bacteria	Methylocystaceae; genus_NA*	Methane oxidation	0.59	0.00	0.00
Bacteria	Comamonadaceae; Methylibium	Methanol oxidation	49.64	1.36	0.70
Bacteria	Methylophilaceae; Methylophilus	Methanol oxidation	0.00	0.01	0.01
Bacteria	Methylophilaceae; Methylotenera	Methanol oxidation	0.00	0.01	0.00
Bacteria	Methylophilaceae;genus_NA	Methanol oxidation	0.00	1.42	1.09
Archaea	Methanobacteriaceae;Methanobacterium	Methanogenesis	0.46	0.83	0.14
Archaea	Methanobacteriaceae; Methanobrevibacter	Methanogenesis	0.00	0.53	0.00
Archaea	Methanobacteriaceae; genus_NA	Methanogenesis	0.00	3.75	28.87
Archaea	Methanocellaceae; Methanocella	Methanogenesis	0.00	0.00	0.00
Archaea	Methanocellaceae; Rice_Cluster_I	Methanogenesis	1.29	4.51	0.00
Archaea	Methanospirillaceae; Methanospirillum	Methanogenesis	0.01	6.79	0.00
Archaea	Methanosaetaceae; Methanosaeta	Methanogenesis	0.00	0.01	0.00

**NA = unclassified*.

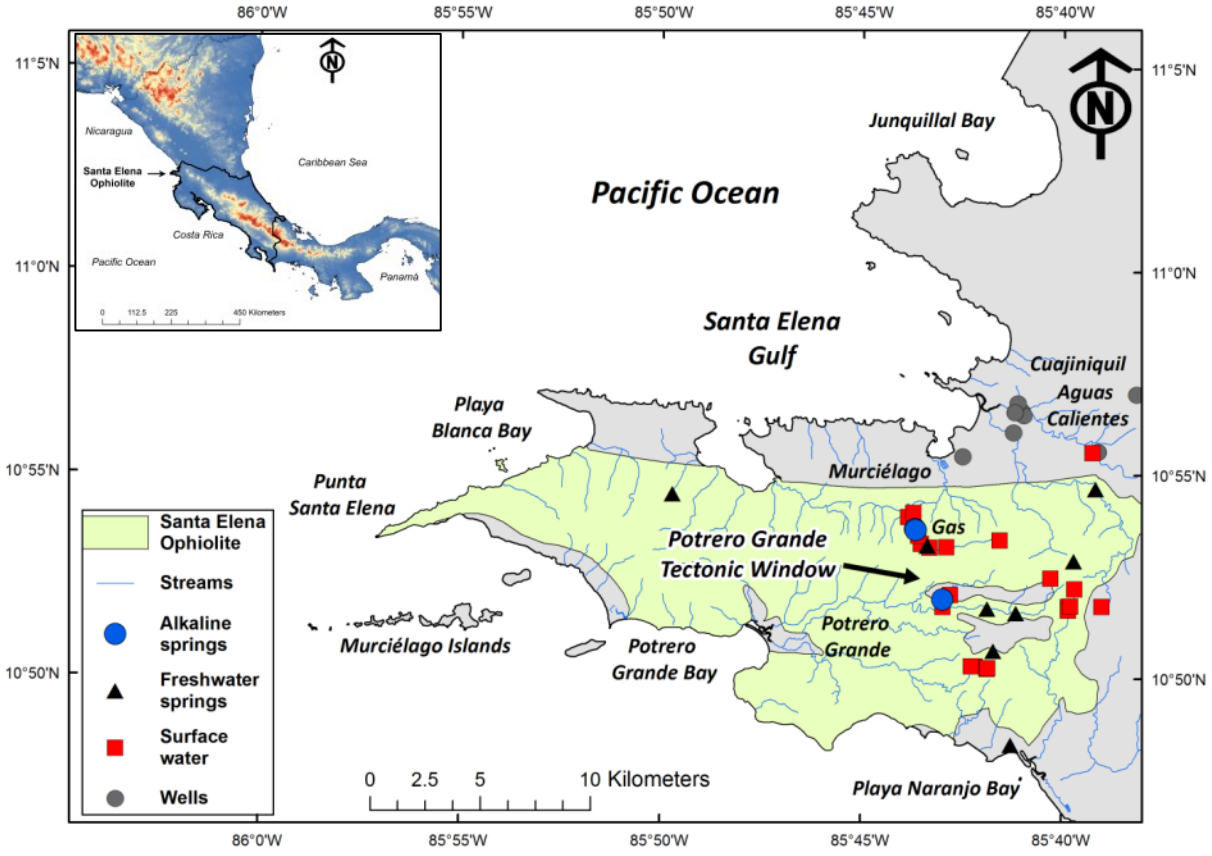

Figure 1: Map of the study area. Blue highlighted area denotes Santa Elena Ophiolite, dominated by ultramafic mantle rocks based on *Gazel et al.* [2006]. Sample locations are color coded: alkaline spring systems within Murciélago and Potrero Grande watersheds are identified by red crosses. Black and blue squares represent freshwater springs and wells, respectively. Open circles stand for surface water sites. Blue lines are perennial and intermittent streams. Inset shows an overview of Central America.

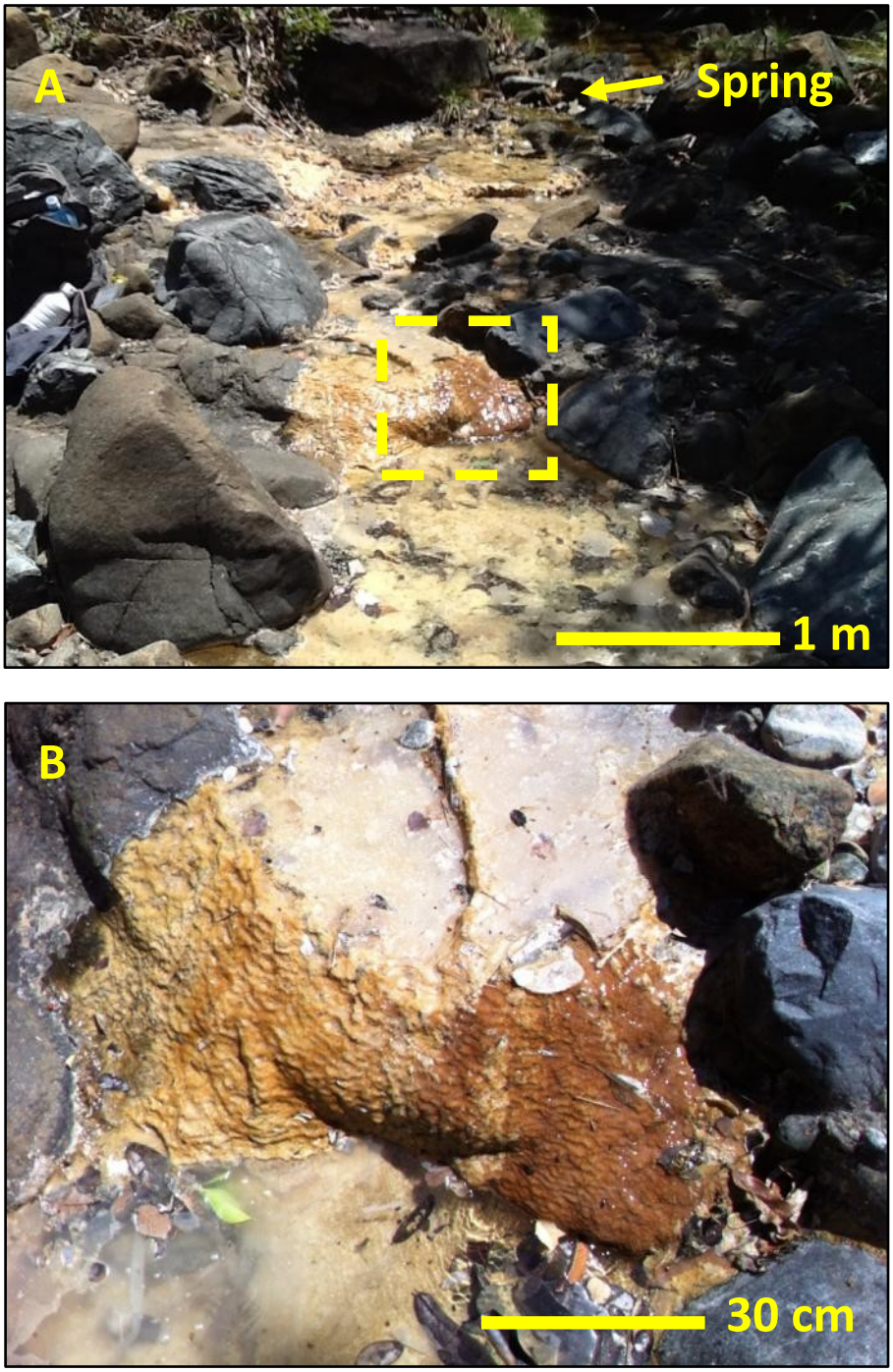

Figure 2: A) Image of the hyperalkaline spring at Quebrada Danta site (within the Potrero Grande tectonic window) showing pool on the left stream bank with extensive yellow-brown precipitates. These precipitates form small travertine terraces. B) Enlargement of yellow dash-square area. Note high water turbidity, organic matter, travertine deposits, and white supernatant crust are due to atmospheric CO2 uptake.

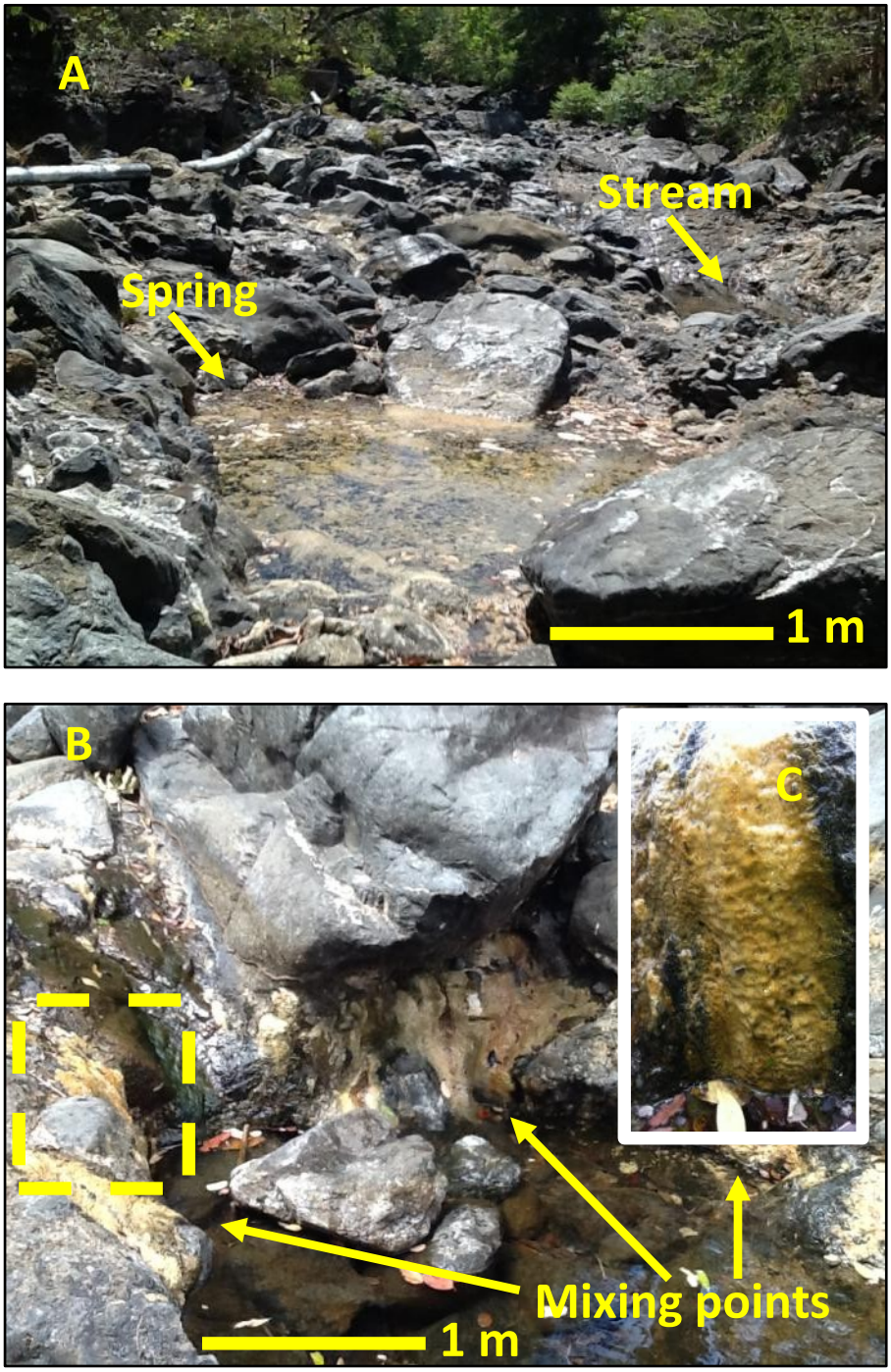

Figure 3: *A)* Image of the hyperalkaline spring at Río Murciélago site showing pool on the right stream bank with presence of yellow-brown precipitates. *B)* Image of yellow-brown precipitates covering riparian bedrocks and mixing points of hyperalkaline fluids and stream water. Dilution with receiving stream water occurs rapidly. C) Enlargement of yellow dashed-square area in B. Preciptates in contact with stream water.

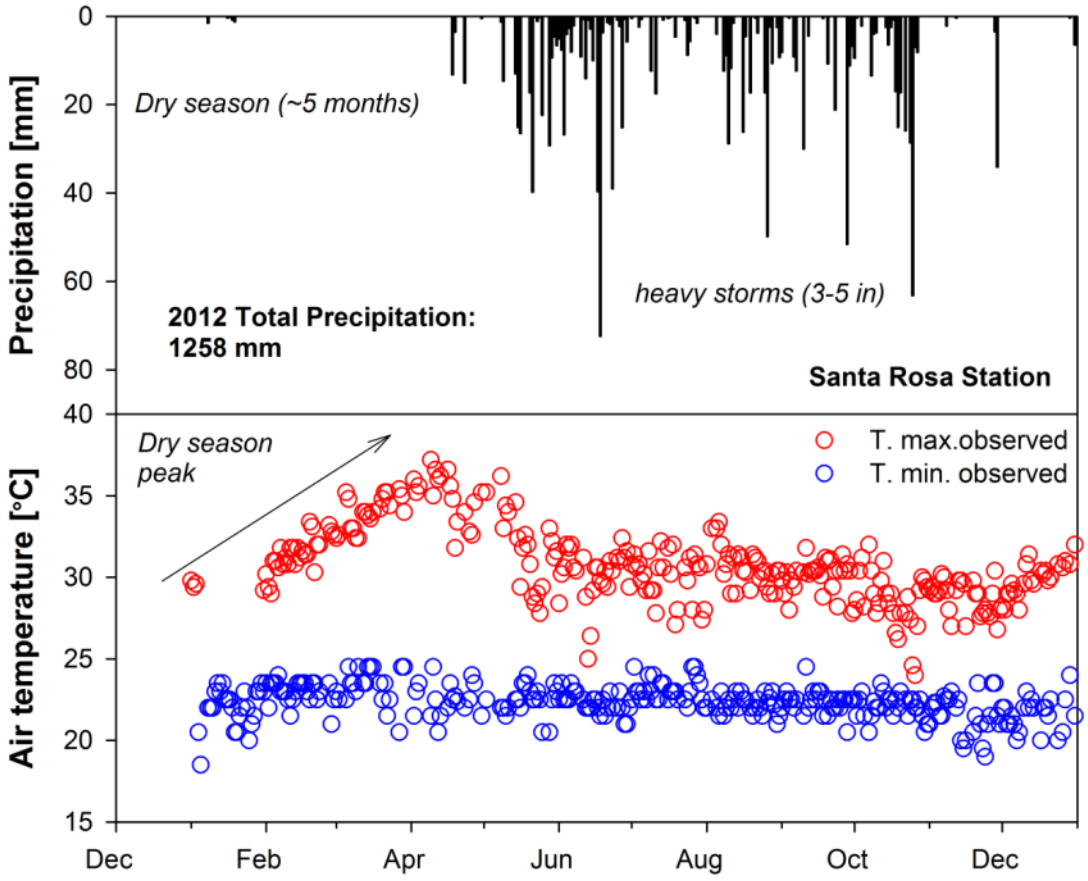

Figure 4: Santa Elena climate generalities. Top) Daily precipitation [mm]. Bottom) Maximum and minimum ambient temperatures [°C] during the 2012 water year. Maximum temperature (April) is close to 40°C. Minimum temperature is on average 23°C.

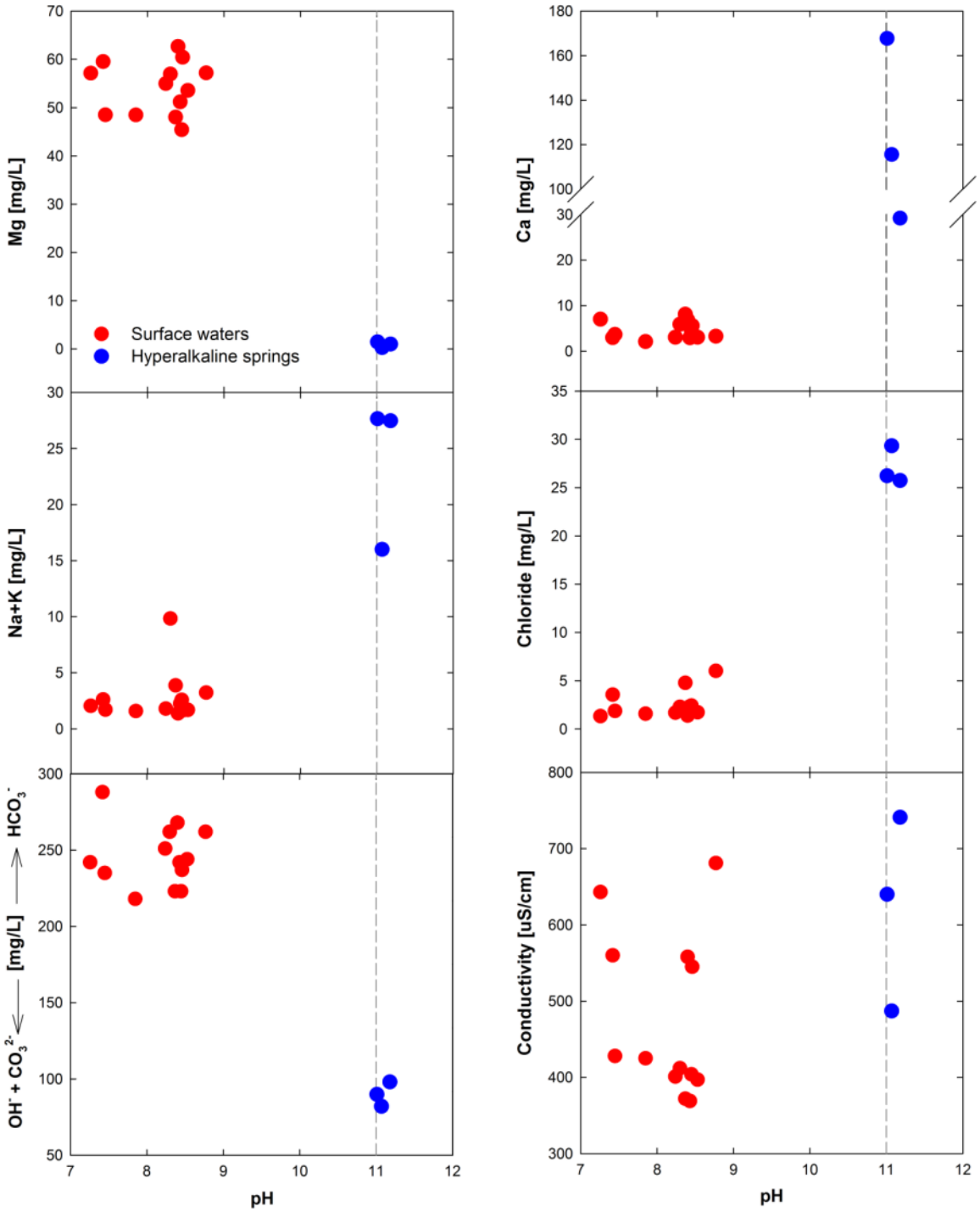

Figure 5: Surface water and hyperalkaline spring water chemical composition. Gray dashed line represents pH=11.0. Hyperalkaline fluids are characterized by high Ca, N+K, and chloride concentrations while surface waters show an inverse composition dominated by Mg and bicarbonate. Hydroxide and carbonate were only detected within the hyperalkaline springs.

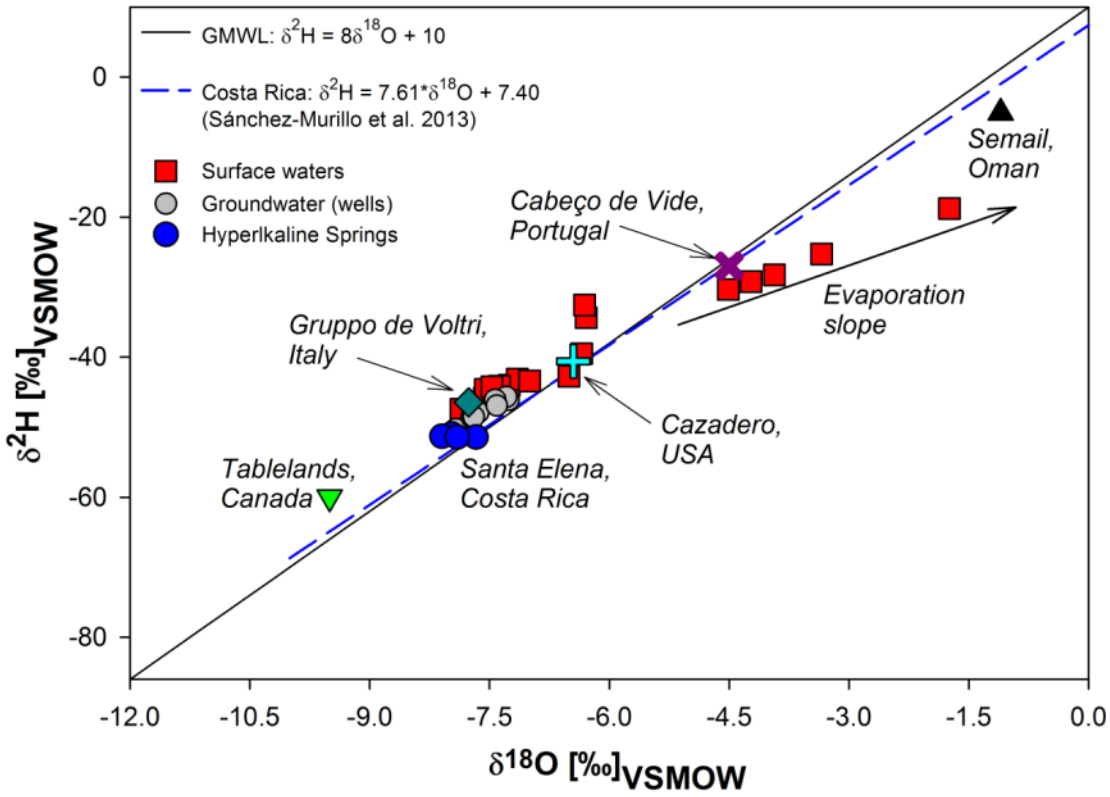

Figure 6: Stable isotope ($\delta^{18}O$ and $\delta^{2}H$) composition [‰] of surface water (red squares), groundwater wells (gray circles), and hyperalkaline springs (blue circles) in the Santa Elena Ophiolite. Surface water samples follow an evaporation enrichment line as travel distance increases. Hyperalkaline springs show a similar isotopic signature compared with groundwater samples from 12 deep wells. Global and Costa Rica meteoric water lines are included to reference meteoric water origin. Mean stable isotope composition in similar subtropical and temperate locations are color coded: Hahwalah Wadi Jizi, Semail, Oman (black triangle) [*Barnes et al. 1978*]; Cazadero, California, USA (cyan cross) [*Barnes et al. 1978*]; Cabeço de Vide, Portugal (purple cross) [*Marques et al. 2008*]; Tablelands, Gros Morne National Park, Canada (green triangle down) [*Szponar et al. 2012*]; Gruppo di Voltri, Italy (dark green rhombus) [*Cipolli et al., 2004*].

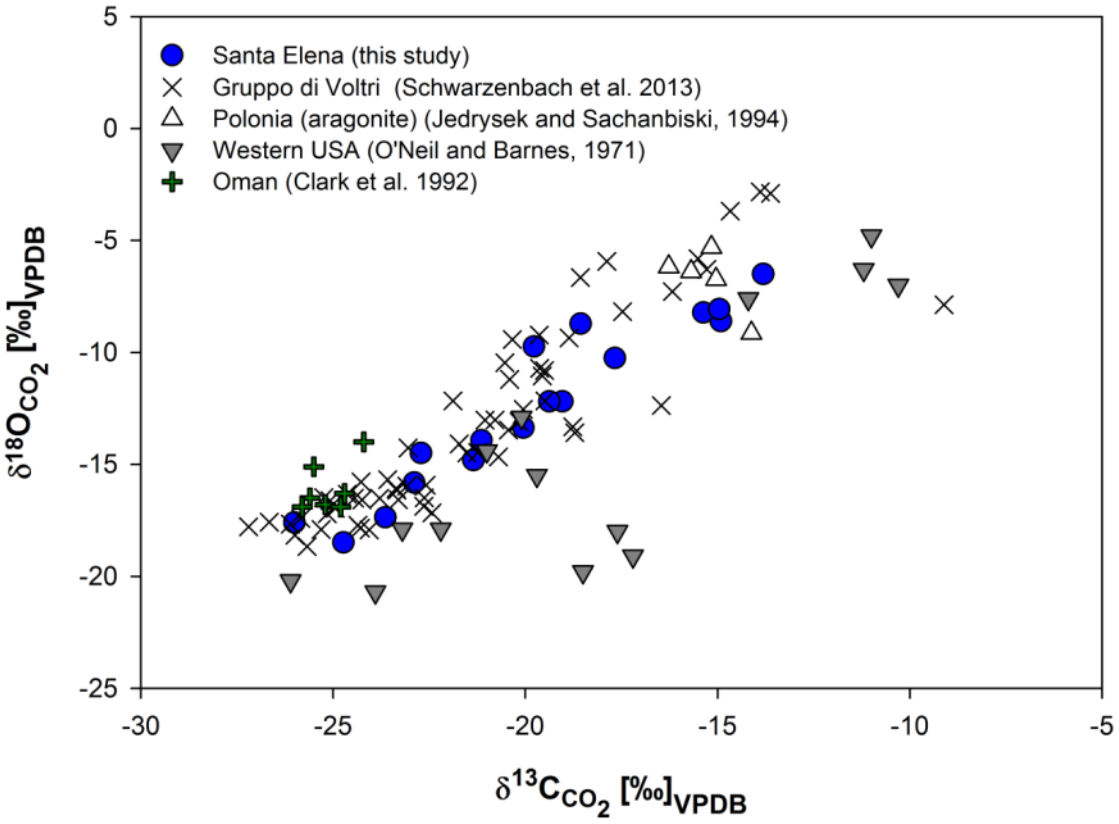

Figure 7: Comparison of Santa Elena $\delta^{13}C$ and $\delta^{18}O$ composition (‰) (blue circles) and summary of similar ultramafic hosted carbonate deposits in subtropical and temperate sites: Gruppo di Voltri, Italy (black crosses) [*Schewarzenbach et al., 2013*]; Polonia (open triangles) [*Jedrysek and Sachanbiski, 1994*]; Western USA (gray triangles down) [*O'Neil and Barnes, 1971*]; Oman (green crosses) [*Clark et al. 1992*]. Santa Elena's carbon and oxygen isotope composition of carbonates is within the range of similar ultramafic hosted carbonate deposits.

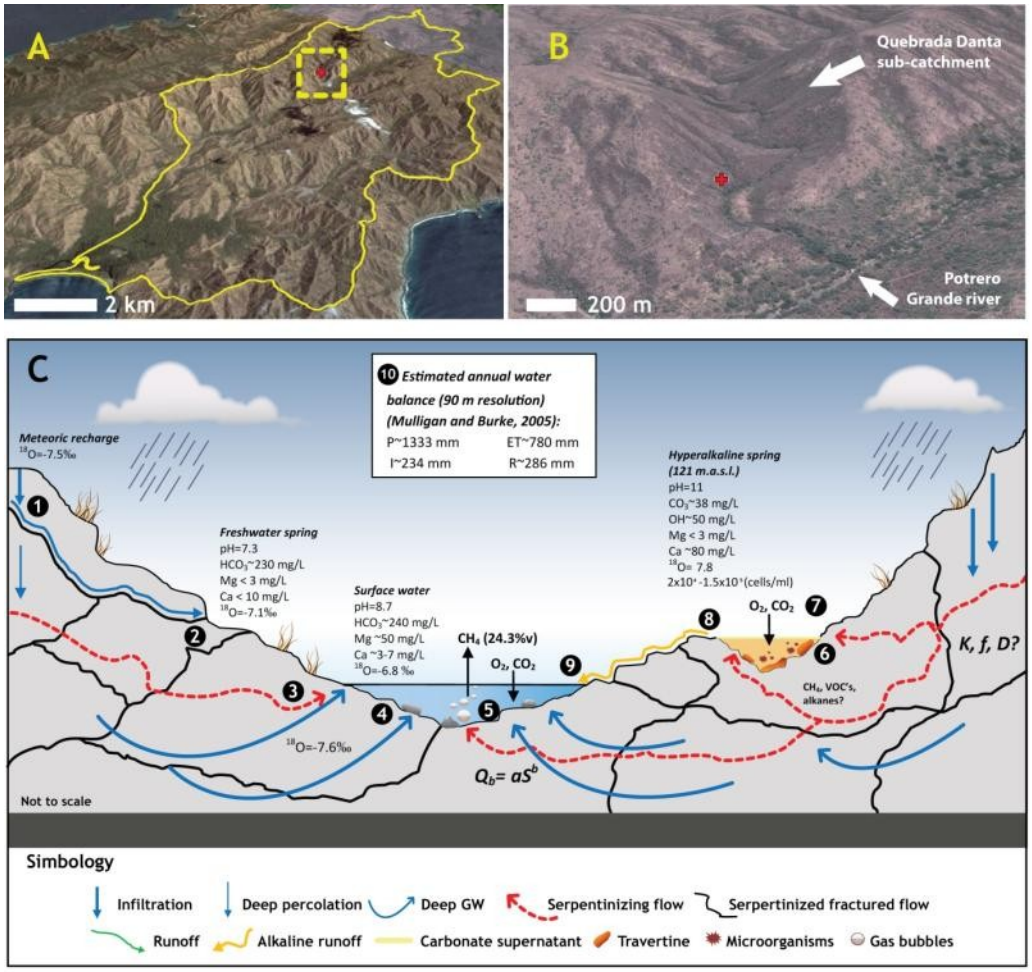

Figure 8: Schematic representation illustrating the hyperalkaline baseflow process proposed for the Santa Elena Ophiolite. A) Digital elevation overview of Potrero Grande watershed (Landsat Image, USGS, 90 m). Yellow line represents watershed boundary and yellow dashed-square denotes Quebrada Danta subcatchment. Red cross corresponds to the hyperalkaline system. B) Enlargement of yellow dashed-square area over Quebrada Danta subcatchment; mean basin slope is ~33%. Vegetation is scarce on hillslopes; but mostly concentrated in the riparian zones of the floodplain. C) A conceptual hyperalkaline baseflow process coupled with measured water chemistry and field observations. Soil profile is relatively absent (less than 20 cm). Infiltration occurs directly through the ultramafic formation [1]. Piston-type flow may occur within serpertinized fractured macropores (i.e. faults) producing freshwater springs if the system is open in respect to CO_2 [2]. These flow paths appear to be relatively shallow. Deep groundwater flow feeds the creek during the dry season [4]. Baseflow discharge is a function of storage, where *a* corresponds to the characteristic recession timescale (presumably low due to high evapotranspiration). Hydraulic parameters such as conductivity (K), drainage porosity (*f*), and aquifer thickness (*D*) are unknown. If the system responds as a linear reservoir, then *b=1*. Deep groundwater flow may dilute the signature of active serpentinizing [3]. However, active serpentinizing flow paths could also emerge as hyperalkaline

springs probably with an exponential-piston flow distribution due to the constant structural changes [6]. Hyperalkaline fluids form riparian pools coated by a $CaCO_3$ supernatant film where travertine terraces are evident and potential heterotrophic microbial methanogenesis may also occur [7, 8]. The hyperalkaline fluids are characterized by high pH, Ca, and low Mg. The fluids mix with receiving stream waters at low rates and volumes, thus, dilution occurs rapidly [9]. As measured in the Río Murciélago watershed methane emanations (24.3% v/v) occur at the streambed [5]. Other hydrocarbons may be produced during the serpentinization process. Based on the *Mulligan and Burke* [2005] regional hydrological model (90 m resolution), recharge could be approximately 18% of the water budget whereas runoff could reach up to 21% during the wet season and evapotranspiration is roughly 60%. Shallow storage could be as lower as 3%.

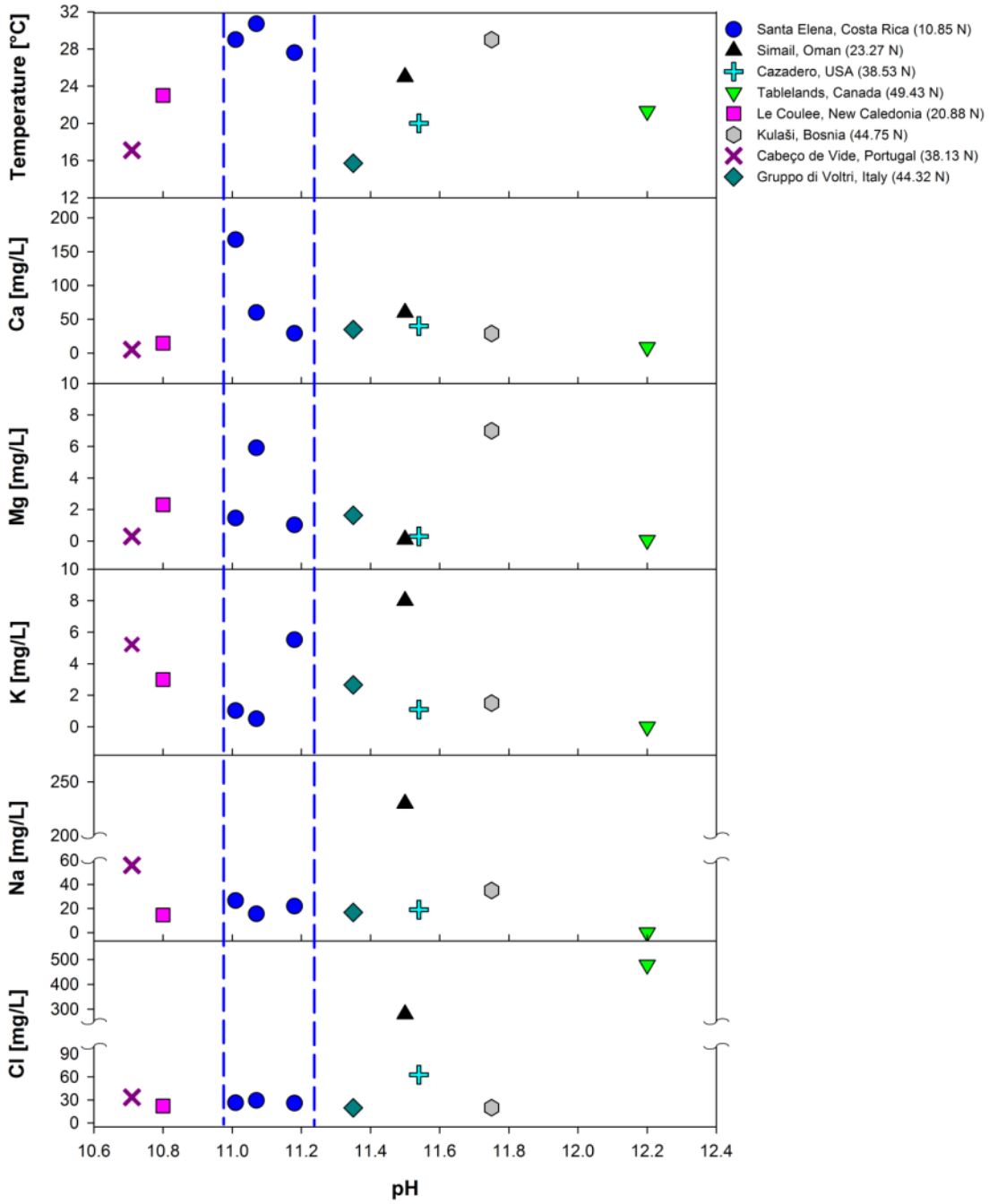

Figure 9: Comparison of Santa Elena aqueous geochemistry and mean composition of hyperalkaline springs in similar subtropical and temperate locations: Hahwalah Wadi Jizi, Semail, Oman [*Barnes et al. 1978*]; Cazadero, California, USA [*Barnes et al. 1978*]; Le Coulee 1, New Caledonia [*Barnes et al. 1978*]; Kulaši, Bosnia [*Barnes et al. 1978*]; Cabeço de Vide, Portugal [*Marques et al. 2008*]; Tablelands, Gros Morne National Park, Canada [*Szponar et al. 2012*]; Gruppo di Voltri, Italy [*Cipolli et al. 2004]*. Numbers in parentheses denote latitude in decimal degrees. Blue dashed-lines emphasize Santa Elena lower and upper pH limits.

Supplementary Tables

The following supplementary tables are provided in a digital format.

Table S1: Description of sampling locations during field explorations (January and March, 2013) in the Santa Elena Ophiolite.

Table S2: Chemical composition of samples from Santa Elena springs and surface waters during the first field expedition in January 2013.

Table S3: Chemical composition of samples from Santa Elena springs and surface waters during the second field expedition in March 2013.

Table S4: Microbial characteristics and 16S rRNA tag sequence diversity measurements for the hyperalkaline spring samples.

Table S5: Taxonomic assignments for all the Bacterial 16 rRNA tag sequences. Values represent % of the total sequences per sample. Only taxa that comprise at least 1% of total sequences in one sample are shown (NA=unclassified).

Table S6: Taxonomic assignments for all the Archaeal 16 rRNA tag sequences. Values represent % of the total sequences per sample. Only taxa that comprise at least 1% of total sequences in one sample are shown. (NA=unclassified).

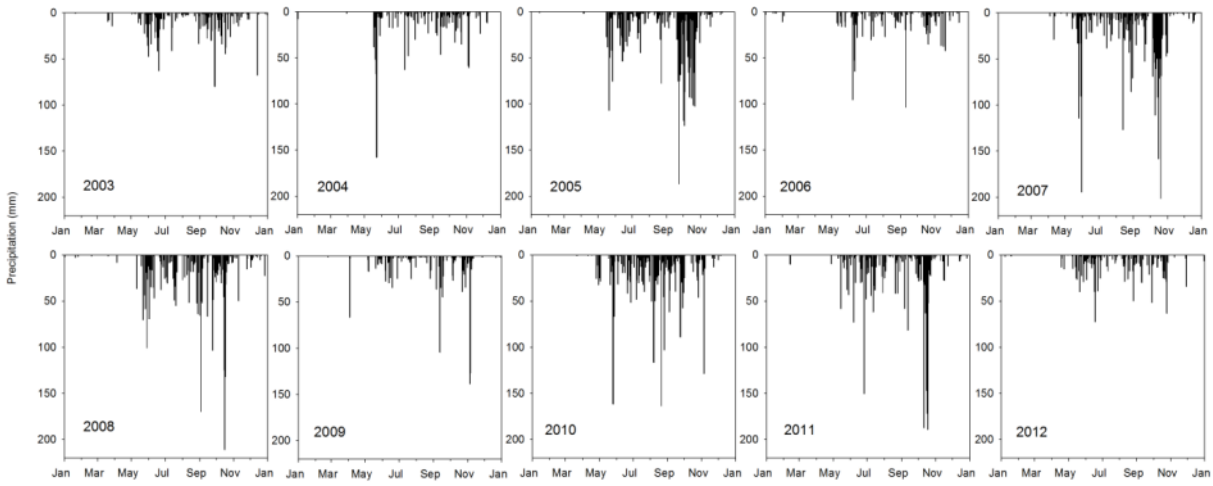

Figure S1: Daily precipitation [mm] from 2003-2012 at the Santa Rosa climatological station.

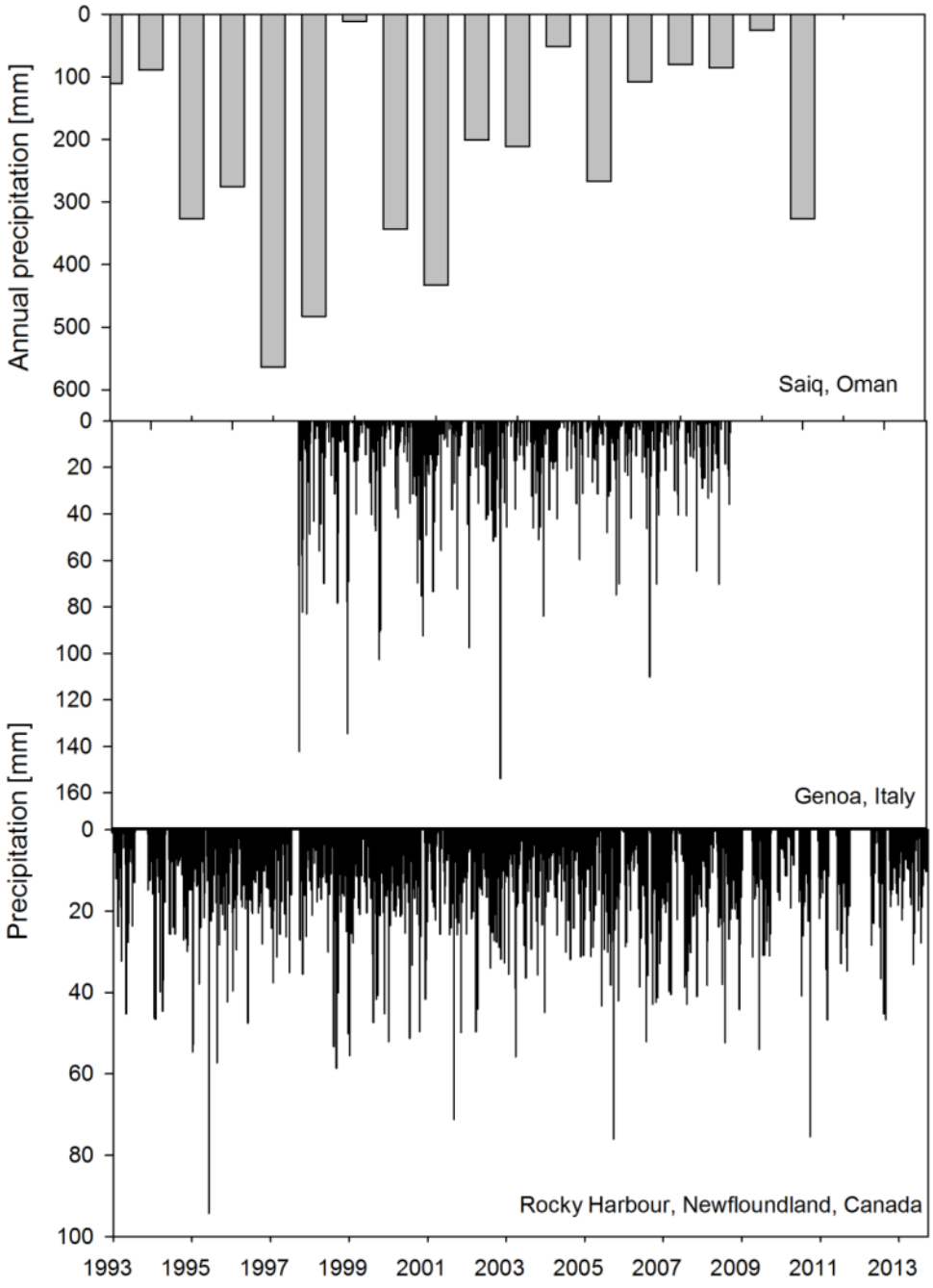

Figure S2: Comparison of daily precipitation records (1993-2013, Newfoundland, Canada and 1997-2008, Genoa, Italy) and yearly precipitation totals (1993-2011, Saiq, Oman) obtained from the National Climatic Data Center (National Oceanic and Atmospheric Administration: http://www.ncdc.noaa.gov/cdo-web/search).

CHAPTER IV

Conclusions

Baseflow recession characteristics and their relationship to landscape, geomorphic, and climatic attributes have been a matter of debate among the hydrology community for several decades. Despite this debate, the spatial heterogeneity and intrinsic complexity of baseflow processes have turned the attention of researchers to *a)* physically-based efforts that permit the parameterization of hydraulic parameters over meso (10^2 km^2) and large (10^3 km^2) catchment areas and *b)* regional analyses that provide a systematic perspective of water sustainability (i.e. surface and groundwater resources) for the upcoming decades. For the inland Pacific Northwest, water managers, understanding how the combination of potential greater ET, earlier spring runoff, and prolonged droughts will affect baseflow regimes has become an imperative.

Results from Chapter I indicate that baseflow coefficients are not strongly related with drainage scale. The most significant parameter controlling the natural release of water as baseflow resulted to be the mean basin slope. The climatic aridity index also could be a useful estimator of baseflow parameters; however, a better understanding of potential changes in precipitation regimes and air temperature is needed. The findings suggest that watersheds located in eastern Washington and northwestern Idaho due to a combination of several factor such as flatter basalt landscapes, low precipitation, and high ET rates could experience even lower recession times and less than 1 mm of minimum annual storage.

Chapter II evaluated baseflow MMTs in natural and human-altered watersheds using stable isotopes and geochemical signals. Baseflow age estimates ranged from 0.42 − 0.62 years (human-altered and basalt-dominated landscape), 0.73 – 1.7 years (mining-altered and predominantly sedimentary rocks), and 0.67 − 3.2 years (forested and granitic-dominated watersheds). Baseflow geochemical data supported the relative water age estimates. Greater residence times were represented by more homogenous water chemistry whereas smaller residence times resulted in more

dynamic compositions. A highly significant power regression ($\tau = 0.11D^{-1.89}$; r^2 = 0.83) was found between the MTT and the damping ratio, indicating greater subsurface travel times as the observed damping ratio decreased. Natural watersheds exhibited a lower damping ratio whereas human-altered watersheds presented greater variability. Relative MTT (i.e. sine-wave approach and damping ratio) and bMTT were greater in watersheds composed mainly of metamorphic and sedimentary basement rocks while watersheds in basalt formation presented smaller travel times. Overall, isotope ratios in the inland PNW showed a temperature-dependent seasonality with a regional meteoric water line of $\delta^2H = 7.42 \cdot \delta^{18}O + 0.88$ (n = 316; r^2 = 0.97). Low d-excess values for precipitation in the inland PNW revealed the incorporation of local recycled water vapor into the traveling air masses and secondary basin scale evaporation processes. Despite the observed seasonal variation in precipitation, the seasonal stream $\delta^{18}O$ variation was very small. However, a significant depletion in surface waters was observed during the 2012 spring due to a large snowmelt event. Overall, the human-altered watershed showed greater isotopic variability, especially during the summer flows. Isotopic differences found in stream $\delta^{18}O$ time series across the study watersheds highlighted the relative contributions of depleted groundwater reservoirs in the streamflow regime.

The baseflow recession characteristics provided in Chapters I and II will enhance physically-based modeling by reducing the use of trial and error approach to calibrate baseflow or deep percolation conditions. By knowing baseflow characteristics such as minimum annual storage and recession timescales, land managers and environmental agencies could prioritize efforts and resources in areas where potential future droughts may drastically affect overall ecosystems services.

Baseflow conditions were also studied in a tropical environment where serpentinization is actively occurring. Field explorations in the Santa Elena Ophiolite, Costa Rica provide strong evidence of active serpentinization in the area. In the hyperalkaline fluids, Mg was highly depleted probably due to serpentine formation and brucite precipitation in the subsurface, whereas Ca was abundant along with high concentrations of hydroxide, carbonates, and chloride. Further, the combination

of active methane vents and extensive carbonate deposits also provide evidence of active serpentinization, though, methane may also form through methanogenic organisms. Signatures of methanogenic archaea from the orders Methanobacteriales, Methanocellales and Methanomicrobiales detected in the hyperalkaline fluids suggest that methanogenesis is an important process at this system. Further evidence for active serpentinization could give the possible presence of H_2 in the spring waters, which will be considered in future studies.

Natural well-mixed surface waters were characterized by a dominant Mg-HCO_3^- system, which represents ~95% of the major ions composition. Stable isotope data shows notable groundwater to surface water connectivity in the main perennial rivers where the hyperalkaline fluids were discovered. Most importantly, spring seepage temperature and isotopic composition (i.e. plotted on the local meteoric water line) strongly suggest no isotopic enrichment or any external heat source such as hydrothermal activity.

Overall, the long rainy season coupled with high rainfall intensity mainly controlled by coastal convective storms position the Santa Elena Ophiolite as an analogue of an early humid Earth where meteoric water inputs were abundant and mainly dominated by changes in the global circulation and sea surface temperature regimes. Given the distribution of mafic-ultramafic rocks on other planetary environments (e.g. Mars), the unique Santa Elena's environment will serve as a natural laboratory to better and fully characterize the planetary conditions that can support life. Likewise, variations in the carbonate mineralogy of veins or layered deposits can give insight into changing fluid compositions and element transport that might be a result of seasonal changes in the hydrological cycle.

Future work on the carbonate deposits formed by discharge of the hyperalkaline springs will serve to refine the search criterion for the surface expression of these systems which could be used to identify both active and inactive serpentinization systems on other planetary bodies. Further evaluations will require continuous physical-chemical monitoring (i.e. resolution of minutes to hours) coupled with sampling of hyperalkaline fluids on an event basis (i.e. single storm responses) to determine the role of rapid meteoric recharge in serpentinization rates and

chemosynthetic organisms as well as depicting the evolution of the hyperalkaline fluids composition throughout the baseflow recession regime.